The Dissertation Committee for Andrew Dike Hughes
Certifies that this is the approved version of the following dissertation:

EXPERIMENTAL CONTRIBUTIONS TO THE THEORY AND APPLICATION OF MOLECULAR RECOGNITION

Committee:

_____
Eric V. Anslyn, Supervisor

_____
Brent Iverson

_____
Christopher Bielawski

_____
Jason Shear

_____
Kevin Dalby

EXPERIMENTAL CONTRIBUTIONS TO THE THEORY AND APPLICATION OF MOLECULAR RECOGNITION

by

Andrew Dike Hughes, B.S.

Dissertation

Presented to the Faculty of the Graduate School of

The University of Texas at Austin

in Partial Fulfillment

of the Requirements

for the Degree of

Doctor of Philosophy

The University of Texas at Austin

May 2008

For Mom and Dad

Acknowledgements

I would like to thank Anslyn group members past and present for support and advice. The culture in the Anslyn group is amazing, and has certainly been the best part of graduate school. Special thanks must be extended to Frantz, Karl and Marco for extensive scientific discussions, and to Byron and Chance for sheer reliability. Thanks also to Pedro Metola for help in procuring last minute analytical data for this dissertation, and to Himali, Sonia and Shuhui for well-timed smiles and candy.

I would like to thank Eric Anslyn for being a role model both scientifically and personally. Eric has found a life he loves, and he inspires me to do the same.

Much of the credit for any of my success in graduate school must go to my wife Julie. She keeps me centered.

Finally, I would like to thank all of my family and friends for all of their love and support. Special thanks to Bryan and Isaiah for all of the phone calls, to Evan for all of the coffee, to Adrial for all of the umbrellas, and to the gang down at the Poison Arrow.

EXPERIMENTAL CONTRIBUTIONS TO THE THEORY AND APPLICATION OF MOLECULAR RECOGNITION

Publication No._____

Andrew Dike Hughes, Ph.D.

The University of Texas at Austin, 2008

Supervisor: Eric V. Anslyn

Molecular recognition is a major branch of modern organic chemistry, and it resides at the forefront of supramolecular chemistry. Supramolecular chemistry refers to the study of the noncovalent intermolecular interaction that are crucial for biological processes, catalytic systems, the organization of crystalline or solution phase superstructures, and molecular recognition to name a few examples. The following dissertation reports research efforts from the Anslyn group into three topics of fundamental interest to the molecular recognition community: cooperativity, array

sensing, and the development of highly selective sensors for minimally functionalized analytes. Chapter 1 is a review of the most fundamental points of molecular recognition as it applies to the experimental work that follows.

Intermolecular association phenomena are driven by multiple discrete, noncovalent interactions, and cooperativity is a measure of the efficiency with which these interactions are employed in a given system. Cooperativity is poorly understood despite its ubiquity in biological and molecular recognition contexts. The first synthetic host-guest system exhibiting positive cooperativity in water is reported in Chapter 2.

The utility of sensitive but unselective sensors when applied in an array format has recently come to light. Chapter 3 details an array of polyaromatic fluorophores dissolved in an aqueous surfactant solution that was used to sense nitrated explosives. This exceptionally unselective quenching process was able to detect and discriminate nitrated explosives such as RDX and TNT at concentrations as low as 19 μM.

Finally, Chapters 4 and 5 report different approaches to the sensing of enantiomeric excess in α-chiral alcohols using an indicator displacement paradigm. Chapter 4 explores unprecedented efforts to convert the Sharpless catalytic epoxidation system to the first Ti^{IV}-based molecular recognition system. Chapter 5 focuses upon a two-stage approach of derivatization of the α-chiral alcohol to a metal chelating ligand followed by employment of the derivative in an indicator displacement assay.

Table of Contents

List of Tables

List of Figures

List of Schemes

Chapter 1. Molecular Recognition: An Overview

1.1 Introduction

Chemistry is called the central science because of its position between physics and biology. Within chemistry, supramolecular chemistry lies toward the biological end of the discipline. Making molecules is the art/science of synthetic chemistry, while the study of weak interactions that assemble molecules is known as supramolecular chemistry. At some point, as the complexities of supramolecular systems grow, life results and the biologists take over.[1,2]

Within supramolecular chemistry lies molecular recognition. Molecular recognition is the organizing force behind supramolecular chemistry that enables the construction of its most complex structures. Any instance of preference in intermolecular interactions can be explored in terms of molecular recognition. The scale of this notion can be demonstrated using DNA. The preference of a strand of DNA base pairs for its complementary strand is the result of the preference of single base pairs, for example, cytosine for guanine. Cytosine prefers binding to guanine over adenine for reasons of shape and electrostatic complementarity, but the double helix formation is largely driven by hydrophobic effects (Figure 1.1).

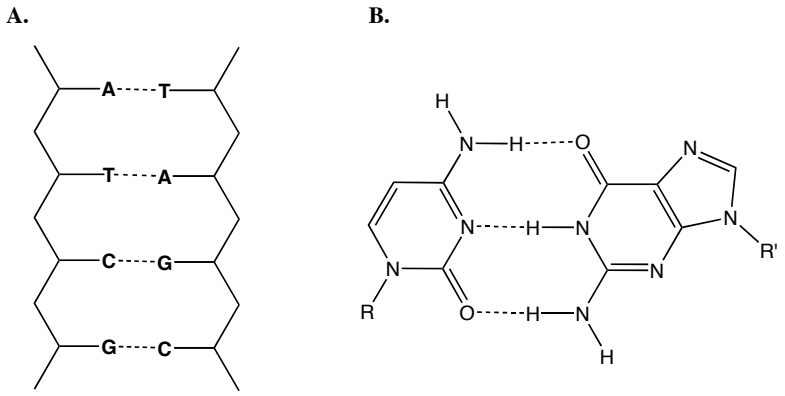

Figure 1.1 ***Scales of molecular recognition.*** The formation of the DNA double helix can be considered as a molecular recognition event at different scales, and is driven by a mixture of hydrogen bonds, shape complementarity and the hydrophobic effect.

Myriad processes drive molecular recognition, both specific and non-specific, and the purpose of Chapter 1 is to provide an overview of what is known about these processes. The scope of this chapter has been dictated by the studies that follow it, each of which begins with a review of the theory and literature more specific to that study.

1.2 The Lock and Key Principle

The dominant paradigm of molecular recognition has been the lock-and-key principle (Figure 1.2). Emil Fischer first deployed this metaphor to explain the substrate specificity of enzymes, and the clarity of the visual argument it presents has led to its ubiquity in explaining the principles that drive specificity in molecular recognition.[3] The lock-and-key principle is probably also responsible for the tendency of researchers to define molecular recognition phenomena in terms of hosts and guests: a large host molecule having a concave binding site envelopes a smaller guest molecule that has peripheral binding functional groups.[4,5] The lock-and-key concept is simple. The alignment of complementary functional groups between a host and a guest dictates the quality of their association. In the case of extremely specific hosts such as enzymes and antibodies, the binding process has been tuned to bind a single molecule to near complete exclusion of others. Most synthetic hosts display some degree of cross reactivity and are therefore selective but not specific. If two guests are in solution, the guest that can engage the various binding events of the host with the best fit will bind more strongly, but in the absence of competitive binders both guests might associate.

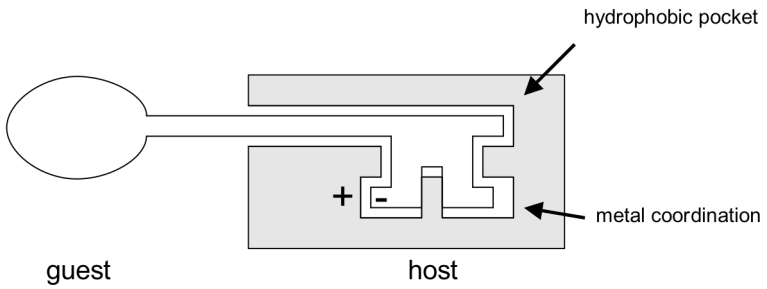

Figure 1.2 ***Lock and key.*** The lock and key paradigm asserts that host-guest affinity is the product of shape and functional group complementarity.

1.2.1 Preorganization

Inherent in the lock-and-key paradigm is the concept of preorganization. The various binding events that drive host-guest assembly, such as metal-coordination, ion-pairing, and hydrogen bonding are directional, and are most effective when employed at precise angles and distances (Scheme 1.1).[6,7,8] Molecular preorganization of host and guest binding sites to maximize the quality of each binding event will inevitably improve the total affinity of the host for the guest. The term *pre*-organized is used to emphasize that functional group positioning has been set prior to binding, in the synthesis of the host (Figure 1.3).[9] Preorganization provides two conspicuous benefits in selective binding. First, the entropic cost of arranging the various binding events of the host around the guest has been paid in the synthesis of the host. This advantage improves the Gibbs free energy of the binding event. Second, the enforcement of binding group location by the covalent structure of the host discourages rearrangement of the host to accommodate other binding partners. This improves the selectivity of the binding event. Preorganization is intimately related to the topic of cooperativity, which is covered extensively in Chapter 2 of this dissertation.

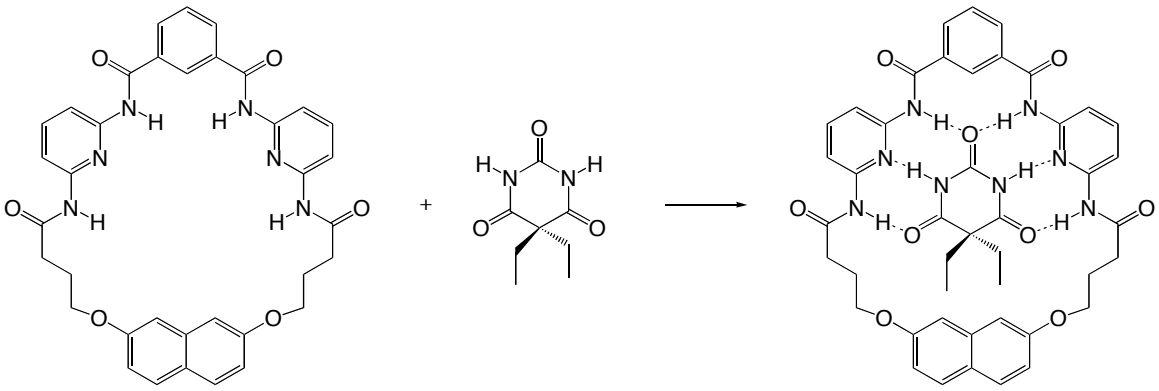

1.1 **1.2**

Scheme 1.1 ***A nice fit.*** Barbitol, **1.2**, binds to host **1.1** strongly in chloroform. The arrangement of host hydrogen bond donors and acceptors is highly complementary to appropriate sites on the guest. The cyclization of the host restricts conformations of the unbound host, so that the structural enforcement of guest binding does not exact as large of an entropic penalty.

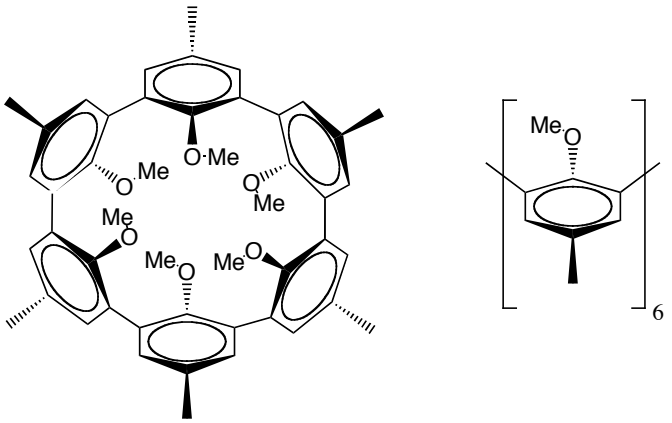

1.3 **1.4**

Figure 1.3 ***The importance of preorganization.*** The binding of Li^+ and Na^+ by the hemispherand **1.3** releases almost four times as much Gibbs free energy as the binding of the same cations by the less preorganized open chain host **1.4**.

1.3 Fundamental Intermolecular Interactions

The organization of binding events is essential to their effectiveness, but the nature of the binding event itself constitutes the driving force of an interaction. For example, hydrogen bonds (H-bonds) are strong enough to effect host-guest binding only when numerous H-bonds are used in concert (See Figure 1.3), while only a single metal-ligand coordination is sometimes sufficient to join two species in solution. In this section, the major intermolecular interactions are reviewed as well as the role of solvent in molecular recognition.

1.3.1 Electrostatics

Most of the binding events in solution are driven by Coulombic forces *i.e.* the alignment of electrostatics. Regions of opposite charge will attract and align, while like charges will repel each other and will be positioned accordingly. Electrostatic interactions vary in intensity, from the abutment of fully charged species in an ion-pair or salt bridge (Figure 1.4A), to the van der Waals forces that describe the attractive component of the transient polarization of adjacent electron clouds (Figure 1.4F). Every combination of ion, dipole, and induced-dipole can be expected to form a stabilizing

interaction of some strength (Figure 1.4).[10,11] Ion-dipole interactions are at the heart of the seminal example of host-guest interaction: cation binding by crown ethers.[12]

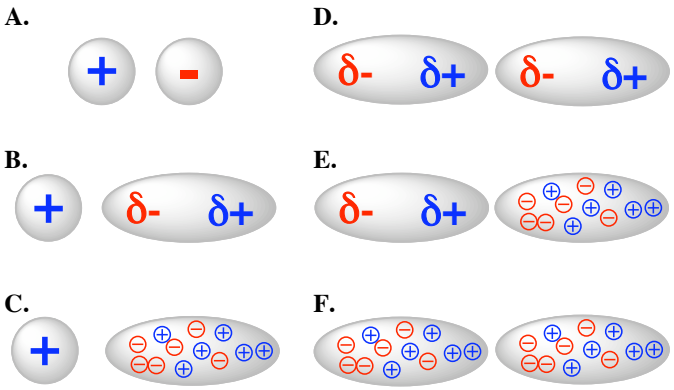

Figure 1.4 ***Basic electrostatic interactions.*** (A.) ion-ion, (B.) ion-dipole, (C.) ion-induced dipole, (D.) dipole-dipole, (E.) dipole-induced dipole, (F.) induced dipole-induced dipole.

1.3.1.1 Crown ethers and cryptands

The first crown ether was synthesized serendipitously by Charles Pederson (Scheme 1.2). Pederson's synthetic target was the diphenolic ether **1.5** which was intended to serve as a chelating vanadyl (VO) ligand, but he was intrigued by a minor side product that had a bizarre propensity to dissolve in aqueous sodium hydroxide despite the absence of an acidic proton. Upon determining the structure of **1.6** Pederson claims to have immediately realized that the "sodium ion had fallen into the hole in the center of the molecule and was held there by the electrostatic attraction between its positive charge and the negative dipolar charge on the six oxygens."[12] Although transition metal chelating species were well known, the ability of crown ethers to bind the alkali metals set them apart[13] and hinted at the importance of the principles of complementarity and preorganization that would be articulated thereafter.

Other researchers, most notably Lehn and Cram, built upon Pederson's work. Lehn expanded crown ethers to bicycles to create cages for cations that he called cryptands (Figure 1.5).[14] Cram also expanded polyethers to create rigid, highly ordered structures like the hemispherand in Figure 1.3 above.[15] Pederson, Lehn and Cram shared

the Nobel Prize in Chemistry in 1987 for their work, and are credited with founding supramolecular chemistry.

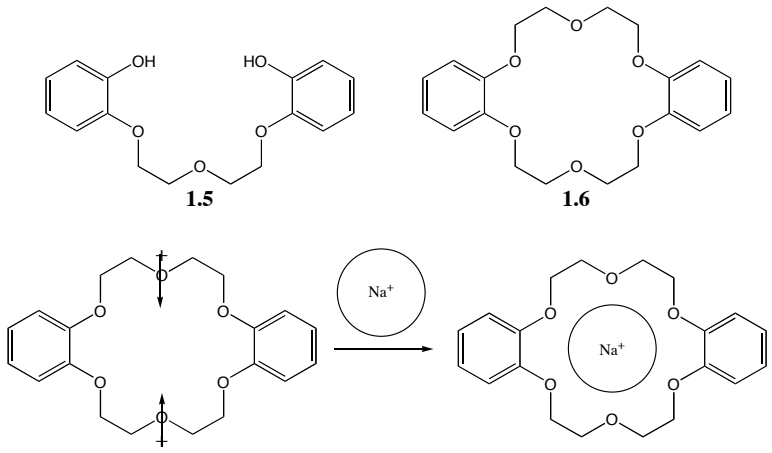

Scheme 1.2 ***Pederson's crown ether.*** In attempting to synthesize **1.5**, Charles Pederson inadvertently generated **1.6** as a side product. He was intrigued by the sodium binding properties of **1.6**, that are the result of the highly organized arrangement of the negative end of the ether dipole.

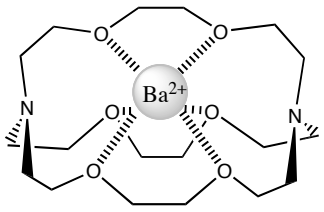

Figure 1.5 A cryptand. Compound **1.7**, developed by Lehn, binds alkali-earth cations (group IIA) preferentially to the alkali (group IA).

1.3.1.2 Ion-pairing

Ion-pairs or salt bridges have been used extensively as binding events in molecular receptors. An interesting example from the Lehn group converts a transition metal binding octaaza-cryptand to a host for anions simply by protonating the amines of the parent metal host (Figure 1.6). The same structural features of preorganization are operating whether the host is acting as a cation or anion host. Due to the fact that the

fluoride in Figure 1.6 is directionally associating with the hydrogens of the ammonia groups, these binding events could also be described in terms of hydrogen bonding.[16]

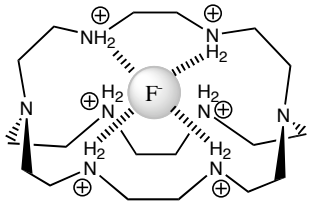

1.8

Figure 1.6 ***Octaaza-cryptand.*** By having ammoniums instead of amines, cryptand **1.8** is capable of binding anions. It is selective for fluoride based upon the size of its cavity.

1.3.1.3 Hydrogen bonding

Hydrogen bonding refers generally to any attractive interaction in which the participants share a hydrogen. Usually the hydrogen is covalently attached to one participant and ionically associated to the other.[17] Innumerable examples of hydrogen bonding exist in biological and synthetic molecular recognition events (see Figure 1.1 and). Hydrogen bonding also imparts structure to water, and water's propensity to donate and accept hydrogen bonds tends to disrupt host-guest hydrogen bonds in bulk aqueous solution. For this reason, hydrogen-bonding interactions tend to become more important in low dielectric fields, such as the hydrophobic depths of a folded protein, or in the solid state.[18]

1.3.1.4 π-bonding

The final topic on electrostatics in molecular recognition, π-bonding, deals not only with dipoles but also with quadrapoles (Figure 1.7). In general, the quadrupole of an aromatic molecule is positive in the center and negative in the vicinity of the π-cloud above and below the ring. Accordingly, favorable interactions between aromatic rings tend to occur in an edge-to-face or slip stacked manner. The π-cloud has also been shown to interact with cations and dipoles.[19,20] Another interesting π-bonding interaction

is the face-to-face stacking of alternating electron-rich and electron-poor aromatic systems. The nature of the aromatic dipole is inverted by substituting electron withdrawing groups around the ring, the net result being a quadrapole moment that is positive at the faces of the ring and negative in the plane. Well-ordered systems have been designed that capitalize upon alternating electron demand between aromatic faces in combination with the hydrophobic effect (Figure 1.8).[21]

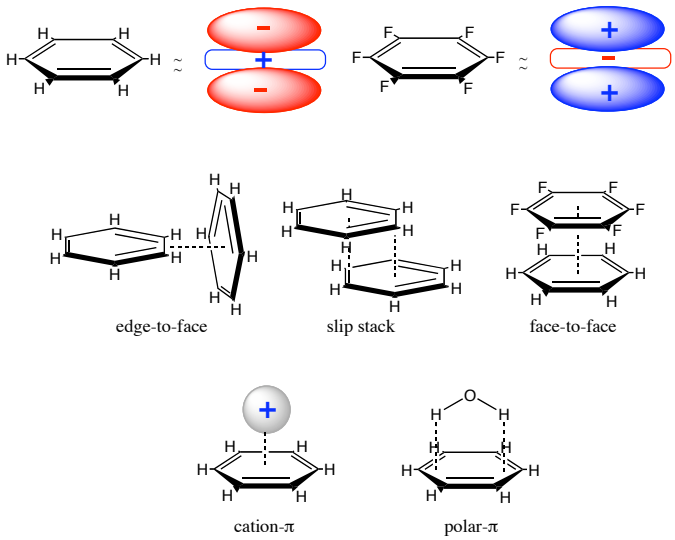

Figure 1.7 ***π-bonding phenomena.*** π-bonding phenomena are electrostatic interactions based upon the quadrapolar nature of aromatics.

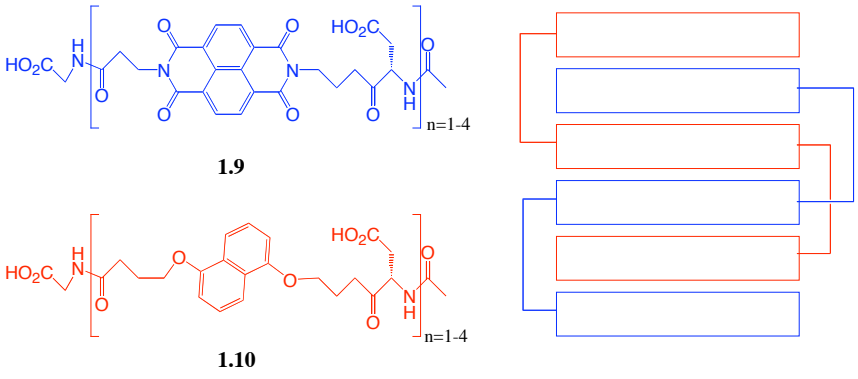

Figure 1.8 ***Order imparted through π-stacking.*** Oligomers of electron deficient (blue) and electron rich (red) aromatics associate in water. The Gibbs free energy of the association becomes more favorable as a function of oligomer length. A diagram of the stacked assembly is shown on the right.

1.3.2 Metal coordination

Metal coordination is one of the strongest intermolecular interactions. To use a metal-ligand interaction to drive host-guest assembly, the key is to make the host-ligand a stronger binder of the metal in question so that the metal reveals unsaturated coordination sites to the incoming guest, but is not stripped by the guest from the host. The incorporation of metal ions into a host also has startling structural implications.[22] In Scheme 1.3, a host for phosphate developed by the Anslyn group has an incorporated Cu^{II} for the duel purpose of organizing the binding cavity and coordination of phosphate.

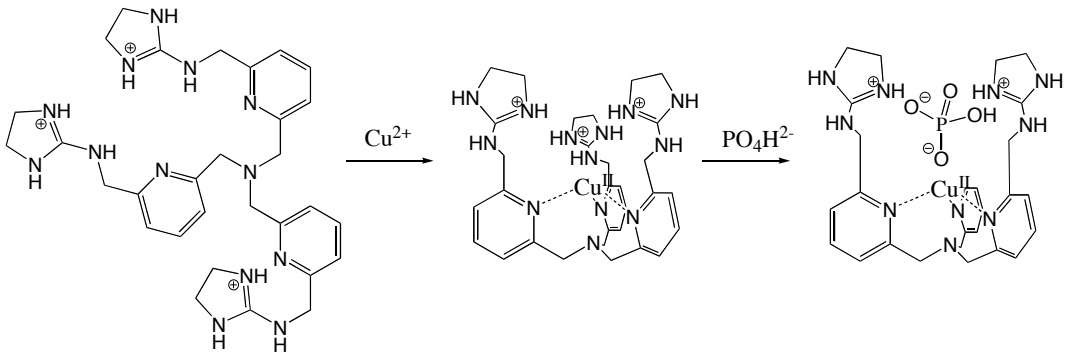

Scheme 1.3 ***Installing a metal-coordination binding site.*** The addition of Cu^{2+} to ligand **1.11** organizes the guanidinum groups to form a tetrahedral binding cavity for inorganic phosphate. One guanidinium in the structure on the right has been omitted for clarity.

The Fabbrizzi group has published extensively on metal-containing host compounds.[23] One example from their group takes the structure modifying nature of metals one step further by incorporating a translocation event that can activate or deactivate the host binding to histidine (Scheme 1.4).[24]

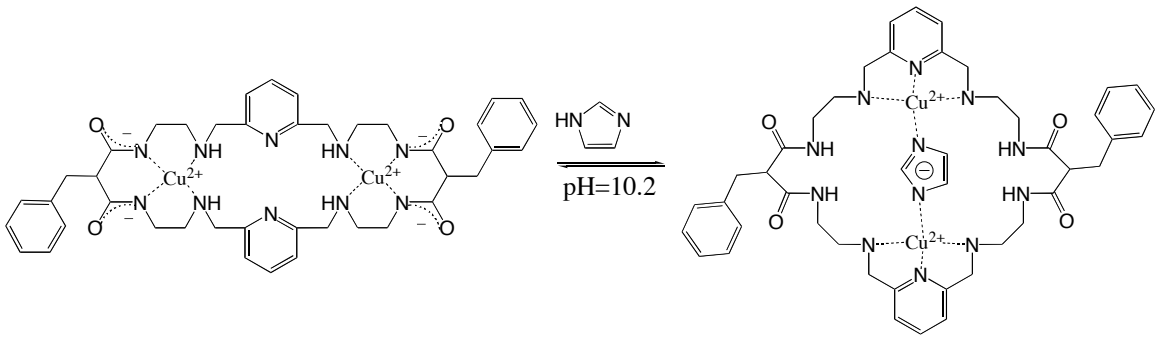

1.13 **1.13'**

Scheme 1.4 ***pH-dependent host activity.*** Compound **1.13** is non-functional as an imidazole host, however, at low pH the amide groups become protonated and the Cu^{2+} ions translocate to afford host **1.13'** which is an effective imidazole host because of open coordination sites on the two copper ions.

1.3.3 Reversible covalent bonds

Although they are not a part of supramolecular chemistry as defined by Lehn,[1] covalent bonds having high kinetic lability or reversibility have regularly been incorporated into host molecules. The most commonly exploited reversibly covalent transition has been the binding of boronic acids to dioxygen functionalities such as catechols, diols, and α-hydroxycarboxylic acids (Scheme 1.5). Boronic acids have proven especially useful for binding to saccharides and other polyhydroxylated natural products. James and Shinkai have been especially active in this area.[25] Scheme 1.6 shows a fluorescent receptor from the James group that is selective for D-glucosamine hydrochloride.[26] The Anslyn group has also reported a number of boronic acid based receptors for naturally occurring analytes including tartrate, citrate and heparin.[27]

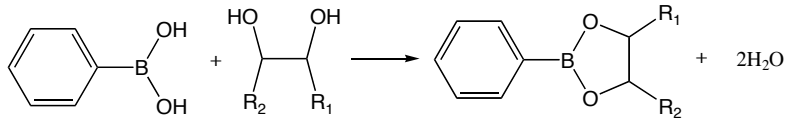

1.14

Scheme 1.5 ***Boronic acid binds a diol.*** A reversible covalent bond formation useful for molecular recognition.

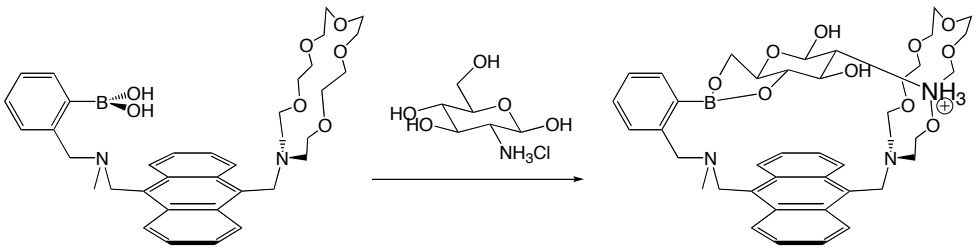

1.15

Scheme 1.6 ***A sensor employing reversible covalent bonding.*** D-glucosamine hydrochloride was shown to bind the boronic acid/azacrownether **1.15** in 33% ethanol in water at pH 7.18.

1.3.4 Solvent effects

Solvation is integral to molecular recognition. Most binding events are orders of magnitude more pronounced in the gas phase than in solution because there is no competition from solvent. Solvation and molecular recognition are highly analogous processes, and for molecular recognition to occur in solution it must be more energetically favorable for the host and guest to be solvated as a complex than to exist independently in solution.

The role of solvent is one of the most challenging facets of molecular recognition and is still not completely understood. Solvent effects are of two types: those that promote binding and those that disrupt it. Both types of effect are most pronounced in water. The role of water in molecular recognition is reviewed more extensively in Chapter 2.

1.3.4.1 The hydrophobic effect

The hydrophobic effect is the tendency of non-polar molecules to aggregate in water. When a small amount of specificity is imparted to this aggregation by shape complementarity or by the presence of one of the previously discussed binding interactions, then molecular recognition is at work. The hydrophobic effect is believed to be entropically driven for small solutes and enthalpically driven for large ones.[28] A network of hydrogen bonds characterizes bulk water. Large solutes interfere with this

network, and are therefore enthalpically unfavorable to dissolve. Smaller solutes, on the other hand, can exist without reducing the number of hydrogen bonds to each water molecule, but restrict the orientations available to water in maintaining this network. Such restriction is entropically unfavorable and therefore the aggregation of smaller solutes is entropically driven.

The binding of the cyclodextrin macrocycles to organics in water is an example of a strong binding event that is predominantly driven by the hydrophobic effect.[11] A specific example of a system that shows strong binding that is driven almost exclusively by water comes from the Diedrich group (Figure 1.9).[29]

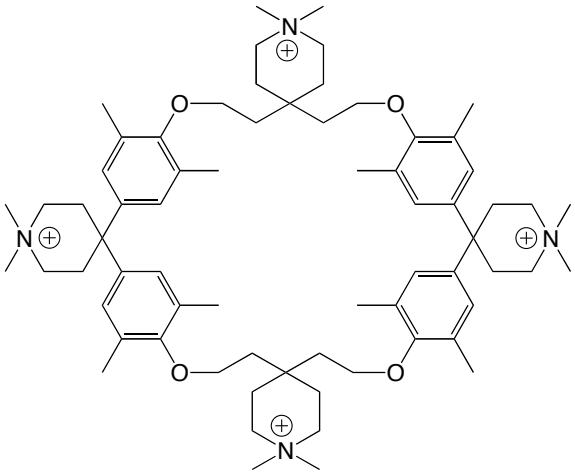

1.16

Figure 1.9 ***A host for pyrene.*** Host **1.16** is a water-soluble macrocycle that binds pyrene in almost exclusive *via* the hydrophobic effect.

1.3.4.2 Competition from solvent

In the case of binding events with a polar component such as ion-pairing, hydrogen-bonding and even metal coordination, water and other polar solvents are almost always a detriment. The binding moieties are stabilized by interactions with the solvent and the energetic benefits of association dwindle rapidly when going from polar to non-polar solvents. Figure 1.10 shows an example from the Hamilton group of a hydrogen

bonding interaction that is strong in 5% THF/$CDCl_3$, but is essentially inactive in DMSO.[30]

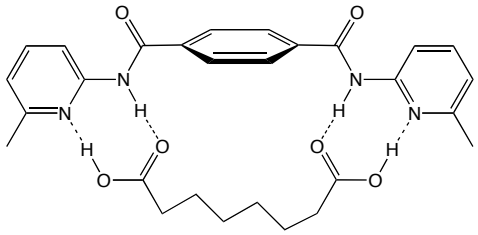

1.17

Figure 1.10 ***Sensitivity to solvent.*** Complex **X.A** is stable in deuterated chloroform but dissociates in the presence of DMSO.

1.4 Optical Sensors from Supramolecular Systems

The term host has been used to describe the larger of two binding partners in molecular recognition. In non-natural systems it is also true that the host tends to be the synthetic partner and was often designed and synthesized with a certain target guest. If that guest is an analyte of interest then it is ideal if the binding of the host can report the presence and concentration of the analyte. A host molecule that is fitted with such a signaling mechanism is called a sensor.[31]

The modes of binding guests that a host may have were reviewed in the preceding sections. This section focuses on the signaling motifs that have been employed to develop sensors using supramolecular chemistry. Signaling strategies can employ covalently attached signaling units, or they can rely upon the displacement of a non-covalently bound, or reversibly covalently bound indicator using a technique known as indicator displacement analysis. A signaling unit is defined as any functionality that can effect a spectrophotometric signal change (UV-Visible absorbance, fluorescence or circular dichroism) upon binding an analyte.

1.4.1 Covalently attached signaling moieties

The general strategy for developing sensors with covalently attached signaling units is straightforward (Figure 1.11). A binding site that is known or expected to bind with the analyte of interest is covalently bound to a signaling element *via* a linking unit. The importance of the linker is to emphasize that the binding site and signaling unit must be able to serve in their respective capacities without interfering with each other.

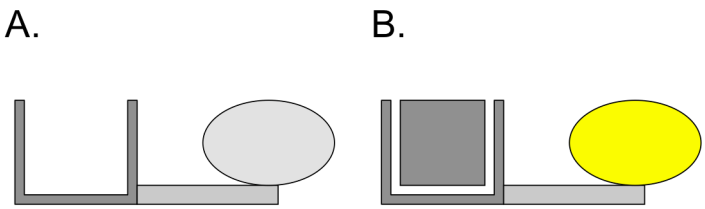

Figure 1.11 ***Covalent sensor design.*** The binding site is attached to the signaling unit by a linker. (A.) In the absence of analyte, the host is silent. (B.) The analyte is complementary to the binding site and is bound, causing an observable modulation in the optical properties of the signaling unit.

A great number of covalently attached signaling systems use a fluorescence-signaling motif in order to take advantage of the "near-ultimate detectability" of fluoresence.[32] Fluorescence may be turn-on or turn-off depending on whether analyte binding increases or decreases the intensity of emission. Three major mechanisms of fluorescence sensing that will be covered in this section are off-on photoinduced electron transfer (PET), on-off PET and monomer-excimer systems.[33]

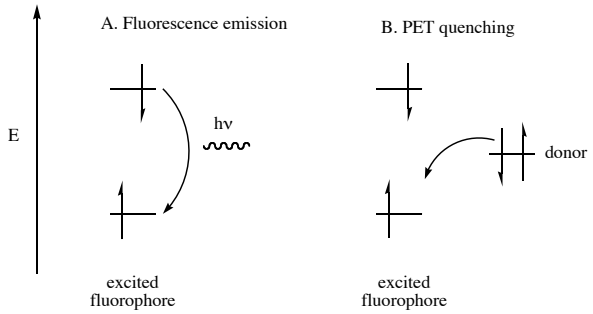

Figure 1.12 ***PET quenching.*** (A.) Radiative relaxation of an excited fluorophore. (B.) Non-radiative electron transfer process.

The PET process is a relaxation pathway for excited fluorophores that is competitive with fluorescent emission, and it is therefore a quenching process (Figure 1.12). A number of turn-on fluorescent sensors have been developed that utilize the interruption of PET by an analyte as a signal generation motif. The most common technique is the installation of an amine next to the fluorophore. The lone pair of the amine donates to the excited fluorophore and quenches fluorescence. Protonation or metallation of the amine ties up the lone pair of the amine, thus eliminating or reducing PET and signaling the presence of the analyte. Two systems exhibiting fluorescence off-on sensing are shown in FIGURE, one from Czarnik (Scheme 1.7A) and the other from Verhoeven(Scheme 1.7B).[34,35] The James D-glucosamine hydrochloride sensor in Scheme 1.5 also utilizes a PET based fluorescence off-on mechanism.

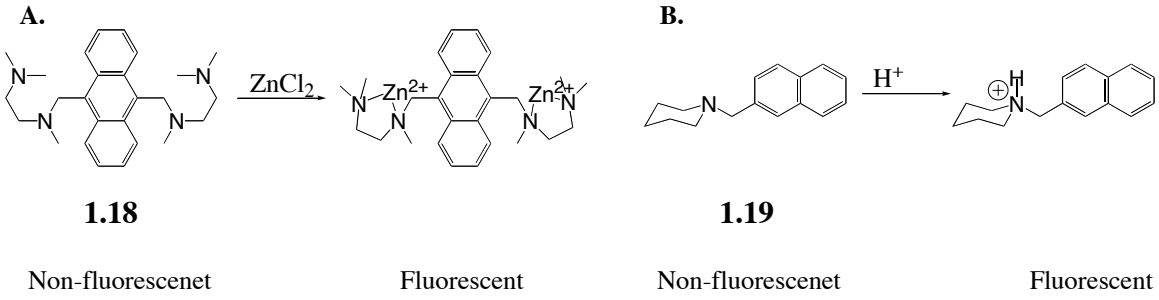

1.18 **1.19**

Non-fluorescenet Fluorescent Non-fluorescenet Fluorescent

Scheme 1.7 ***Off-on fluorescence by suppression of PET.*** A sensor for Zn^{2+}, **1.18**, and a sensor for acidic protons, **1.19**, both exhibiting off-on signaling motifs.

On-off PET systems work inversely from their off-on brethren, either by binding a analyte that has an electron donating group of the proper energy, or perhaps more elegantly, by bringing an intramolecular donor in proximity with the fluorophore upon substrate binding. A Zn^{2+} sensor from the Fabrizzi group that operates in such a way is shown in Scheme 1.8.[36]

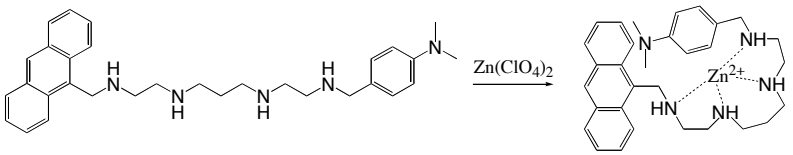

1.20

Scheme 1.8 ***On-off fluorescence sensor.*** When Zn^{2+} is bound by compound **1.20**, the aniline quencher of **1.20** is brought close to the anthracene fluorophore and fluorescence is quenched. The coordination geometry around Zn^{2+} in the bound structure is tetrahedral.

Another class of covalent signaling strategies utilizes the wavelength difference between the monomer and excimer emissions of certain fluorophores. The intensity of excimer emission is related to the proximity of the fluorophores in solution. The closer they are the more likely that the excited species will couple with the ground state species and relaxation will occur *via* emission of the excimer. The design strategy for excimer sensors is to induce the interaction or association of two monomers upon substrate binding. The effect is an off-on sensor in either case because the monomer or excimer emission will be growing in and one need only observe that emission wavelength. An example of an excimer disruption signaling technique from the Shinkai labs is shown in Scheme 1.9.

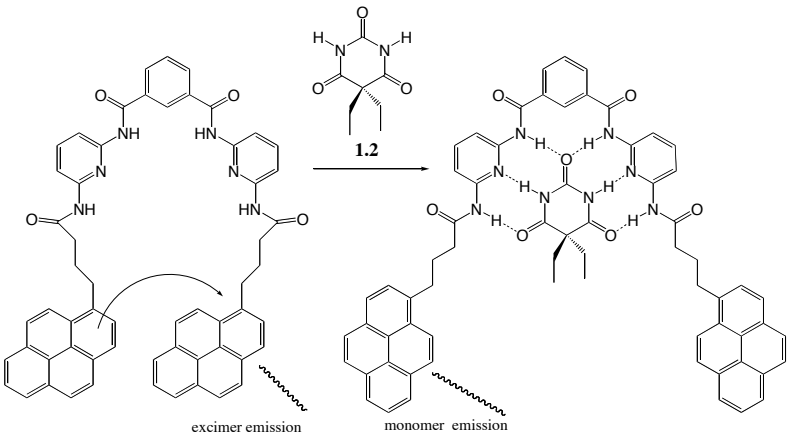

1.21

Scheme 1.9 ***A sensor with excimer disruption.*** Binding of barbitol disrupts the excimer of compound **1.21** and results in a turn on of monomer fluorescence.

1.4.2 Indicator Displacement Assays

Sensors having covalently attached indicators have proven successful in many cases, but the laborious synthesis of large receptor molecules is only exacerbated by the addition of a signaling subunit. To address this problem, a non-covalent signaling protocol has become quite prevalent: indicator displacement assays (IDAs). The design of an IDA is shown in Scheme 1.10. IDA's rely upon a competition between indicator and analyte for the host cavity. The indicator must absorb or emits light differently when bound to the host or free in solution. The system is tuned by the choice of indicator, the solvent the pH and the concentration all of which are modularly variable to find the system with the highest sensitivity to a desired analyte.[37]

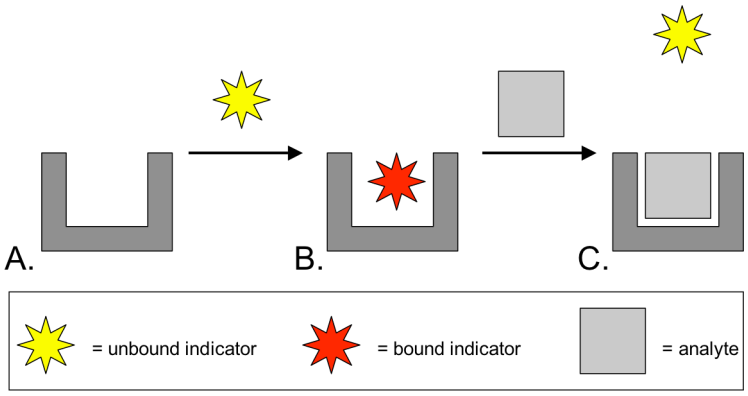

Scheme 1.10 ***The basics of indicator displacement assays.*** (A.) The host alone (B.) An indicator is added that has different optical properties when bound to the host. (C.) An analyte displaces the indicator resulting in a color change. The presence of the analyte is thus signaled.

The Anslyn group has been particularly active in developing IDA technology, two systems they have developed appear in Scheme 1.11.[38] One of the difficulties of developing IDAs is finding the right indicator that will respond colorimetrically to the types of binding events installed on the host. The Zn^{2+} and boronic acids systems, **1.22** and **1.23**, shown in Scheme 1.11 both rely on deprotonation of their respective catecholic indicator and are useful in aqueous systems. Asymmetric analytes for which IDAs have been developed are discussed in Chapter 4.

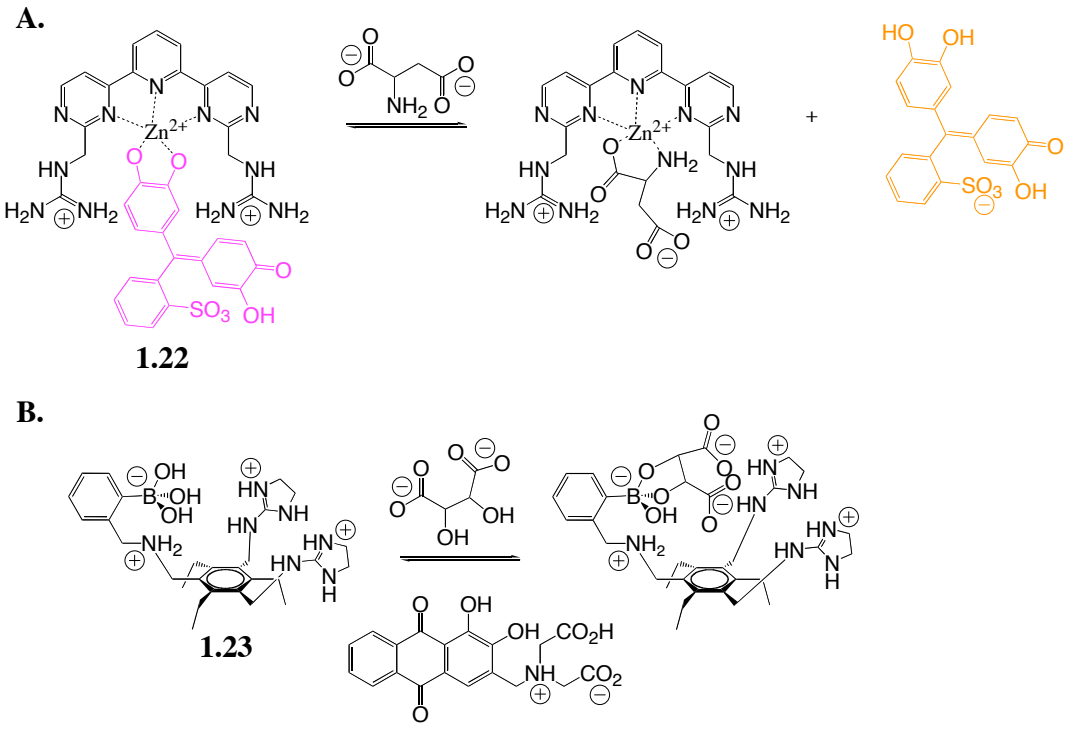

Scheme 1.11 ***IDAs from the Anslyn group.*** Both systems operate in aqueous methanol around pH 7.4. (A.) A sensing ensemble for amino acids that is selective for aspartate. The indicator is pyrocatechol violet. (B) A sensing ensemble for tartrate and malate, tartrate is shown. The indicator is alizarin complexone. The indicator host complex is not shown for clarity. This system was effective at quantifying the total concentration of tartrate and malate in a series of commercial wines and grape juices.

1.5 Summary

This chapter has been a review of the most important molecular association phenomena with selected examples from the literature. The adaptation of molecular recognition hosts for sensing applications was also explored. The purpose of this chapter was to give an overview of molecular recognition that complements the in-depth coverage of the topics in later chapters: cooperativity, array sensing and the development of an enantioselective IDA for α-chiral alcohols.

1.6 References from Chapter 1

1. Lehn, J.-M. *Supramolecular Chemistry: Concepts and Perspectives.* (VCH-Weinheim, 1995).

2. "Design of Complexes Between Synthetic Hosts and Organic Guests" Cram, D. J.; Cram, J. M. *Acc. Chem. Res.* **1978**, *11*, 8-14.

3. *The Lock and Key Principle. The State of the Art – 100 Years On* (Ed.: J.-P. Behr), Wiley, New York, **1994**.

4. Steed, J. W.; Atwood, J. L. *Supramolecular Chemistry*. John Wiley & Sons: Chichester, 2000.

5. "The Design of Molecular Hosts, Guests, and Their Complexes" Cram, D. J. *Angew. Chem. Int. Ed.* **1988**, *27*, 1009-1020.

6. "Preorganization: From Solvents to Spherands" Cram, D. J. *Angew. Chem. Int. Ed.* **1986**, *25*, 1039-1057.

7. "Host-Guest Complexation. 35. Spherands, the First Completely Preorganized Ligand Systems" Cram, D. J.; Kaneda, T.; Helgeson, R. C.; Brown, S. B.; Knobler, C. B.; Maverick, E.; Trueblood, K. N. *J. Am. Chem. Soc.* **1985**, *107*, 3645-3657.

8. "Hydrogen Bonding and Molecular Recognition: Synthetic, Complexation, and Stuctural Studies on Barbituate Binding to an Artificial Receptor" Chang, S. –K.; Van Engen, D.; Fan, E.; Hamilton, A. D. *J. Am. Chem. Soc.* **1991**, *113*, 7640-7645.

9. "Host-Guest Complexation. 29. Expanded Hemispherands" Cram, D. J.; deGrandpre, M.; Knobler, C. B.; Trueblood, K. N. *J. Am. Chem. Soc.* **1984**, *106*, 3286-3292.

10. "Supramolecular Chemistry. 42. Electrostatics in Molecular Recognition" Schneider, H. J.; Blatter, T.; Eliseev, A.; Ruediger, V.; Raevsky, O. A. *Pure. App. Chem.* **1993**, *65*, 2395-2334.

11. Anslyn, E. V.; Dougherty, D. A. *Modern Physical Organic Chemistry*. University Science Books, Sausalito, 2004.

12. "The Discovery of Crown Ethers" Pederson, C. J. *Angew. Chem. Int. Ed. Engl.*, **1988**, *27*, 1021-1027.

13. (a)"Cyclic Polyether and Their Complexes with Metal Salts" Pederson, C. J. *J. Am. Chem. Soc.* **1967**, *89*, 2495-2496. (b) "Cyclic Polyether and Their Complexes with Metal Salts" Pederson, C. J. *J. Am. Chem. Soc.* **1967**, *89*, 7017-7036.
(c)"New Macrocyclic Polyether" Pederson, C. J. *J. Am. Chem. Soc.* **1970**, *92*, 391-394.

14. (a) "Diaza-polyoxa-macrocycles et macrobicycles" Dietrich, B.; Lehn, J. –M.; Sauvage, J. –P. *Tetrahedron Lett.* **1969**, *10*, 2885-2888. (b) "Cryptates: The Chemistry of Macropolycyclic Inclusion Complexes" Lehn, J. –M. *Acc. Chem. Res.* **1978**, *11*, 49-57.

15. (a) "Structural Parameters that Control Association Constants between Polyether Host and Alkylammonium Guest Compounds" Timko, J. M.; Helgeson, R. C.; Newcomb, M.; Gokel, G. W.; Cram, D. J. *J. Am. Chem. Soc.* **1974**, *96*, 7097-7099. (b) "Host-Guest Chemistry" Cram, D. J.; Cram, J. M. *Science*, **1974**, *183*, 803-809. (c) "Host-guest Complexation, Concept and Illustration" Kyba, E. P.; Helgeson, R. C.; Madan, K.; Gokel, G. W.; Tarnowski, T. L.; Moore, S. S.; Cram, D. J. *J. Am. Chem. Soc.* **1977**, *99*, 2564-2571.

16. "Anion Receptor Molecules: Synthesis of an Octaaza-cryptand and Structure of its Fluoride Cryptate" Dietrich, B.; Lehn, J. –M.; Guilhem, J.; Pascard, C. *Tetrahedron Lett.* **1989**, *30*, 4125-4128.

17. Pauling, L. *The Nature of the Chemical Bond, 3rd Ed.* (Cornell University Press, New York, 1960).

18. Jeffrey, G. A. *An Introduction to Hydrogen bonding.* Oxford: Oxford University Press, 1997.

19. "Substantive effects on cation- π interactions: A quantitative study" Hunter, C. A., Low, C. M. R., Rotger, C.; Vinter, J. G.; Zonta, C. *Proc. Natl. Acad. Sci. USA*, **2002**, *99*, 4873-4876.

20. "The Cation-π Interaction" Ma, J. C.; Dougherty, D. A. *Chem. Rev.* **1997**, *97*, 1303-1324.

21. "Aromatic Oligomers that Form Hetero Duplexes in Aqueous Solution" Gabriel, G. J.; Iverson, B. L. *J. Am. Chem. Soc.* **2002**, *124*, 15174-15175.

22. "Formation of Artificial Receptors by Metal-Templated Self-Assembly" Linton, B.; Hamilton, A. D. *Chem. Rev.* **1997**, *97*, 1669-1680.

23. Fabbrizzi, L.; Licchelli, M.; Pallavicini, P.; Parodi, L.; Taglietti, A. *Transition Metals in Supramolecular Chemistry*; Sauvage, J. P., Ed.; John Wiley & Sons: New York, 1999.

24. "A Sleeping Host Awoken By Its Guest: Recognition and Sensing of Imidazole-Containing Molecules Based on Double Cu^{2+} Translocation Inside a Polyaza Macrocycle" Fabrizzi, L.; Foti, F. Patroni, S.; Pallavicini, P.; Taglietti, A. *Angew. Chem. Int. Ed.* **2004**, *43*, 5073-5077.

25. "Boronic Acid-Based Sensors" Wang, W.; Gao, X., Wang, B. *Curr. Org. Chem.* **2002**, *6*, 1285-1317.

26. "Selective D-glucosamine hydrochloride fluorescence signalling based on ammonium cation and diol recognition" Cooper, C. R.; James, T. D. *Chem. Commun.* **1997**, 1419-1420.

27. "Guidelines in Implementing Enantioselective Indicator-Displacement Assays for α-Hydroxycarboxylates and Diols" Zhu, L.; Zhong, Z.; Anslyn, E. V. *J. Am. Chem. Soc.* **2005**, *127*, 4260-4269.

28. "Two Faces of Water" Chandler, D. *Nature*, **2002**, *417*, 491.

29. "^{1}H NMR Investigation of Host-guest Complexation between a Macrocyclic Host of the Cyclophane Type and Aromatic Guests in Aqueous Solution" Diederich, F.; Griebel, D. *J. Am. Chem. Soc.* **1984**, *106*, 8037-8046.

30. "Molecular Recognition: A Remarkably Simple Receptor for the Selective Complexation of Dicarboxylic Acids" Garcia-Tellado, F.; Goswami, S.; Chang, S. –K.; Geib, S. J.; Hamilton, A. D. *J. Am. Chem. Soc.* **1990**, *112*, 7393-7394.

31. (a) "Supramolecular Optical Chemosensors for Organic Analytes" Bell, T. W., Hext, N. M. *Chem. Soc. Rev.* **2004**, *33*, 589-598. (b) "Sensors and Switches from Supramolecular Chemistry" Fabrizzi, L.; Poggi, A. *Chem. Soc. Rev.* **1995**, *24*, 197-202.

32. "Emerging fluorescence sensing technologies: From photophysical principles to cellular application" de Silva, A. P.; Eilers, J.; Zlokarnik, G. *Proc. Natl. Acad. Sci. USA* **1999**, *96*, 8336-8337.

33. "Signaling Recognition Events with Fluorescent Sensors and Switches" de Silva, A. P.; Gunaratne, H. Q. N.; Gunnlaugsson, T.; Huxley, A. J. M.; McCoy, C. P., Rademacher, J. T.; Rice, T. E. *Chem. Rev.* **1997**, *97*, 1515-1566.

34. "Chemical Communication in Water Using Fluorescent Chemosensors" Czarnik, A. W. *Acc. Chem. Res.* **1994**, *27*, 302-308.

35. “Photoinduced Electron Transfer in Polychromophoric Systems. 2. Protonation Directed Switching between Tri- and Bichromophoric Interaction” Mes, G. F.; van Ramesdonk, H. J.; Verhoeven, J. W. *J. Am. Chem. Soc.* **1984**, *106*, 1335-1340.
36. “A Zinc(II)-Driven Intramolecular Photoinduced Electron Transfer” Fabbrizzi, L.; Licchelli, M.; Pallavicini, P.; Taglietti, A. *Inorg. Chem.* **1996**, *35*, 1733-1736.

37. “Teaching Old Indicators New Tricks” Wiskur, S. L.; Ait-Haddou, H.; Anslyn, E. V.; Lavigne, J. J. *Acc. Chem. Res.* **2001**, *34*, 963-972.

38. (a) “Optical sensing of inorganic anions employing a synthetic receptor and ionic colorimetric dyes” Niikura, K.; Bisson, A. P.; Anslyn, E. V. *J. Chem. Soc., Perkin Trans. 2*, **1999**, 1111-1114. (b) “Teaching Old Indicators New Tricks: A Colorimetric Chemosensing Ensemble for Tartrate/Malate in Beverages” Lavigne, J. J.; Anslyn, E. V. *Angew. Chem. Int. Ed.* **1999**, *38*, 3666-3669. (c) “Achieving Large Color Changes in Response to the Presence of Amino Acids: A Molecular Sensing Ensemble with Selectivity for Aspartate” Ait-Haddou, H.; Wiskur, S. L.; Lynch, V. M.; Anslyn, E. V. *j. Am. Chem. Soc.* **2001**, *123*, 11296-11297.

Chapter 2. A Cationic Host Displaying Positive Cooperativity in Water.

2.1 Introduction

Noncovalent and reversibly covalent molecular interactions such as hydrogen bonding, ion-pairing, metal-coordination and the hydrophobic effect, to name only a few, are the basis of the field of supramolecular chemistry. These intermolecular interactions are often referred to simply as binding events. Binding events in isolation are rarely strong enough to effect the molecular recognition and self-assembly processes that define supramolecular chemistry, and therefore they usually operate multilaterally. Multiple binding events always result in an enhancement of the Gibbs free energy released upon binding, and this phenomenon is known as cooperativity. If one considers binding events as discrete interactions with fundamental strengths of binding, then the cooperativity of a bimolecular interaction composed of multiple binding events will have an associated efficiency. If the Gibbs free energy released in a cooperative interaction is less than the sum of the Gibbs free energies of the constituent binding events, then the system is considered to exhibit negative cooperativity. If the Gibbs free energy of the cooperative interaction exceeds the sum of its binding events then the system is considered to exhibit positive cooperativity.

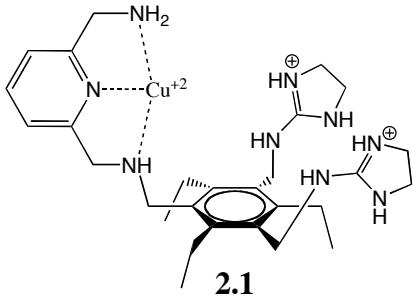

2.1

In the study discussed in this chapter, the thermodynamics of binding between tetracationic host **2.1** and a series of polycarboxylate guests in water were determined using UV-Vis titration and isothermal titration calorimetry (ITC) and analyzed in terms

of cooperativity. It was found that **2.1**, which contains two guanidinium groups and a coordinatively unsaturated Cu^{II} center, exhibits positive cooperativity when binding all of the polycarboxylates, and that this positive cooperativity is enthalpic in origin. This is one of the first examples of positive cooperativity in water using a synthetic host.

2.1.1 Background and Significance

Cooperativity is a general effect that has been explored in a number of closely related phenomena, including: the chelate effect,[1,2,3] multivalency,[4,5] and cooperativity.[6,7,8,9,10] These terms are often used interchangeably, but some trends have been established. The chelate effect is typically reserved for metal binding by polydentate ligands. Early studies of cooperativity and multivalency, which typically involve more complicated host-guest systems, co-opted this term to explain the increases in binding affinity when multiple binding events occur between two substrates,[3] but soon researchers formulated the concepts of cooperativity and multivalency to describe larger systems. The difference between cooperativity and multivalency is subtler. Multivalency tends to be reserved for the largest of binding events in which the multiple interactions between two substrates do not occur simultaneously, thereby resulting in a stepwise progression of the binding event and a number of degenerate partially bound states between the actors.[4,11] In biological systems, multivalency is often deemed the cluster effect.[12,13] Cooperativity occurs in systems undergoing multiple binding events at short range where all of the binding moieties engage simultaneously; it is an especially fitting descriptor of binding in cavities. Therefore the interaction between the closely positioned cationic moieties of **2.1** as they bind polyanionic species is best described as cooperativity. It should be noted that cooperativity and multivalency are conflated in the literature, and many of the conclusions of chelation, multivalency and cooperativity studies seem transferable between systems. However, cooperativity should not be confused with allosteric cooperativity, which is seen when hemoglobin binds multiple diatomic oxygen molecules. Allosteric cooperativity is a fundamentally different phenomenon than that discussed herein.

Positive cooperativity represents an optimal mode of binding in which the various discrete binding events that collectively drive a host-guest interaction are being employed to their full capacity, and indeed, exceed the binding strength that could be expected via the summation of the individual Gibbs free energies of binding. Negative cooperativity does not imply that the affinity between two species is weakened by the multiplicity of their interactions; on the contrary, polyvalent interactions are almost without exception far stronger than any of the constituent binding events in isolation. Maximizing positive cooperativity in water is an especially important goal because water has long been one of the most difficult media for the molecular recognition chemist, despite being the exclusive solvent *in vivo*.

The principles of complementarity and preorganization elucidated by Cram, Lehn and other early students of noncovalent interactions, seem so obvious to the modern supramolecular chemist that it is almost possible to forget that these ideas spawned the fields of molecular recognition and supramolecular chemistry.[14,15] The goal of research into the origin of positive cooperativity is to delineate new maxims that will validate and shape the very intuition of future supramolecular chemists. A general strategy for achieving positive cooperativity in host-guest systems would signify a comprehensive understanding of binding phenomena. Finally, a thorough understanding of cooperativity will allow researchers to maximize binding interactions without simply tacking on functional groups, a scenario with practical benefits in the pharmaceutical industry. Lipinski's rule of five recommends that potential therapeutic agents be under 500 Da, and the ability to modulate the binding site affinity of a compound without dramatically increasing its mass helps researchers work within this constraint.[16]

2.1.2 Theories of Cooperativity

What chemists have come to call cooperativity, Jencks, in 1981,[9] first articulated as additivity in the form of Eq. 1. The Gibbs free energy of connection ($\Delta G_S°$) is defined to be positive in the case of positive cooperativity and negative in the case of negative cooperativity. The Gibbs free energy of binding A-B ($\Delta G_{AB}°$) represents the binding of the polyvalent host and guest, while the Gibbs free energy of binding A ($\Delta G_A°$) and B

($\Delta G_B°$) are the strengths when observed in isolation of the constituent binding events that make up the full host-guest interaction observed as $\Delta G_{AB}°$ (Figure 2.13).

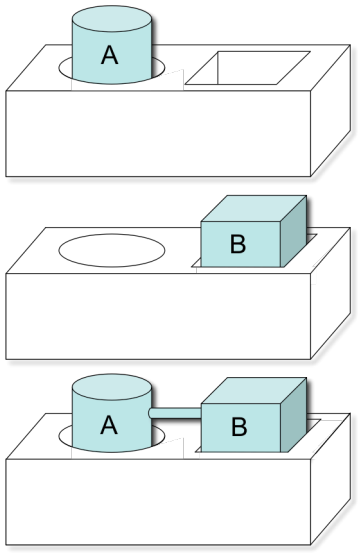

Figure 2.13 ***Binding in Tandem.*** A and B bind the host in different regions. When covalently tethered as A-B they bind the host cooperatively. If the binding of A-B releases more Gibbs' free energy than could be expected from the binding of A and B separately, then the binding of A-B is said to exhibit positive cooperativity.

$$\Delta G_S° = \Delta G_A° + \Delta G_B° - \Delta G_{AB}° \quad (1)$$

As an extension of Jencks' delineation of ΔG_S, our group has previously defined $\Delta H_S°$ and $T\Delta S_S°$ as the enthalpy and entropy of connection (Eqs. 2 and 3).[6] $\Delta H_S°$ is positive when enthalpy contributes to positive cooperativity and negative when enthalpy contributes to negative cooperativity, while $T\Delta S_S°$ is negative when entropy contributes to positive cooperativity and positive when entropy contributes to negative cooperativity. These thermodynamic variables of connectivity maintain a Gibbs-Helmholtz type dependency (Eq. 4). For clarity the term $-T\Delta S_S°$ is used, which is positive when the entropy of connection contributes to positive cooperativity just like $\Delta G_S°$ and $\Delta H_S°$.

$$\Delta H_S° = \Delta H_A° + \Delta H_B° - \Delta H_{AB}° \quad (2)$$

$$T\Delta S_S^\circ = T\Delta S_A^\circ + T\Delta S_B^\circ - T\Delta S_{AB}^\circ \quad (3)$$

$$\Delta G_S^\circ = \Delta H_S^\circ - T\Delta S_S^\circ \quad (4)$$

Jencks' analysis of cooperative binding was very similar to theories about metal chelation: for entropic reasons, covalently tethering two or more binding moieties and engaging them simultaneously will yield positive cooperativity, unless the binding moieties are tethered in such a way that they interact poorly with their complement on the host. It can be deduced that an entropic benefit must be gained in the tethering of multiple binding events because the entropic penalty of losing translational motion must be paid once in total, instead of once for each of the binding events. The deleterious effects of improperly tethered binding functional groups are similarly easy to imagine (Figure 2.14); as such, one would expect enthalpy to scale imperfectly as the binding events between a host and guest multiply, unless the host and guest are able to associate in a configuration ideal for all of the constituent binding events.

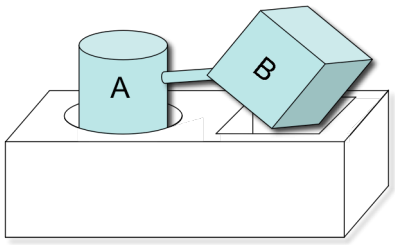

Figure 2.14 ***An Imperfectly Tethered Pair of Binding Events.*** As it is tethered to binding event A in this example, binding event B is unable to fully interact with the binding pocket of the host. The enthalpy of binding event B will not be fully expressed in the binding of the ditopic guest A-B, and negative cooperativity will result.

The thermodynamic truisms that Jencks illuminated are indispensable considerations for any analysis of cooperativity; however the prediction that positive cooperativity will tend to be entropic in nature has not been realized experimentally (*vide infra*). This is due in part to the complexities of the solution phase, especially with competitive solvents such as water. Competitive solvents are able to engage charged and

polar binding moieties in hydrogen bonding, dipole-dipole interactions and charge-dipole interactions. Some examples of ion pairing and metal coordination binding events in water are known to be entropically driven by solvent rearrangement,[17, 18] and it has been shown that the reduced solvation surface of the "whole" guest (A-B) versus the "parts" (A and B) can contribute to an entropic disfavorability of tethering (Figure 2.15).[6] Another reason that the entropic benefit of connection is not commonly observed to give a positive Gibbs free energy of connection is that tight binding appears to result in a loss of conformational freedom.

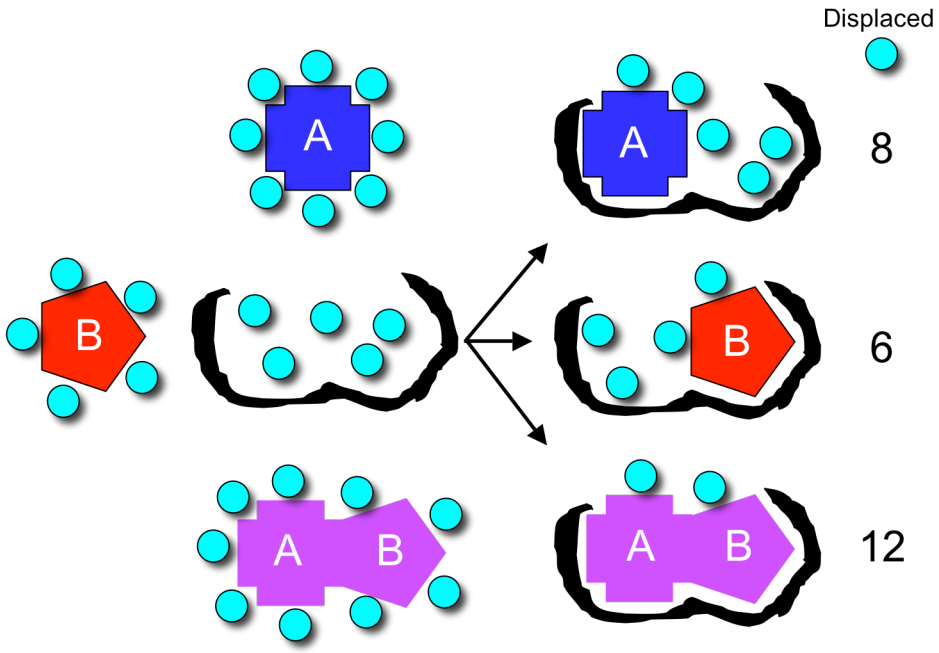

Figure 2.15 ***A Very Simple Model of Solvent Displacement.*** In competitive solvents such as water, symbolized here as turquoise circles, liberation of the solvent sphere of the host and guest to the disordered bulk solution lends an entropically favorable element to binding events. When A or B enter the binding cavity alone they displace a total of 14 solvent molecules, however when they bind as A-B they release only 12 solvent molecules because of surface area lost upon tethering A and B.

The ability of complementary binding functionalities (e.g. a hydrogen bond donor and acceptor) to interact is easily compromised when such functionalities are each part of a larger molecule incorporating multiple discrete binding moieties. As all of the binding

interactions between a host and guest seek their complementary parts, it is logical to consider that they will not all be able to access the ideal distance and conformation that represents the most stable mode of interaction for that binding event. Jencks supposed that the proper spacing and orientation of binding events constitutes the fundamental difficulty in achieving positive cooperativity; however, enthalpy has often been found to scale efficiently as the number of binding events grows.[3,5] Just as positive cooperativity has not emerged from entropic benefits, so has negative cooperativity not been regularly linked to enthalpy.[3,6]

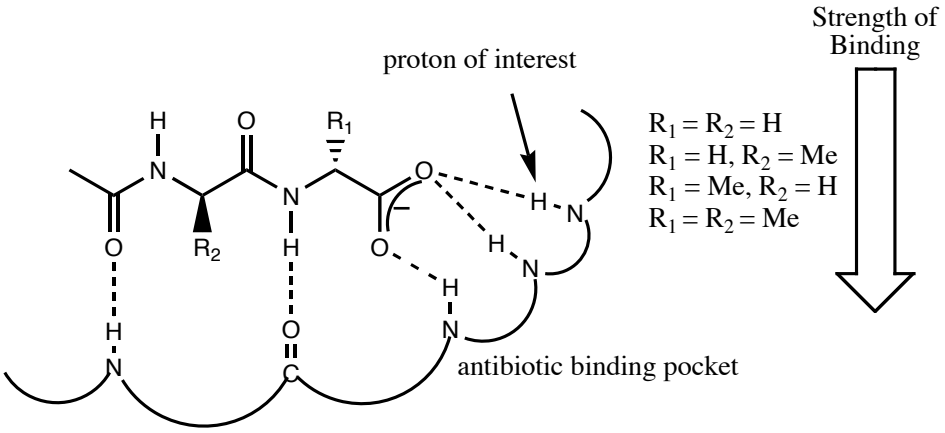

Figure 2.16 ***Dipeptide Binding to Antibiotics.*** Williams showed that the presence of methyl groups at the R-positions (alanine versus glycine) enhanced both the total affinity of binding and the ^{1}H NMR chemical shift of the "proton of interest," which was correlated to exothermicity. Hence it was concluded that hydrophobic stabilization elsewhere in the binding pocket reduced residual motion and allowed the carboxylate – amide hydrogen bond to strengthen. This trend was observed using both eremomycin and teicoplanin A_3-1 antibiotics.

A corollary to Jencks' original considerations has been proposed by Williams and has proven useful in providing a more complete picture of the nature of cooperative binding.[8] Williams analyzed the binding of vancomycin group antibiotics with bacterial cell wall analogues and found a correlation between the $-\Delta G°$ of the binding event, the hydrocarbon surface area of the peptide and the ^{1}H NMR shift of the amide protons of the antibiotic upon binding the carboxylate terminus of the peptide (Figure 2.16).[19,20] The ^{1}H NMR shift was considered a measure of the strength of this hydrogen bond. Williams

concluded that the hydrophobic binding from the latter part of the peptide dampened residual motion in the binding cavity and allowed the carboxylate-amide hydrogen bond to become stronger and more exothermic. The settling of the ligand into the binding pocket is enthalpically favorable; however, the loss of residual motion and binding mode diversity are entropically unfavorable (Figure 2.17).

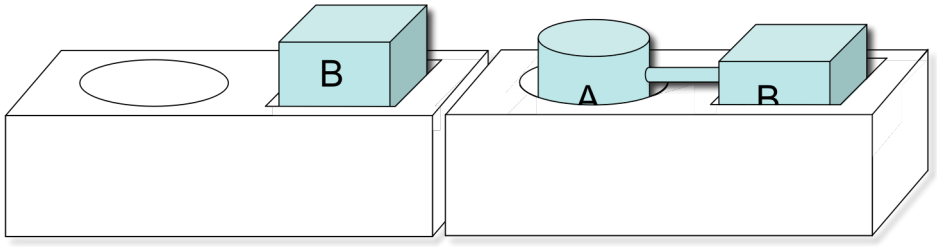

Figure 2.17 ***Settling into the Binding Pocket.*** When A-B binds the host both binding events are dampening the residual motion of the system, and therefore both binding events are able to interact more strongly with the host than when A or B binds the host separately. This stronger binding is enthalpically favorable, but the loss of residual motion is entropically unfavorable.

A second study by Williams focused upon the dimerization of the vancomycin group antibiotics.[10] Using van't Hoff methods to parse $\Delta H°$ and $\Delta S°$ from $\Delta G°$, it was observed that antibiotics that dimerize with a more favorable $-\Delta G°$ also undergo structural tightening as determined by ^1H NMR analysis. However, the amount of Gibbs free energy released upon dimerization was mitigated by the entropically unfavorable loss of residual motion. Williams has proposed that this enthalpy-entropy compensation effect is general, and should be a major determinant of cooperativity: positive cooperativity will be enthalpically driven while entropic factors will contribute to negative cooperativity. Jencks' and Williams' theories of cooperativity are complementary in that they both consider different aspects of polyvalent binding, all of which are contributing to different degrees, but these theories differ in their predictions of the thermodynamic source of positive and negative cooperativity. Whether the enthalpy-entropy compensation effect is primal in cooperativity or is only evident in specific systems remains to be seen. As thermodynamic studies of cooperativity continue to be

published, it is becoming increasingly clear that multiple factors contribute to Jencks' original analysis of positive cooperativity.

2.1.3 Studies in Cooperativity

One of the first studies of cooperativity to judiciously parse binding events as prescribed by Jencks was from the Breslow group.[3] Using ITC, the binding of β-cyclodextrin monomers and covalent dimers with mono- and ditopic hydrophilic substrates was examined in water using ITC (Figure 2.18). The binding of ditopic substrates to the β-cyclodextrin dimers was routinely three to four times more exothermic than the relevant monotopic interaction. Conversely, the entropies of binding, which were favorable in all of the monotopic instances, became sharply unfavorable in the ditopic systems. The entropic contribution to negative cooperativity ($T\Delta S_S°$) overwhelmed the enthalpic gains, and in all of the host-guest combinations which Breslow studied negative cooperativity was in effect. This study strongly supports Williams' arguments that enthalpic gains toward positive cooperativity will tend to be counterbalanced by entropic losses in residual motion and internal rotation. Interestingly, an earlier ditopic system described by Breslow that contained a more rigid spacer between the β-cyclodextrin units appears to display positive cooperativity, although it was not reported as such; unfortunately this system was not dissected in a formal thermodynamic study of cooperativity.[21]

Whitesides *et al.* have reported a trivalent interaction based upon the vancomycin-dipeptide interaction.[22] C_3-symmetric tris-vancomycin and tris-dialanine derivatives were synthesized, and their association was compared to that of the monovalent vancomycin-dialanine in water (Figure 2.19). In this case, the enthalpy of the trivalent receptor was only slightly more than three times that of the isolated vancomycin-dialanine interaction (-40 kcal/mol versus -12 kcal/mol) but again, entropic losses contributed to negative cooperativity. Whitesides credited the loss in entropy of connection to the use of a rather flexible linker from the dialanine subunit to the benzene

core and posited that the system could be redesigned with a more rigid spacer to effect positive cooperativity.

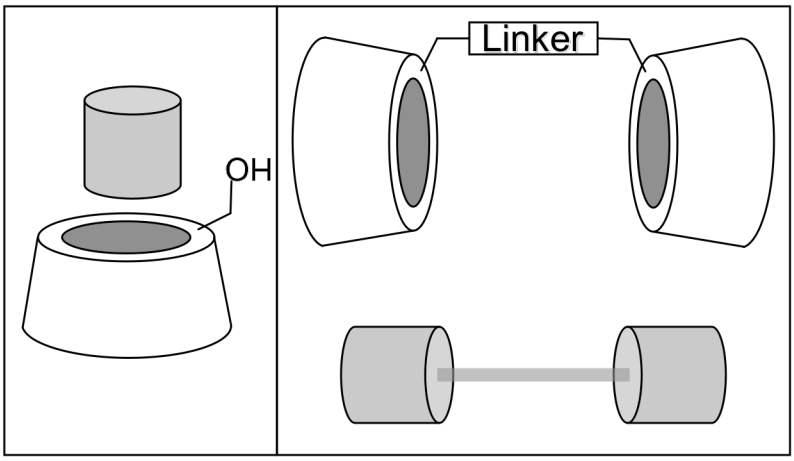

Figure 2.18 ***β-Cyclodextrin Dimers Studied by Breslow.*** The grey cylinders are hydrophobic groups: adamantyl, naphthyl, and *tert*-butylphenyl. The toroids represent β-cyclodextrin which was covalently dimerized using a dithiol, 2,6-bipyridine and a biphenyl linker. Binding of the ditopic guests to the β-CD dimers was more than twice as exothermic as the monomeric equivalents on the left, however negative cooperativity resulted due to the loss of entropic favorability in the dimeric system.

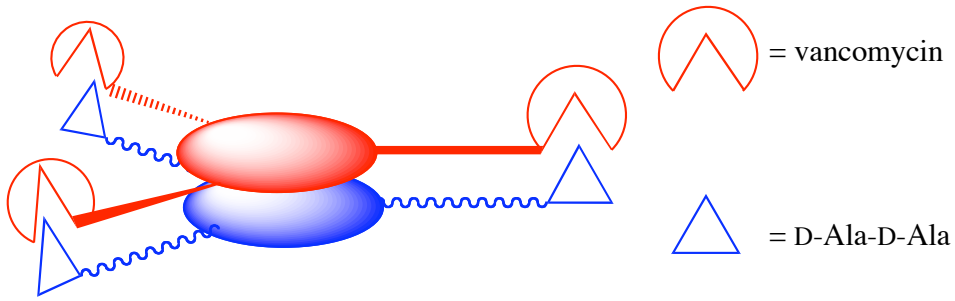

Figure 2.19 ***A Trivalent Vancomycin-dipeptide System.*** The binding of trivalent vancomycin and dialanine derivatives was more than three times as exothermic as the monovalent interaction. Negative cooperativity was due to an unfavorable entropy of tethering, probably due to the highly flexible linker in the tris-alanine compound which loses significant internal rotation upon binding.

One of the few definitive examples of positive cooperativity comes from the Anslyn group. In chloroform, *cis*-1,3-cyclohexanediol releases more than twice the

Gibbs free energy upon association with host **2.2** as is released when cyclohexanol binds to host **2.3** (Figure 2.20).[23] These data were collected without the benefit of ITC, but it is informative that positive cooperativity appears to be more accessible in an organic solvent than in water.

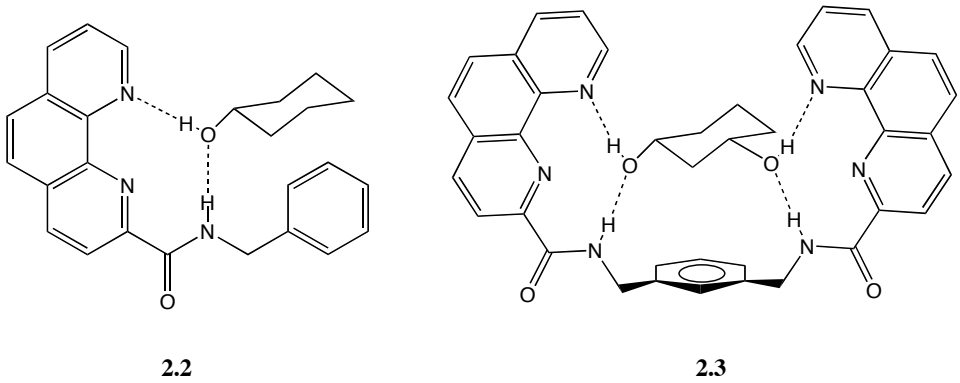

2.2 **2.3**

Figure 2.20 ***An Example of Positive Cooperativity.*** In chloroform, host **2.3** binds *cis*-1,3-cyclohexanediol ($\Delta G°$ = 4.18 kcal/mol) more than twice as strongly as **2.2** binds cyclohexanol ($\Delta G°$ = 1.5 kcal/mol).

The role of solvation in cooperativity was the goal of another study from the Anslyn group. The binding of host **2.4** to a series of polycarboxylate guests was monitored by ITC and UV-Vis (Figure 2.21). As the number of carboxylates on the guest increased, the increase in binding affinity was attributable to enthalpic gains but was once again unfavorable with respect to entropy. In this study it was determined that the loss of residual motion and internal rotation was probably insufficient to result in the observed negative entropy of connectivity ($-T\Delta S_S°$). Instead it was concluded that the loss of solvation area when the guest carboxylates are tethered together is a major contributor to negative cooperativity in this system (see Figure 2.15).

While $\Delta G°$ normally becomes more favorable as binding events are tethered, the entropic loss that accompanies enthalpic strengthening and loss of solvated surface area has regularly been implicated in a final analysis of why negative cooperativity results.[3, 6, 22] In light of the seemingly inescapable entropic penalty of strong binding, we reason that a system that displays positive cooperativity must have a fundamental binding

quality that is not present in the constituent binding moieties in isolation: an "X-factor". From the literature, one example of such an "X-factor" seems to be active in the prodigious chelating ability of EDTA.[1] In EDTA, the polyanionic character is believed to have a destabilizing effect upon the unbound form so that its ability to bind cations is strongly assisted by the exothermic release associated with the relief of several electrostatic repulsions. Similarly, spherand type cation receptors have been shown to bind more strongly when the unbound host suffers from configurational deformation due to the repulsion of electron pairs between oxygens in the binding pocket.[24] Systems such as spherands and EDTA, which have a conspicuous destabilizing force in the unbound state, seem to be archetypes around which a formal demonstration of positive cooperativity in water could be designed. We wondered if an organic receptor employing a mixture of metal coordination and ion-pair binding events could be a possible candidate for a system displaying positive cooperativity in a manner similar to the EDTA chelating effect.

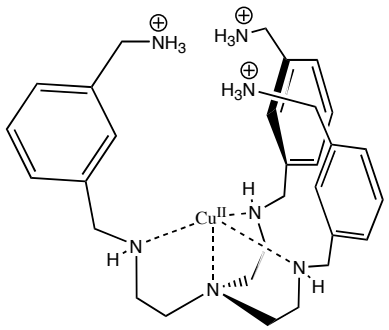

2.4

Figure 2.21 ***Negative Cooperativity Due to Reduction in Solvation Area.*** When **2.4** was bound with a series of carboxylate guests, the loss of solvent accessible surface area as the guests were tethered resulted in negative cooperativity.

To achieve positive cooperativity our strategy was to exploit the destabilizing effect of electrostatic repulsion in order to instill in the full host a secondary binding force unavailable to the constituent binding moieties. In this way we hoped to promote positive cooperativity in water, or at least to observe a system whose negative cooperativity was minimal compared to previous systems. We hypothesized that any

progress toward a positively cooperative system would come from enthalpic gains derived from the alleviation of electrostatic repulsions in the unbound host. We therefore chose host **2.1** because the steric gearing of the 2,4,6-triethylbenzene core will force the charged groups close to each other and because it was easy to conceive of a modular dissection of the metal-coordination versus the ion-pairing binding events.

2.1.4 Design Criteria

Host **2.1** is tetracationic and therefore able to accommodate up to four carboxylate groups in a small guest molecule such as 1,2,3,4-butanetetracarboxylate (**2.7**). Two carboxylates can chelate at the Cu^{II} center (although the axial coordination bond is longer and weaker than the equatorial),[25,26,27] leaving one carboxylate for each of the guanidiniums. In this way host **2.1** is conceptually cleavable into its Cu^{II} center **2.5** and its bis-guanidinium portion **2.6** (Figure 2.22), with each part able to accommodate up to two carboxylates per guest. The purpose of segregating the individual binding events is to accurately quantify the strength of binding portions A and B, $\Delta G_A°$ or $\Delta G_B°$, as defined by Jencks.[9]

The copper site has been isolated in the form of the bis-aminomethylpyridine Cu^{II} ligand-metal complex **2.5**. The bis-guanidinium site is isolated in model host **2.6** in which the portion of host **2.1** that is equipped with a tridentate copper ligand has been capped with an acyl amide group, rendering it nonfunctional as an anion binding site in the competitive aqueous media. It is important to note that any hydrophobic binding in host **2.1** from the face of the aromatic ring will be similarly available in **2.6**, so all of the overt binding functionalities in host **2.1** have been accounted for in the two model hosts. Therefore, any positive cooperativity will be an intrinsic property of the specific arrangement of these binding entities in host **2.1**.

Each host and guest has one or more associated counter ions. The cationic hosts have exclusively chloride counter anions, while the anion guests have exclusively sodium cations. The salt metathesis that is inherent in our studies always involves the generation of the same salt (NaCl), and is therefore not what differentiates the host-guest thermodynamics. For similar reasons, the buffer concentration and solution pH are kept

constant throughout. A discussion on ionic strength is included in the Experimental Details section of this chapter.

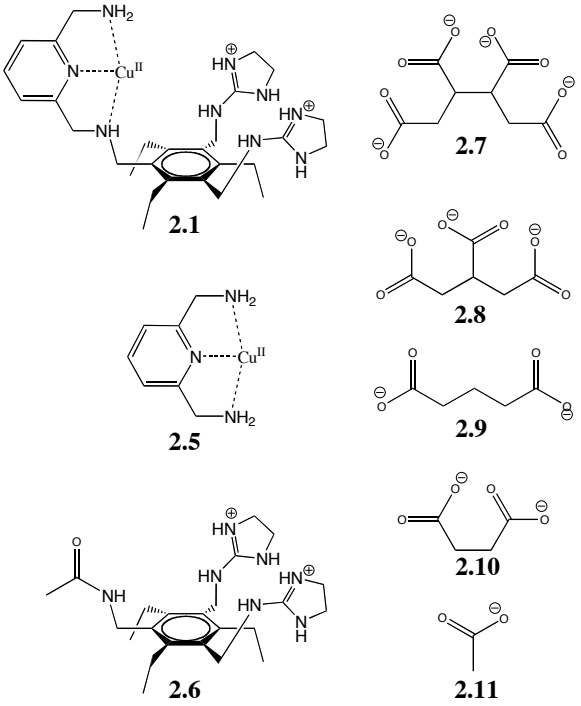

Figure 2.22 ***Cationic Hosts and Anionic Guests.***

2.2 Results and Discussion

2.2.1 Synthesis

The synthesis of **2.1** involves the coupling of the metal-chelating arm precursor **2.17** to the modified triethylbenzene **2.18**. The synthesis of **2.17** is addressed in Scheme 2.12. Diol **2.12** is monotosylated in the presence of Ag_2O to produce **2.13**, the tosylate of which is then displaced by phthalate to form **2.14**. **2.14** is converted with hydrazine to the aminoalcohol **2.15**, which is then Boc-protected at the amine. The boc-protected aminoalcohol **2.16** is then oxidized to the aldehyde **2.17** using hypervalent iodide.

To form **2.1**, **2.17** was reductively aminated using the known amine **2.18** followed by sodium borohydride.[28] Compound **2.19** was triply deprotected with trifluoroacetic acid

and then converted to the chloride salt *via* an ion-exchange column. The Cu^{II} complex **2.1** was generated *in situ* prior to use in binding studies (Scheme 2.13).

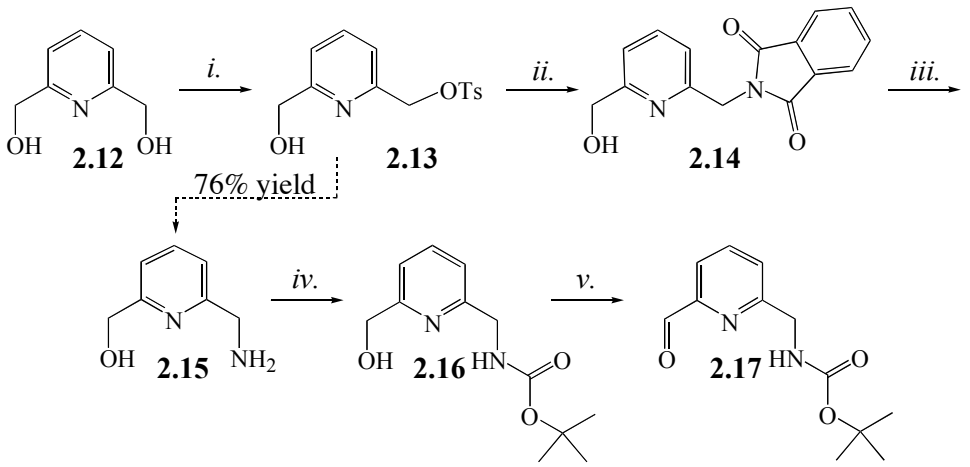

Scheme 2.12 ***Synthesis of the Chelating Arm of* 2.1.** (*i.*) TsCl, KI, Ag_2O, DCM, -20 °C to rt, 4 h, 63% (*ii.*) K-phthalimide, DMF, 40 °C, 4 h (*iii.*) N_2H_4, EtOH, reflux, 7 h (*iv.*) Boc_2O, NEt_3, DCM, rt, 2 h, 73% (*v.*) Dess-Martin periodinane, DCM, rt, 0.5 h, 85%.

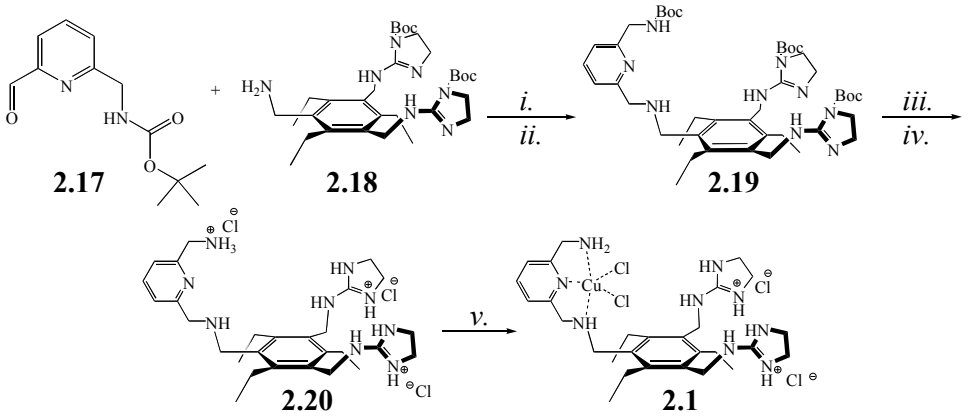

Scheme 2.13 ***Synthesis of* 2.1.** (*i.*) toluene, 50 °C, 5 h (*ii.*) $NaBH_4$, MeOH, rt, 4.5 h, 80% (*iii.*) 1:1 TFA/DCM, rt, overnight, 96% (*iv.*) Cl^- ion-exchange column (*v.*) $Cu^{II}Cl_2$ (aq.)

The synthesis of host **2.5** is detailed in Scheme 2.14. **2.21** was generated as a side product from the tosylation of **2.13** (Scheme 2.13). The tosylates were then doubly displaced by phthalate to form **2.22**, which was then converted to the diammonium **2.23**

using concentrated hydrochloric acid. The Cu^{II} complex was generated *in situ* prior to use in binding studies.

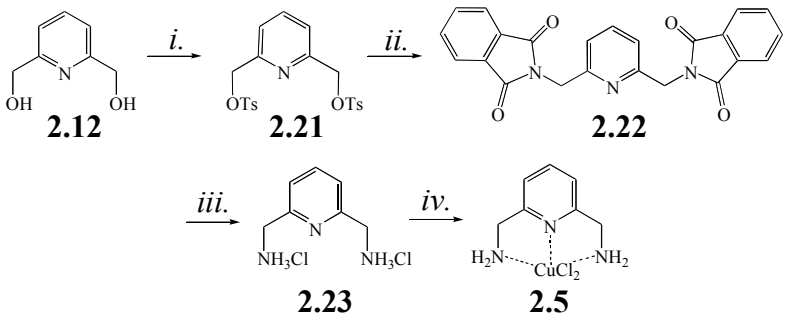

Scheme 2.14 ***Synthesis of*** **2.5.** (*i.*) TsCl, KI, Ag_2O, DCM, -20 °C to 0 °C, 4 h, 17% (*ii.*) K-phthalimide, K_2CO_3, DMF, 160 °C, overnight, 96% (*iii.*) HCl (conc.), reflux, 4 h, 46% (*iv.*) $Cu^{II}Cl_2$ (aq.)

The synthesis of **2.6** is detailed in Scheme 2.15. The benzylamine **2.24** was acylated using acetic anhydride to furnish **2.25**, which was then doubly deprotected to yield **2.26**. Boc-protected guanidine groups were installed *via* methylthioimidazole **2.27**, forming **2.28**, which was deprotected with trifluoroacetate and converted to the chloride salt by passage down an ion exchange column.

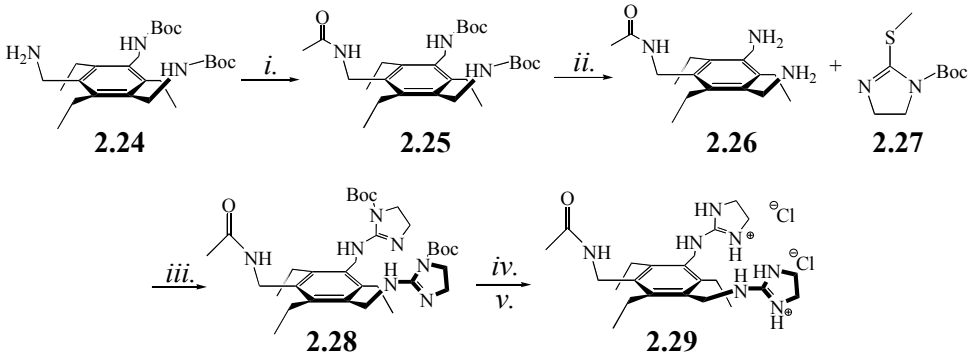

Scheme 2.15 ***Synthesis of*** **2.6.** (*i.*) Ac_2O, DCM/ 0.5 M NaOH, rt, 1 h, 53% (*ii.*) TFA, DCM, rt, overnight, 85% (*iii.*) AcOH, MeOH, 45 °C, 8 h, 73% (*iv.*) TFA, DCM, rt, 2 h, 81% (*v.*) Cl^- ion exchange column.

2.2.2 Binding Studies

The results of binding studies between hosts **2.1**, **2.5**, and **2.6**, and the pertinent carboxylate guests are shown in Table 2.1. The ITC titrations were undertaken in HEPES-buffered (60 mM, pH 7.4) solution with the host molecule in the cell and the guest carboxylate as the titrant. When possible, affinity constants from ITC were confirmed using UV-Vis spectroscopy. For the UV-Vis titrations, the Cu^{II} absorbance shift as a function of guest added was plotted and fit to a 1:1 binding curve in order to obtain the association constant.[29]

Host	Guest	K_a (M^{-1}) UV-Vis	K_a (M^{-1}) ITC	ΔG (kcal/mol) UV-Vis	ΔG (kcal/mol) ITC	ΔH (kcal/mol)	TΔS (kcal/mol)
2.1	acetate	$5 \pm 1 \times 10^2$	Enthalpically neutral	-3.7 ± 0.2			
	succinate	$6 \pm 2 \times 10^3$	$2.6 \pm 0.4 \times 10^3$	-5.1 ± 0.2	-4.7 ± 0.1	-0.2 ± 0.1	4.5 ± 0.1
	glutarate		$1.4 \pm 0.2 \times 10^3$		-4.3 ± 0.1	0.7 ± 0.2	5.0 ± 0.2
	tricarballate		$2.3 \pm 0.3 \times 10^3$		-4.6 ± 0.1	-1.2 ± 0.3	3.4 ± 0.3
	tetracarboxylate		$1.9 \pm 0.3 \times 10^4$		-5.9 ± 0.1	-2.0 ± 0.6	3.9 ± 0.6
2.5	acetate	$3.5 \pm 0.3 \times 10^1$	$1.6 \pm 0.2 \times 10^1$	-2.1 ± 0.1	-1.6 ± 0.1	1.5 ± 0.2	3.1 ± 0.2
	succinate	$1.7 \pm 0.1 \times 10^2$	$1.2 \pm 0.2 \times 10^2$	-3.05 ± 0.04	-2.8 ± 0.1	1.0 ± 0.3	3.8 ± 0.3
	glutarate		$1.1 \pm 0.2 \times 10^2$		-2.8 ± 0.1	1.6 ± 0.5	4.4 ± 0.5
2.6	acetate		$1.3 \pm 0.2 \times 10^1$	-	-1.5 ± 0.1	0.3 ± 0.1	1.8 ± 0.1
	succinate		$4 \pm 1 \times 10^1$	-	-2.2 ± 0.2	-0.2 ± 0.1	1.9 ± 0.1
	glutarate		$5.3 \pm 0.7 \times 10^1$	-	-2.3 ± 0.1	0.3 ± 0.1	2.7 ± 0.1

Table 2.1 ***Host-Guest Binding Affinities and Thermodynamic Values.***

2.2.2.1 Isothermal Titration Calorimetry

ITC has allowed significant insight into the nature of molecular recognition events because of its unique capacity to deliver a full suite of binding data (K_a, ΔG, ΔH and TΔS) in a single titration. ITC's uniqueness derives from the direct observation of heat consumed or generated during an interaction. When a host is added in aliquots to a solution of guest, the exo- or endotherm generated per aliquot diminishes to a baseline as guest is consumed to form the host-guest complex. This saturation behavior generates a sigmoidal or hyperbolic curve whose equation may be solved to determine K_a and therefore ΔG of the interaction. Because the heat characteristics of the interaction

(enthalpy) were observed directly to generate the binding isotherm, the entropy may be determined with the Gibbs-Helmholtz equation.

In ITC, the unitless value *c* refers to the product of the association constant K_a (M^{-1}) and the concentration of the receptor (mol/L) in the sample cell. Wiseman *et al.* originally defined acceptable *c* values as falling between 1 and 1000 to insure a thermogram of sufficient curvature to be fit by the binding isotherm for the determination of K_a and ΔH.[30] Unfortunately, implicit in the study of noncovalent binding events in isolation is the observation of exceptionally low K_a values (10 – 100 M^{-1}), which would require unreasonable experimental concentrations to achieve $c \geq 1$. Some of the ITC data in this study were determined at *c* values as low as ~0.02; however, Turnbull and Daranas have argued that *c* values as low as 0.001 are acceptable provided that the titrations are taken well past the 2 equivalents of ligand used in Wiseman's example, and the thermogram is allowed to develop into a hyperbolic isotherm of sufficient curvature.[31] Indeed, their study supports "the validity of all values of K_a," while advocating "caution in the interpretation of $\Delta H°$." We therefore proceed confidently in our analysis of cooperativity, which is a Gibbs free energy phenomenon, while we cautiously offer thermodynamic explanations of our findings when dealing with the lowest affinity systems ($K_a < 100$).

2.2.2.2 Binding of Acetate and Polycarboxylates to hosts 2.1, 2.5, and 2.6

In the case of acetate (**2.11**) binding to host **2.1** only the UV-Vis data could be used to calculate the binding constant ($K_a = 5 \times 10^2$ M^{-1}, -3.7 kcal/mol) due to the thermoneutrality of the binding event, which makes it insensible to ITC. The ΔG's of **2.1** binding succinate (**2.10**) ($K_a = 2.6 \times 10^3$ M^{-1}, -4.7 kcal/mol), glutarate (**2.9**) ($K_a = 1.4 \times 10^3$ M^{-1}, -4.3 kcal/mol) and tricarballate (**2.8**) ($K_a = 2.3 \times 10^3$ M^{-1}, -4.6 kcal/mol) are all roughly the same, but the thermodynamic bases of these associations are distinct. The enthalpic contribution to **2.1** association with the dicarboxylates is quite small in the case of succinate (ΔH = -0.2 kcal/mol) and unfavorable in the case of glutarate (ΔH = 0.7 kcal/mol). In contrast, the association of tricarballate with host **1** is more exothermic (ΔH

= -1.2 kcal/mol), but the tighter binding results in an apparent entropic penalty as the TΔS term is less favorable by over 1 kcal/mol when the third carboxylate is present (tricarballate TΔS = 3.4 kcal/mol versus average TΔS = 4.8 kcal/mol for the dicarboxylates). This apparent trend of enthalpy/entropy compensation does not extend to 1,2,3,4-butanetetracarboxylate (**2.7**) binding to host **1**, as the enthalpy and entropy both become more favorable (ΔH° = -2.0 kcal/mol, TΔS° = 3.9 kcal/mol) upon addition of the fourth carboxylate.

The binding affinities of the model hosts **2.5** and **2.6** to the small carboxylates acetate, succinate, and glutarate, were also examined. **2.5** showed a small entropically driven affinity for acetate (K_a = 16 M^{-1}, -1.6 kcal/mol) and an affinity of an order of magnitude more for the dicarboxylates. The trend of **2.6** binding is the same as hosts **2.1** and **2.5** with ΔG° generally decreasing (more exergonic) as the number of guest carboxylates increases from one (acetate, K_a = 13 M^{-1}, -1.5 kcal/mol) to two (succinate, K_a = 40 M^{-1}, -2.2 kcal/mol; glutarate, K_a = 53 M^{-1}, -2.3 kcal/mol). The association of **2.6** with all three small carboxylate guests was slightly lower than that of **2.5**, as may be expected given the coordinative nature of the copper-carboxylate interaction of **2.5** in comparison to the pure ion-pairing nature of the guanidinium-carboxylate interaction present in host **2.6**.

2.2.3 Cooperativity Analysis

The binding of mono- and dicarboxylates to the model hosts **2.5** and **2.6** is considered representative of the strength of binding, ΔG°, for carboxylates interacting with the analogous portions of host **2.1**. Using Jencks' Eq. 1 in our analysis of cooperativity, we have assigned the strength of binding at the Cu^{II} center of **2.1** as ΔG_A°, and the strength of binding at the bisguanidinium portion of **2.1** as ΔG_B°. ΔG_A° and ΔG_B° are defined by the strength of binding of a particular guest subunit to **2.5** and **2.6** respectively. The thermodynamic components of connectivity, ΔH_S° and $T\Delta S_S^{\circ}$ (Eq. 2 and Eq. 3) were also calculated to reveal the influences that determine the sign of ΔG_S°. In all cases ΔG_S° is positive and enthalpic in origin (Table 2.2).

The positive ΔG_S° of binding succinate or glutarate to host **2.1** indicates that the binding interaction is more favorable than is predicted by the summation of the ΔG_A° of acetate coordinating to host **2.5** and the ΔG_B° of acetate binding to the diguanidinium moiety modeled on host **2.6**. The difference in binding between the "whole" and the "parts" depends upon whether the "whole" in question is succinate or glutarate.

A-B	A + B	ΔG_{AB}° (kcal/mol)	$\Delta G_A^\circ + \Delta G_B^\circ$ (kcal/mol)	ΔG_S° (kcal/mol)
succinate	$acetate^A + acetate^B$	-4.7 ± 0.1	-3.1 ± 0.1	+1.6 ± 0.1
glutarate	$acetate^A + acetate^B$	-4.3 ± 0.1	-3.1 ± 0.1	+1.2 ± 0.1
tricarballate	$succinate^A + acetate^B$	-4.6 ± 0.1	-4.3 ± 0.1	+0.3 ± 0.1
tricarballate	$glutarate^A + acetate^B$	-4.6 ± 0.1	-4.3 ± 0.1	+0.3 ± 0.1
butanetetracarboxylate	$succinate^A + succinate^B$	-5.9 ± 0.1	-5.0 ± 0.2	+0.9 ± 0.2
butanetetracarboxylate	$glutarate^A + glutarate^B$	-5.9 ± 0.1	-5.1 ± 0.1	+0.8 ± 0.1
A-B	A + B	ΔH_{AB}° (kcal/mol)	$\Delta H_A^\circ + \Delta H_B^\circ$ (kcal/mol)	ΔH_S° (kcal/mol)
succinate	$acetate^A + acetate^B$	-0.2 ± 0.1	+1.8 ± 0.2	+2.0 ± 0.2
glutarate	$acetate^A + acetate^B$	+0.7 ± 0.2	+1.8 ± 0.2	+1.1 ± 0.3
tricarballate	$succinate^A + acetate^B$	-1.2 ± 0.3	+1.3 ± 0.3	+2.5 ± 0.4
tricarballate	$glutarate^A + acetate^B$	-1.2 ± 0.3	+1.9 ± 0.5	+3.1 ± 0.6
butanetetracarboxylate	$succinate^A + succinate^B$	-2.0 ± 0.6	+0.8 ± 0.3	+2.8 ± 0.7
butanetetracarboxylate	$glutarate^A + glutarate^B$	-2.0 ± 0.6	+1.9 ± 0.5	+3.9 ± 0.8
A-B	A + B	$T\Delta S_{AB}^\circ$ (kcal/mol)	$T\Delta S_A^\circ + T\Delta S_B^\circ$ (kcal/mol)	$-T\Delta S_S^\circ$ (kcal/mol)
succinate	$acetate^A + acetate^B$	+4.5 ± 0.1	+4.9 ± 0.2	-0.4 ± 0.2
glutarate	$acetate^A + acetate^B$	+5.0 ± 0.2	+4.9 ± 0.2	+0.1 ± 0.3
tricarballate	$succinate^A + acetate^B$	+3.4 ± 0.3	+5.6 ± 0.3	-2.2 ± 0.4
tricarballate	$glutarate^A + acetate^B$	+3.4 ± 0.3	+6.2 ± 0.5	-2.8 ± 0.6
butanetetracarboxylate	$succinate^A + succinate^B$	+3.9 ± 0.6	+5.7 ± 0.3	-1.8 ± 0.7
butanetetracarboxylate	$glutarate^A + glutarate^B$	+3.9 ± 0.6	+7.1 ± 0.5	-3.2 ± 0.8

Table 2.2 ***Cooperativity Values***

Succinate displays greater positive cooperativity than glutarate, and all of succinate's positive cooperativity stems from its positive ΔH_s° (+1.8 kcal/mol), which is able to compensate for the negative cooperativity of its $-T\Delta S_S^\circ$ (-0.4 kcal/mol). Glutarate on the other hand is the only "whole" guest whose positive ΔG_s° is derived in part from a positive $-T\Delta S_S^\circ$. The positive entropy of connection is likely the result of the desolvation of the C3 methylene of glutarate upon binding host **2.1**, an entropically favorable event that is not accounted for in the two acetate interactions that were used to determine the strength of glutarate's constituent binding events. This analysis is further supported by the less positive ΔH_S° of the glutarate interaction. The same desolvation process that

leads to a positive $-T\Delta S_S°$ could be enthalpically costly in accordance with the current theory of the endothermic nature of some forms of hydrophobic binding.[32]

While the dicarboxylates were considered "whole" with respect to acetate "parts," they served as "parts" in the study of larger "whole" guest molecules tricarballate and 1,2,3,4-tetracarboxylate. Succinate and glutarate have been examined to allow for the different possible binding conformations of tricarballate and the tetracarboxylate to host **2.1**. 1,2,3,4-Butanetetracarboxylic acid, for example, may chelate Cu^{II} in a manner resembling succinate or glutarate (Figure 2.23). While the succinate type 7-member ring formed with Cu^{II} is known to be more stable,[33] the glutarate type 8-member ring may be induced depending upon the preferred geometry of interaction at the bisguanidinium portion of **2.1**. A succinate type chelation mode by 1,2,3,4-butanetetracarboxylate would present two β-carboxylates toward the bisguanidiniums while a glutarate type chelation mode would present two γ-carboxylates.

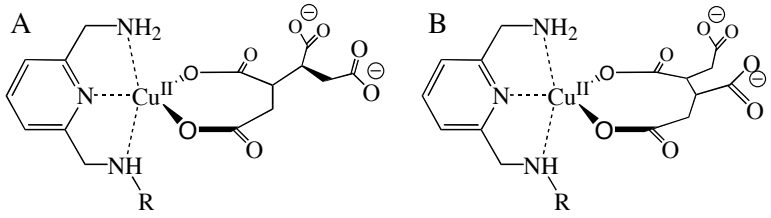

Figure 2.23 ***Chelation Modes of 1,2,3,4-Butanetetracarboxylate.*** Succinate-like (A) and glutarate-like (B) chelation around the Cu^{II} center of **2.1**.

The latter mode of bisguanidinium binding is best represented by glutarate while the former is best represented by succinate, thus necessitating the use of both dicarboxylates as model guests for interaction with model hosts **2.5** and **2.6**. Considering 1,2,3,4-butanetetracarboxylate as a "whole" guest made of glutarate-like "parts" is somewhat unfair due to the presence of the glutarate methylene group at carbon 3 that is not represented in the tetracarboxylate. In this way, succinate, which does not have the extra methylene is an inherently better approximation of one half of 1,2,3,4-butanetetracarboxylate, and indeed we observed some important differences between the

two dicarboxylates when used as parts in both the tricarballate and 1,2,3,4-tetrabutanecarboxylate cooperativity analysis (see below).

The least positive cooperativity in Table 2.2 is seen in the binding of tricarballate to host **2.1**. Tricarballate can be dissected as either a succinate and an acetate, or as a glutarate and an acetate. Also, the tricarballate could bind host **2.1** in two ways: (1) with succinate or glutarate type chelation (like that shown for 1,2,3,4-butanetetracarboxylate in Figure 2.23) of the copper which allows the remaining carboxylate to engage the diguanidinium portion of **2.1,** or (2), with a single carboxylate coordination of the Cu^{II} while the guanidinium groups are associating with the dicarboxylate. Whether the dicarboxylate in question is succinate or glutarate, the highest absolute sum of $\Delta G_A°$ plus $\Delta G_B°$ results when $\Delta G_A°$ is either dicarboxylate chelating copper and $\Delta G_B°$ is the interaction between acetate with host **2.6**. Therefore, as a means of underestimating any positive cooperativity this mode of segregation is used in Table 2.2.

The low $\Delta G_S°$ of binding tricarballate appears to be rooted in the relatively small $T\Delta S_{AB}°$ term of tricarballate binding to host **2.1**. When moving from either dicarboxylate to tricarballate binding to **2.1** the entropic term is decreased by over 1 kcal/mol. The concomitant improvement in $\Delta H_{AB}°$ indicates that tighter binding could be reducing residual motion in the binding pocket. Also, any chelation present in tricarballate binding that was not present in the dicarboxylate binding will further freeze out rotational motion.

1,2,3,4-Butanetetracarboxylate may be considered as a "whole" constructed of two succinate "parts" ($succinate^A$ + $succinate^B$) or two glutarate "parts" ($glutarate^A$ + $glutarate^B$) as shown in Figure 2.23. Both modes of dissection yield positive cooperativity, however the positive cooperativity is less when glutarates are the "parts" in question (+0.8 kcal/mol versus +0.9 kcal/mol for succinate "parts"). The dependence of $\Delta G_S°$ upon the dicarboxylate used in the cooperativity analysis can be attributed to the extra methylene on glutarate. Glutarate binding to host **2.5** ($\Delta G_A°$) and to host **2.6** ($\Delta G_B°$) is strongly entropically favorable. As such, the entropy of connection ($-T\Delta S_S°$) is strongly negative (-3.2 kcal/mol) because 1,2,3,4-butanetetracarboxylate binding to host **2.1** does not involve the desolvation of two methylene carbons present in the two model binding events (one for glutarate in each event). Similarly the $\Delta H_S°$ is more positive in

the case of glutarate^{A} + glutarate^{B} due to the more endothermic binding of glutarate to the model hosts. The enthalpic cost of glutarate desolvation makes it an imperfect model guest, therefore the $\Delta G_S°$ of 1,2,3,4-butanetetracarboxylate when succinate^{A} + succinate^{B} are the component binding events is probably a more accurate quantification of the system's positive cooperativity.

2.2.3.1 The Basis of Positive Cooperativity in Water Using Ion-Pairing

The importance of observing the constituent binding functionalities of host **2.1** in isolation is apparent upon comparison of the binding strength of the acetate-**2.1** complex (UV/Vis data; K_a = 5 x 10^2 M^{-1}, -3.7 kcal/mol) with that of the acetate-**2.5** complex (UV/Vis data; K_a = 35 M^{-1}, -2.1 kcal/mol). The mode of binding in both of these systems is similar: a coordinative interaction between the Cu^{II} center and the acetate, yet acetate affinity to **2.1** is much higher. This binding model is supported in that both affinity constants were determined by observing the change in absorbance of the Cu^{II} *d-d* transition, a spectral shift associated with interaction at the Cu^{II} center.[34] A second point of interest is that acetate binding to **2.5** was shown to be endothermic (+1.5 kcal/mol) while acetate binding to the full host **2.1** was found to be enthalpically neutral. As a result, the binding can be monitored by UV/Vis spectroscopy but not by ITC. The stronger binding of acetate to **2.1** appears to be driven by some exothermic event that counterbalances the endothermicity of the carboxylate-Cu^{II} coordination event as seen in **2.5**. This exothermic event seems to be fundamental to **2.1** since it emerges in the binding of a single anion, acetate, outside of a cooperativity analysis. Such an intrinsic property also seems manifest when plotting $T\Delta S_S$ against ΔH_S.

The slope of the trendline in Figure 2.24 is greater than 1, indicating that $T\Delta S_S$, which is positive in instances of negative cooperativity, is increasing faster than the enthalpy of connection, ΔH_S. That an unfavorable $T\Delta S_S$ would undermine the favorable contributions of ΔH_S is in line with Williams' theory of cooperativity.[9] In this case some "X-factor" has imbued host **2.1** with an inherent exothermicity when binding anions, and this exothermicity appears to be providing a region of positive cooperativity before the favorable ΔH_S is overtaken by the unfavorable $T\Delta S_S$. We believe this to be the first time

that the enthalpy and entropy of connectivity have been plotted against each other. The result is strong graphical support for a general entropic basis of negative cooperativity in water and an enthalpic basis for positive cooperativity that is evident in **2.1**, and is perhaps a general feature of multiply charged, sterically rigidified binding cavities.

When considering the differences between host **2.1** and the model hosts **2.5** and **2.6** with which the strengths in isolation of the various binding events have been determined, the most outstanding feature of **2.1** is the close proximity of the positive charges. The destabilizing effect of multiple like charges has been implicated in the strongly exothermic binding prowess of EDTA with various metal ions.[1] The electrostatic strain when the cationic binding moieties are forced into close proximity in the synthesis of **2.1** is relieved in some part by the binding event with anionic carboxylates.

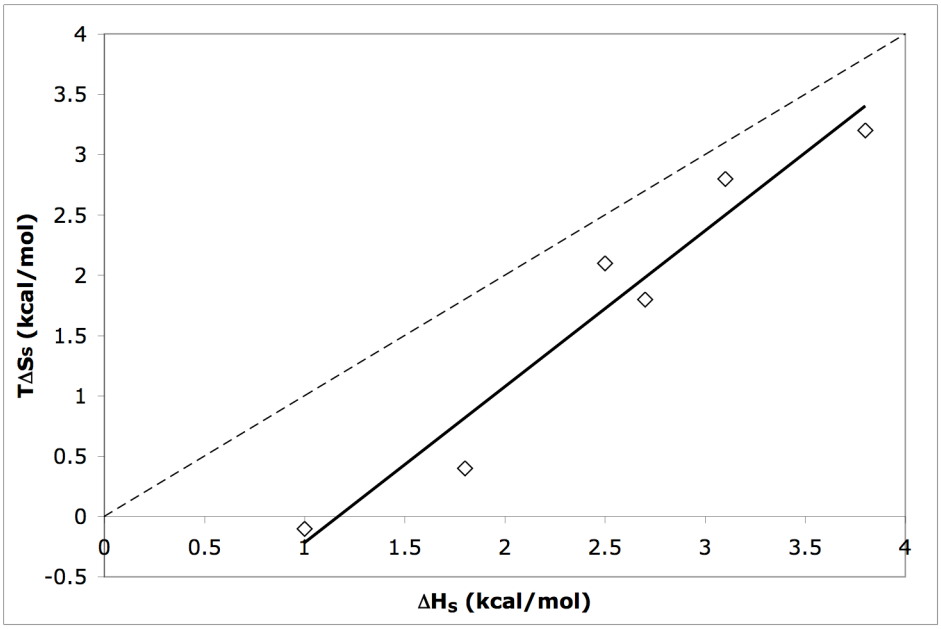

Figure 2.24 ***The Entropy of Connectivity Versus the Enthalpy of Connectivity.*** The diamonds are the cooperativity analyses from Table 2.2 with a trendline in solid black. The dotted line represents the balance of ΔH_S and $T\Delta S_S$, below which positive cooperativity results from enthalpic effects and above which negative cooperativity results from entropic effects. Note that $T\Delta S_S$ is used here without a negative sign.

If the destabilization of the unbound host is the sole source of the positive cooperativity, then the strength of this effect must be at least +1.6 kcal/mol. This estimation is based upon the assumption that the system would display negative cooperativity in the absence of the electrostatic repulsions that destabilize the unbound host because negative cooperativity has been the conclusion in nearly all of the previous cooperativity studies in water.[3, 6, 22] The contribution of charge clustering in host **2.1** to positive cooperativity must be in all cases slightly negated by the forces of negative cooperativity, such as improper binding functional group alignment and reduced solvent displacement upon tethering. Therefore the system displaying maximal positive cooperativity (succinate binding **2.1**; +1.6 kcal/mol) probably represents a fair estimate of the binding enhancement borne from destabilizing the unbound structure of **2.1**.

2.2.3.2 Anion Selectivity

Prior to the addition of one of the carboxylate guests to host **2.1**, the host solution is not devoid of anions. While probably not proximal to the cationic host in solution, a counter ion exists for each of the charges on **2.1**. Why then is chloride not able to relieve the electrostatic destabilization of **2.1**? The answer must be that chloride is indeed providing some anionic relief to **2.1** in line with its own binding affinity to Cu^{II} and guanidinium type cations. The stronger binding carboxylate anion is able to associate more strongly with the cationic moieties and in turn provide greater relief of electrostatic repulsion. An interesting future study would be to attempt to distinguish between an anion's specific affinity for a positively charged binding moiety and its shape specific ability to inhabit a binding cleft and stabilize the host as a whole against electrostatic repulsive destabilization.

2.3 Conclusion

This cooperativity analysis of host **2.1** represents an example of positive cooperativity in water where all binding moieties of the host and guest are covalently attached as described by Jencks. The source of positive cooperativity was shown to be

enthalpic in this case. Although the precise source of this enthalpic positive cooperativity is unclear, we believe it is rooted in the destabilizing effect of the electrostatic repulsion in the unbound form of **2.1**. The proximity of the chelated Cu^{II} ion to the two guanidinium functional groups represents the most fundamental difference between **2.1** and hosts **2.5** and **2.6** whose carboxylate affinities were employed as the strength of the binding functional groups of **2.1**.

The observation of positive cooperativity also implies that the carboxylate guests must be able to access the cationic binding sites of host **2.1** at or near the ideal distance and orientation involved in the binding of representative fragment carboxylates (acetate, succinate and glutarate) with hosts **2.5** and **2.6**. Any disruption of the individual binding events when employed in tandem contributes to negative cooperativity.[9]

In the system discussed herein we have shown negative cooperativity to be the providence of the entropy of connection ($-T\Delta S_S°$), which was negative in almost all cases. The unfavorable entropy of connection likely results from diminished solvent accessible surface area on larger guest molecules and the reduced residual rotational and vibrational motion in the binding pocket as the host-guest association becomes tighter. While enthalpic gains were generally countered by a diminishing $-T\Delta S_S°$, a fundamental enthalpic favorability associated with tethering the binding events of host **2.1** resulted in a positive $\Delta G_S°$, which we have estimated to be at least 1.6 kcal/mol for this system. **2.1** employs its metal-coordination and ion-pairing binding sites in such a way that the net $\Delta G_S°$ is more favorable than would be predicted by the summation of the strength in isolation of each binding event ($\Delta G_A° + \Delta G_B°$), resulting in a final analysis of positive cooperativity for all of the guest A-B systems analyzed in this paper. We suspect that many other systems might show a similar effect when submitted to a full thermodynamic analysis.

2.4 Experimental Details for Chapter 2

2.4.1 General

Reactions were run under an atmosphere of argon unless otherwise indicated. The chemicals were obtained from Acros Organics, Aldrich, Fisher, and Mallinckrodt and used without further purification unless otherwise noted. Methylene chloride and triethylamine were distilled over calcium hydride. Water used during the analysis of the hosts and guests or in the preparation of the hosts and guests for analysis was distilled, deionized and filtered. All products were dried for at least 6 hours prior to spectral analysis. A Varian Gemini 400 MHz NMR was used to obtain ^{1}H and ^{13}C spectra. The chemical shifts were referenced relative to TMS, used as an internal standard. A MicroMass AutoSpec-Ultima spectrometer was used to obtain high-resolution mass spectra. The UV-visible absorption measurements were recorded on a Beckman DU640 spectrometer. ITC thermograms were recorded using an isothermal titration calorimeter from Microcal, Inc., MA.

2.4.2 UV-Visible Titrations

A typical UV/Vis titration proceeded as follows, although concentrations were altered as necessary. A cuvette with HEPES buffered water (60 mM, pH 7.4) served as the blank. A second cuvette was filled with 1 mL of a solution of the Cu^{II} containing host (0.8 mM) in buffered water (HEPES, 60 mM, pH 7.4) and the spectrum of this solution was recorded. A second solution identical to the first except for the presence of guest (20.27 mM) was added in aliquots to the cuvette and the spectrum recorded between aliquots. The wavelength of maximum difference between the original solution of host and the final addition of guest was determined and the absorbance at this wavelength was plotted against guest concentration. Binding constants were calculated by iterative curve fitting in ORIGIN using a 1:1 binding algorithm.[29] Errors reported are those returned by Origin after curve fitting.

2.4.3 ITC experiments

ORIGIN 5.0 software (Microcal, Inc.) was used to calculate the equilibrium constant and to determine the standard molar enthalpy. The weakness of the observed binding events required that the binding ratio be fixed at 1:1 prior to curve fitting of the thermogram.[17, 31] A typical ITC experiment is as follows, although concentrations were altered as necessary, usually to generate a sufficiently prominent heat effect from the reaction. A buffered solution of water (HEPES, 60mM, pH 7.4) was loaded in the reference cell in all cases. A solution of the host (2 mM) in buffer solution (HEPES, 60mM, pH 7.4) was loaded into the titration cell. The syringe was loaded with around 250 μL of guest (43.5 mM) also in HEPES buffer (60 mM, pH 7.4). The syringe was positioned in the calorimeter and the following parameters set: Injection size: 10 μL, temperature: 26 ºC, injection interval: 300 s, cell feedback: 15 μcal. Some titrations experienced aggregation during the early injections. These data were removed and the curve fit to the remaining points as described in reference [35].

The ΔH's have been corrected to account for the heat of ionization of the HEPES buffer (ΔH_{ion} = 3.92 kcal/mol) according to Eq. 5.[1, 36] The protonation state of the carboxylate guests was calculated from published pK_a values, and it was assumed that the host-guest interaction would promote the full ionization of the guest molecule.[37] The fraction of the guest still protonated at pH 7.4 was therefore used as an estimate for N. The portion of the ΔGº not attributable to the exothermicity of the binding event was then added to the TΔS portion using Eq. 6. Because the binding of tricarballate and 1,2,3,4-butanetetracarboxylic acid to host **2.1** were most affected by this correction, it served chiefly to prevent the overestimation of the enthalpic contributor to positive cooperativity. Conversion of averaged raw data from Table 2.6 is shown in Table 2.3.

$$\Delta H_b = \Delta H_{obs} - N\Delta H_{ion} \quad (5)$$

$$T\Delta S_b = T\Delta S_{obs} - N\Delta H_{ion} \quad (6)$$

Guest	Host	ΔH_{obs} kcal/mol	$T\Delta S_{obs}$ kcal/mol	N	ΔH_{ion}*N kcal/mol	ΔH_{adj} kcal/mol	$T\Delta S_{adj}$ kcal/mol
succinate	1	-0.21±0.04	4.45±0.09	0.017	-0.07	-0.14±0.04	4.52±0.09
succinate	2	0.94±0.35	3.76±0.36	0.017	-0.07	1.08±0.35	3.83±0.36
succinate	3	-0.23±0.05	1.93±0.21	0.017	-0.07	-0.16±0.05	2.00±0.21
glutarate	1	0.55±0.12	4.83±0.15	0.046	-0.18	0.73±0.12	5.01±0.15
glutarate	2	1.43±0.30	4.21±0.31	0.046	-0.18	1.61±0.30	4.39±0.31
glutarate	3	0.13±0.03	2.47±0.09	0.046	-0.18	0.31±0.03	2.65±0.09
tricarballate	1	-1.43±0.30	3.17±0.31	0.087	-0.34	-1.09±0.30	3.51±0.31
tetracarboxylate	1	-3.48±0.73	2.38±0.74	0.027 + 0.365	-1.54	-1.94±0.73	3.92±0.74

Table 2.3 ***Heat of ionization adjustments.***

2.4.3.1 ITC Error Analysis

The raw ITC data for all runs is shown in Table 2.4. The number of repeat titrations is less than ideal. It is recommended that future studies employ three repeats of each titration for a more rigorous error analysis.

Host	Guest	[H] mM	[G] mM	K_a M^{-1}	ΔG kcal/mol	ΔH kcal/mol	$T\Delta S$ kcal/mol
2.1	succinate	0.45	8.77	2571	-4.66	-0.210	4.455
	glutarate	1.45	32.66	1361	-4.28	0.551	4.838
	tricarballate	1.26	20.17	2342	-4.60	-1.504	3.107
	tricarballate	0.45	10.85	2342	-4.60	-1.350	3.259
	tetracarboxylate	0.45	8.95	19430	-5.86	-3.484	2.347
2.5	acetate	2.00	192.50	16	-1.64	1.448	3.098
	succinate	2.00	41.74	115	-2.82	0.942	3.758
	glutarate	2.00	43.54	108	-2.78	1.428	4.207
2.6	acetate	4.07	162.12	13	-1.52	0.312	1.075
	succinate	4.07	83.48	34	-2.09	-0.225	1.869
	succinate	4.68	85.76	42	-2.22	-0.173	2.050
	glutarate	4.07	87.08	53	-2.36	0.126	2.484
	glutarate	4.07	87.08	54	-2.37	0.138	2.503
	glutarate	4.07	82.36	48	-2.30	0.125	2.427

Table 2.4 ***Raw data from all ITC titrations.***

Errors were calculated as the average of two standard deviations for all titrations for which independently repeated data was available (Table 2.5; K_a = 14%; ΔH = 21%). The only exception was the error of succinate binding to host **2.6** (K_a = 30%; ΔH = 37%), which was larger than the average error and was therefore applied as such. This averaging method was used because in all cases it returned greater error than did Origin upon curve fitting. Standard deviation was calculated using Eq. 7.[38]

$$\sigma = \sqrt{\frac{\sum_{i=1}^{N}(x_i - \bar{x})^2}{N-1}} \tag{7}$$

The host-guest data after averaging of repeats and application of percent error, but before adjustment for heat of ionization of buffer are shown in Table 2.6. The ΔG error was calculated as the difference in ΔG based the given value of K_a and the value of ΔG based upon the lower limit of the K_a. For example, the K_a value for succinate binding to host **2.1** is shown as 2571±306 M^{-1}. The ΔG is therefore -4.66 kcal/mol with a lower limit of -4.58 kcal/mol based upon a K_a of 2265 M^{-1} (2571 - 306). The difference between the primary ΔG value and the possible ΔG within error is 0.08 kcal/mol. The logarithmic nature of K_a means that the lower limit is "more different" than the upper limit in terms of free energy and therefore the lower limit was chosen.

Host	Guest	K_a M^{-1}	K_a avg	σ	((2 x σ)/avg) %	ΔH kcal/mol	ΔH avg	σ	(2 x σ) %
2.1	tricarballate	2342				-1.504			
2.1	tricarballate	2342				-1.350			
			2342	0	0		-1.43	0.07	15
2.6	succinate	34				-0.225			
2.6	succinate	42				-0.173			
			38	5.7	30		-0.20	0.03	37
2.6	glutarate	53				0.126			
2.6	glutarate	54				0.138			
2.6	glutarate	48				0.125			
			52	3.2	12		0.13	0.01	11
avg. ((2 x σ)/avg.) % error					14				21

Table 2.5 ***Error calculation.***

Host	Guest	K_a M^{-1}	ΔG kcal/mol	ΔH kcal/mol	TΔS kcal/mol
2.1	succinate	2571±360	-4.66±0.08	-0.21±0.04	4.45±0.09
	glutarate	1361±191	-4.28±0.09	0.55±0.12	4.83±0.15
	tricarballate	2342±328	-4.60±0.09	-1.43±0.30	3.17±0.31
	tetracarboxylate	19430±2720	-5.86±0.09	-3.48±0.73	2.38±0.74
2.5	acetate	16±2	-1.64±0.07	1.45±0.30	3.09±0.31
	succinate	115±16	-2.82±0.09	0.94±0.35	3.76±0.36
	glutarate	108±15	-2.78±0.09	1.43±0.30	4.21±0.31
2.6	acetate	13±2	-1.5±0.1	0.31±0.07	1.83±0.12
	succinate	38±11	-2.16±0.2	-0.23±0.05	1.93±0.21
	glutarate	52±7	-2.34±0.08	0.13±0.03	2.47±0.09

Table 2.6 ***Raw or averaged data with error applied.***

The TΔS was determined from the ΔG and ΔH values, and its error was determined using standard error propagation protocol like that shown in Eq. 8. The error of the ΔG and ΔH values was squared, added and then the square root of the resultant value was taken to yield z, the error of TΔS. The errors of the cooperativity values in Table 2.2 were similarly determined.

$$z = \sqrt{x^2 + y^2} \tag{8}$$

2.4.3.2 Ionic Strength

When the work described in Chapter 2 was carried out it was assumed that the maintenance of a consistent and relatively high concentration of buffer (60 mM HEPES) would be sufficient to control the ionic strength over the course of each titration and to standardize the ionic strength for the comparison of different host-guest systems. HEPES, however, exists primarily as a zwitter ion at pH 7.4 (FIG), and a recent study using capillary electrophoresis has shown that zwitter ions do not contribute to the ionic strength of the solution.[39] The ionic strength attributable to the HEPES buffer is therefore only due to the deprotonated species which is at a concentration of 25 mM. This results in an ionic strength of 0.025 M.

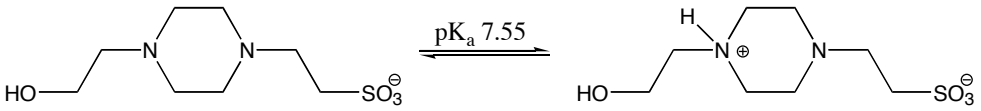

25 mM 35 mM

Scheme 2.16 ***60 mM HEPES at pH 7.4.*** Zwitterions do not contribute to the ionic strength of a solution, therefore only the anionic form of HEPES (left) is setting the ionic strength of the solution.

Because the buffer did not control ionic strength to the extent that was originally envisioned, the ionic strength of each titration with respect to the constituent host and guest is reported in Table 2.7. In most cases the ionic strength started at around 0.01 M,

but in the case of the smaller hosts **2.5** and **2.6** the large amount of guest that was added resulted in a final ionic strength that was greater than the baseline ionic strength due to the buffer anion. Evidence that ionic strength is potentially of minimal importance at these concentrations is seen in the repeat titration of tricarballate into host **2.1**, in which the initial ionic strengths was 0.0045 M and 0.0126 M in separate trials (Table 2.7) yielded identical K_a values (Table 2.4). Still, it is recommended that all future studies employ a fixed concentration of NaCl to maintain ionic strength. Ionic strength (I) was calculated using Eq. 9, where z is the charge of a particular ion and [x] is its concentration.

$$I = \frac{1}{2}\sum_i z_i^2[x_i] \tag{9}$$

Host	Guest	[H] mM	initial ionic strength M	$[G]_{syringe}$ mM	eqs. Guest added	$[G]_{cell}$ mM	ionic strength from incoming guest M	final ionic strength M
2.1	succinate	0.45	0.0045	8.77	4	1.80	0.005	0.010
	glutarate	1.45	0.0145	32.66	4	5.80	0.017	0.032
	tricarballate	1.26	0.0126	20.17	2.5	3.15	0.019	0.032
	tricarballate	0.45	0.0045	10.85	3.5	1.58	0.010	0.014
	tetracarboxylate	0.45	0.0045	8.95	2.5	1.13	0.011	0.016
2.5	acetate	2.00	0.0060	192.50	22	44.00	0.044	0.050
	succinate	2.00	0.0060	41.74	4.5	9.00	0.027	0.033
	glutarate	2.00	0.0060	43.54	5.0	10.00	0.030	0.036
2.6	acetate	4.07	0.0122	162.12	9.0	36.60	0.037	0.049
	succinate	4.07	0.0122	83.48	4.5	18.32	0.055	0.067
	succinate	4.68	0.0140	85.76	4.5	21.06	0.063	0.077
	glutarate	4.07	0.0122	87.08	5.0	20.35	0.061	0.073
	glutarate	4.07	0.0122	87.08	5.0	20.35	0.061	0.073
	glutarate	4.07	0.0122	82.36	4.5	18.32	0.055	0.067

Table 2.7 ***Ionic strength at the beginning and end of each ITC.*** These values do not include the base ionic strength of 0.025 M provided by the buffer. $[G]_{cell}$ is the final concentration of guest added at the saturation or end point of the titration.

2.4.4 Synthesis

Toluene-4-sulfonic acid 6-hydroxymethyl-pyridin-2-ylmethyl ester (2.13) and 2,6-[Bis(toluene-4-sulfonic acid methyl ester)]pyridine (2.21) : 2,6-pyridinedimethanol (**2.12**) (11.029 g, 79.3 mmol) dissolved in CH_2Cl_2 (1 L) was stirred at -25 ºC for 15

minutes. Ag_2O (27.55 g, 118.9 mmol), KI (2.6328 g, 15.86 mmol) and *p*-toluenesulfonyl chloride (16.631 g, 87.23 mmol) were added and the reaction was allowed to warm to room temperature. After 3 hours the reaction mixture was filtered through a silica plug to remove silver salts and products were eluted through with ethyl acetate (100 mL). The solution was concentrated in vacuo to a reddish-white solid. The crude mixture was purified by silica gel column chromatography (solvent ramping from CH_2Cl_2 to ethyl acetate) to yield the desired monotosyl product in 63% yield (13.7 g, 46.7 mmol) as a bright red oil that becomes a solid after a few days under high vacuum. ^{1}H NMR ($CDCl_3$): 7.23 (m, 2H), 7.69 (t, 1H), 7.34 (m, 2H), 7.31 (d, 1H), 7.19 (d, 1H), 5.13 (s, 2H), 4.69 (s, 2H), 2.45 (s, 3H). ^{13}C NMR ($CDCl_3$): 159.0, 152.6, 145.2, 137.7, 132.8, 129.9, 128.1, 120.6, 120.1, 71.5, 63.8, 21.7. HRMS (CI+) C_{14} H_{16} N O_4 S *m/z*: 294.0806; calcd: 294.0800. Also recovered was the ditosyl product in 17% yield (6.1315 g, 13.7 mmol) as a greenish white solid. ^{1}H NMR ($CDCl_3$): 7.80 (d of t, 4H), 7.69 (t, 1H), 7.33 (d, 6H), 5.05 (s, 4H), 2.44 (s, 6H). ^{13}C NMR ($CDCl_3$): 153.5, 145.2, 137.9, 132.7, 129.9, 128.1, 121.4, 71.3, 21.7. HRMS (CI+) C_{21} H_{22} N O_6 S_2 *m/z*: 448.0891; calcd 448.0889.

(6-Aminomethyl-pyridin-2-yl)-methanol (2.15): 2.13 (1.57 g, 5.34 mmol) in DMF (10 mL) was added dropwise to a solution of potassium phthalimide (1.01 g, 5.45 mmol) in DMF (35 mL). The reaction was stirred for 5 hours at 40 ºC then cooled to room temperature. Water (50 mL) was added and the solution extracted with DCM (3 x 40 mL). The organic layer was dried over sodium sulfate and concentrated *in vacuo* and the solid residue was washed with light petroleum ether then dried again under vacuum to hard off-white solid, **2.14** (1.49 g, 5.55 mmol). Unpurified **2.14** was stirred in absolute ethanol (75 mL), 98% hydrazine (0.25 mL, 7.96 mmol) was added and the suspension stirred 4 hours at reflux. After cooling, suspension filtered and concentrated *in vacuo* to fluffy brown solid. Crude solid dissolved in 0.1 N HCl (30 mL) and washed with $CHCl_3$ (30 mL). The aqueous layer was neutralized with $NaHCO_3$ and continuously extracted for 36 hours with $CHCl_3$. The organic layer was dried over sodium sulfate and concentrated *in vacuo* to yield the product as colorless oil. X-ray quality crystals emerged from oil after 2 weeks slow evaporation. 76% yield. ^{1}H NMR ($CDCl_3$): 7.60 (t,

1H), 7.21 (d, 1H), 7.10 (d, 1H), 4.68 (s, 2H), 3.89 (s, 2H), 3.19 (b, 3H). ^{13}C NMR ($CDCl_3$): 163.4, 163.2, 140.4, 122.7, 121.8, 67.5, 50.3. HRMS (CI+) C_7 H_{11} N_2 O *m/z*: 139.0873; calcd: 139.0871.

(6-Hydroxymethyl-pyridin-2-ylmethyl)-carbamic acid *tert*-butyl ester (2.16): 2.15 (0.584 g, 4.22 mmol) and triethylamine (1.2 mL, 8.61 mmol) were dissolved in $CHCl_3$ (10mL). Di-*tert*-butyl carbonate (1.84 g, 8.44 mmol) in $CHCl_3$ (2 mL) was added dropwise and the reaction stirred 2 hours at room temperature. The solution was concentrated *in vacuo* and the solid residue dissolved in ethyl acetate (50 mL). The organic layer was washed with water (3 x 10 mL), dried over sodium sulfate and concentrated *in vacuo*. Product purified on silica gel chromatography (solvent ramping from DCM to 9:1 DCM:MeOH) to yield white solid (0.730 g, 3.06 mmol). 73% yield. ^1H NMR ($CDCl_3$): 7.67 (t, 1H), 7.21 (d, 1H), 7.18 (d, 1H), 5.70 (b, 1H), 4.75 (s, 2H), 4.43 (d, 2H), 1.48 (s, 9H). ^{13}C NMR ($CDCl_3$): 158.6, 156.8, 156.0, 137.4, 120.2, 119.0, 79.7, 64.0, 45.7, 28.4. HRMS (CI+) C_{12} H_{19} N_2 O_3 *m/z*: 239.1398; calcd: 239.1396.

(6-Formyl-pyridin-2-ylmethyl)-carbamic acid *tert*-butyl ester (2.17): 2.16 (0.812 g, 3.4 mmol) was dissolved in DCM (10 mL). (1,1,1-triacetoxy)-1,1-dihydro-1,2-benziodox-ol-3(1H)-one (1.58 g, 3.73 mmol) was added and the reaction stirred at room temperature for 0.5 hours. The suspension was diluted with ether (20 mL) then treated with 1 M NaOH (40 mL) and stirred to dissolve. The organic layer was washed with water (20 mL) and brine (20 mL) then dried over sodium sulfate and concentrated *in vacuo* to light beige solid (0.679g, 2.88 mmol). 85% yield. ^1H NMR ($CDCl_3$): 10.06 (s, 1H), 7.86 (m, 2H), 7.52 (m, 1H), 5.56 (b, 1H), 4.54 (d, 2H), 1.48 (s, 9H). ^{13}C NMR ($CDCl_3$): 193.3, 158.6, 156.0, 152.2, 137.7, 125.9, 120.3, 79.9, 28.4, 27.8. HRMS (CI+) C_{12} H_{17} N_2 O_3 *m/z*: 237.1238; calcd: 237.1239.

1-[N-6-[(1,1-dimethylethoxy)carbonyl]aminomethyl-pyridin-2-ylmethyl]-aminomethyl-3,5-[4,5-dihydro-N-(1,1-dimethylethoxy)carbonyl-imidazol-2-yl]aminomethyl-2,4,6-triethylbenzene (2.19): 2.17 (0.288 g, 0.490 mmol) and **2.18** (0.110 g, 0.466 mmol) were dissolved in toluene. Reaction was stirred at 50 ºC for 0.5

hours. Water was removed by azeotrope as a portion of toluene (*ca.* 5 mL) was removed under reduced pressure. The reaction was stirred at 50 ºC for another 0.5 hours and the azeotrope procedure was repeated. The reaction was stirred at 50 ºC for another 0.5 hours, and the solution was concentrated *in vacuo* to 2-3 mL. The oily concentrate dissolved in methanol (3 mL) and $NaBH_4$ was added to the solution, and the reaction stirred at room temperature for 4.5 hours. Water (0.5 mL) and K_2CO_3 (2 g) were added to quench the excess borohydride and neutralize the mixture. The slurry stirred for 10 minutes and was evaporated to dryness *in vacuo*. The residue was stirred with DCM (25 mL), and the precipitate filtered. The filtrate was concentrated *in vacuo*. Product purified on silica gel chromatography (solvent ramping from DCM to DCM:MeOH:ammonia saturated MeOH 10:1:1) to yield a sticky yellow solid (0.301 g, 0.373 mmol). 80% yield. ^{1}H NMR ($CDCl_3$) 7.63 (t, 1H), 7.29 (d, 1H), 7.15 (d, 1H), 6.63 (b, 2H), 5.61 (b, 1H), 4.42 (d, 6H), 4.03 (d, 2H), 3.74 (m, 10H), 2.77 (m, 6H), 1.46 (s, 9H), 1.43 (s, 18H), 1.20 (m, 9H). ^{13}C NMR ($CDCl_3$) 159.6, 156.9, 156.0, 153.5, 152.5, 143.7, 137.1, 134.5, 132.1, 120.9, 119.8, 81.8, 79.4, 55.9, 49.1, 47.3, 46.9, 45.8, 41.1, 28.4, 28.2, 23.1, 22.8, 16.7, 16.6. HRMS (CI+) C_{43} H_{68} N_9 O_6 *m/z*: 806.527092 calcd: 806.529257.

1-(N-6-aminomethyl-pyridin-2-ylmethyl)aminomethyl-2,4,6-triethyl-3,5-[(2-imidazolin-2-yl-amino)methyl]benzene (2.20): **2.19** (0.199 g, 0.246 mmol) was dissolved in DCM:trifluoroacetic acid 1:1, and the reaction was stirred at room temperature overnight. The solvent was removed *in vacuo* to yellow film. The residue was washed with diethyl ether (2x10 mL), dried *in vacuo*, dissolved in water (50 mL), ion-exchanged with Amberlite® IRA-400 (Cl) ion-exchanger, and the product was lyophilized to give **2.20** as its hydrochloride salt (0.116 g). The content of **2.20** in the lyophilized product was determined to be 62% by weight by $CuCl_2$ titration into an aqueous solution of **2.20** and observing the ΔA at 656 nm. The impurities are HCl and H_2O. ^{1}H NMR (D_2O) 7.91 (t, 1H), 7.47 (d, 2H), 4.50 (s, 2H), 4.35 (d, 8H), 3.68 (s, 8H), 2.62 (m, 6H), 1.09 (t, 3H), 1.00 (t, 6H). ^{13}C NMR (D_2O) 159.5, 152.4, 150.5, 147.2, 146.1, 139.8, 130.3, 126.0, 124.0, 124.1, 123.2, 51.2, 45.0, 43.2, 43.1, 41.0, 23.4, 22.9, 15.4. HRMS (Cl-) C_{28} H_{45} N_9 Cl_3 *m/z*: 612.2874 calcd: 612.2864.

2,6-Bisaminomethylpyridine 2HCl (2.23): **2.21** (5.5803 g, 12.47 mmol), potassium phthalimide (4.85 g, 26.2 mmol), and K_2CO_3 (471 mg, 3.4 mmol) were dissolved in dry DMF (45 mL) and taken to 160 ºC where it was allowed to stir overnight. The thick slurry was then vacuum filtered after which the solid was put under high vacuum over night. Without further purification, the 2,6-bisphthalimidomethylpyridine (4.7695 g, 12.01 mmol) was added to conc. HCl (75 mL), and the suspension was refluxed for 4 hours. After cooling to room temperature, the crystalline product was vacuum filtered and washed with ethanol. After drying the white crystals under high vacuum the yield was found to be 44% (5.0695 g, 5.5 mmol). By isolating the aqueous filtrate before the ethanol rinse and reducing its volume *in vacuo* by half a second smaller crystal yield was obtainable. However, the purity of this second crystal harvest proved highly variable. The H^1 NMR pure product was not water free, and the content of **2.23** in the crystalline product was determined to be 90% by weight by $CuCl_2$ titration into an aqueous solution of **2.23** and observing the ΔA at 630 nm. ^1H NMR (D_2O) 7.79 (t, 1H), 7.33 (d, 2H), 4.28 (s, 4H). ^{13}C NMR (D_2O) 151.7, 139.3, 122.3, 42.9. HRMS (CI+) $C_7\ ^1H_8\ ^2H_4\ N_3$ *m/z*: 142.1285 calcd: 142.1282.

[3-(Acetylamino-methyl)-5-(*tert*-butoxycarbonylamino-methyl)-2,4,6-triethyl-benzyl]-carbamic acid *tert*-butyl ester (2.25): In a 60 mL Nalgene bottle, **2.24**[40] (561.1 mg, 1.25 mmol) dissolved in CH_2Cl_2 (3 mL) was treated with acetic anhydride (0.5 mL, 5.29 mmol). The solution was then treated with 0.5 N NaOH (2 mL) and the biphasic system was capped and shaken vigorously with occasional venting for 5 minutes. H_2O (20 mL) and CH_2Cl_2 (20 mL) were added and the mixture transferred to a separatory funnel. The organic layer was separated and concentrated in vacuo to an off-white foam. The crude mixture was purified by silica gel chromatography (solvent ramping from CH_2Cl_2 to 10% ammonia saturated methanol: CH_2Cl_2) to yield the product as an off-white foam (323.3 mg, 0.66 mmol). 53% yield. ^1H NMR ($CDCl_3$) 4.36 (d, 2H), 4.26 (d, 4H), 2.65 (m, 6H), 1.90 (s, 3H), 1.37 (s, 18H), 1.12 (m, 9H). ^{13}C NMR ($CDCl_3$) 174.1, 169.7, 155.238, 143.7, 132.5, 131.8, 79.4, 53.3, 38.6, 38.1, 28.3, 22.8, 20.7, 16.3. HRMS (CI+) $C_{27}\ H_{46}\ N_3\ O_5$ *m/z*: 492.3431 calcd: 492.3437.

N-(3,5-Bis-aminomethyl-2,4,6-triethyl-benzyl)-acetamide (2.26): 2.25 (323.3 mg, 0.66 mmol) was dissolved in CH_2Cl_2:trifluoroacetic acid 1:1, and the reaction was stirred at room temperature 2 hours. The reaction mixture was then concentrated in vacuo to a thick yellow oil, which upon treatment with diethylether yielded a white film on the reaction vessel. The diethylether was pipetted out, and the white film was dried under high vacuum. The white solid was then dissolved in 2N NaOH (100 mL) and extracted twice with CH_2Cl_2 (100 mL and 50 mL). The organic layer was washed with brine (100 mL) then dried with Na_2SO_4. The CH_2Cl_2 was removed in vacuo, and the sample dried under vacuum overnight to a light yellow film (136.5 mg, 0.468 mmol) and was used without further purification. 85% yield. ^{1}H NMR (D_2O) 7.79 (t, 1H), 7.33 (d, 2H), 4.28 (s, 4H). ^{13}C NMR (D_2O) 173.9, 146.7, 144.9, 132.2, 128.0, 38.1, 37.0, 23.2, 23.1, 21.8, 15.4, 15.3. HRMS (CI+) $C_{17}\,{}^1H_{25}\,{}^2H_5\,N_3\,O$ *m/z*: 297.2705 calcd: 297.2703.

1-(N-acyl)aminomethyl-2,4,6-triethyl-3,5-[[4,5-dihydro-N-(1,1-dimethylethoxy)-carbonyl-imidazol-2-yl]aminomethyl]benzene (2.28): 2.26 (562 mg, 1.93 mmol) was dissolved in methanol:acetic acid 10:1 (13.2 mL). N-*t*-Boc-2-methylthio-2-imidazole (855 mg, 3.96 mmol) was added, and the reaction mixture stirred at 50 ºC overnight. The reaction mixture was concentrated in vacuo to a yellow oil then dissolved in CH_2Cl_2 (50 mL). The solution was washed with saturated K_2CO_3 (aq., 50 mL), H_2O (50 mL) and brine (50 mL) and then dried with Na_2SO_4. The crude mixture was concentrated in vacuo and purified by silica gel chromatography (solvent ramping from CH_2Cl_2 to 10% ammonia saturated methanol: CH_2Cl_2) to yield an off-white foam (878.5 mg, 1.4 mmol) in 73% yield. ^{1}H NMR ($CDCl_3$) 6.54 (bs, 2H), 5.68 (bs, 1H), 4.36 (m, 6H), 3.68 (m, 8H), 2.69 (q, 2H), 2.63 (q, 4H), 1.90 (s, 3H), 1.36 (s, 18H), 1.14 (m,9H). ^{13}C NMR (D_2O) 169.8, 153.3, 152.5, 144.3, 143.9, 132.3, 131.4, 81.9, 70.4, 48.8, 46.7, 40.9, 38.3, 28.1, 23.0, 22.8, 16.5, 16.3. HRMS (CI+) $C_{33}\,H_{54}\,N_7\,O_5$ *m/z*: 628.4188 calcd: 628.4186.

1-(N-acyl)aminomethyl-2,4,6-triethyl-3,5-[(2-imidazolin-2-yl-amino)methyl]benzene (2.6): 2.28 (878.5 mg, 1.4 mmol) was dissolved in CH_2Cl_2:trifluoroacetic acid 1:1, and the reaction was stirred at room temperature overnight. The reaction mixture was then

concentrated in vacuo to a thick yellow oil, which upon treatment with diethylether yielded a chalky white precipitate. The ethylether was removed by pipette, and the white solid let to dry under high vacuum overnight. The sample was dissolved in H_2O (50 mL) and ion-exchanged with Amberlite® IRA-400 (Cl) ion-exchanger, and the product was lyophilized to give **2.6** as its hydrochloride salt (0.637 g). The yellowish solid was dissolved in H_2O (10 mL) and determined to consist of 89% **2.6** by weight by adding a known quantity of methanol to an aliquot of the aqueous solution in D_2O and comparing the relative peak integrations. Calculated final yield is 81% (0.565 g, 1.13 mmol). ^1H NMR (D_2O) 4.35 (s, 6H), 3.67 (s, 8H), 2.60 (m, 6H), 1.90 (s, 3H), 1.05 (m, 9H). ^{13}C NMR (D_2O) 173.8, 159.5, 145.6, 144.8, 131.6, 129.7, 43.0, 41.0, 38.3, 22.734, 22.698, 21.8, 15.5, 15.4. HRMS (CI+) $C_{23}\ ^1H_{32}\ ^2H_7\ N_7\ O\ Cl$ *m/z*: 471.3341 calcd: 471.3344.

2.5 References for Chapter 2

[1]. "Additivity and the Physical Basis of Multivalency Effects: A Thermodynamic Investigation of the Calcium EDTA Interaction" Christensen, T., Gooden, D.M., Kung, J.E., Toone, E.J. *J. Am. Chem. Soc.* 2003, *125*, 7357-7366.

[2]. "The Chelate Effect: A Simple Quantitative Approach" Hancock, R.D. Marsicano, F. *J.Chem.Soc., Dalton Trans.* **1976**, 1096-1098.

[3]. "Enthalpic Domination of the Chelate Effect in Cyclodextrin Dimers" Zhang, B., Breslow, R. *J. Am. Chem. Soc.* **1993**, *115*, 9353-9354.

[4]. "Multivalency and Cooperativity in Supramolecular Chemistry" Badjic, J. D., Nelson, A., Cantrill, S. J., Turnbull, W. B., Stoddart, J. F. *Acc. Chem. Res*. **2005**, *38*, 723-732.

[5]. "Polyvalent Interactions in Biological Systems: Implications for Design and Use of Multivalent Ligands and Inhibitors" Mammen, M., Choi, S-K., Whitesides, G.M. *Angew. Chem. Int. Ed*. **1998**, *37*, 2754-2794.

[6]. "Studies into the Thermodynamic Origin of Negative Cooperativity in Ion-Pairing Molecular Recognition" Tobey, S.L., Anslyn, E.V. *J. Am. Chem. Soc.* **2003**, *125*, 10963-10970.

[7]. "Positive ion pair cooperativity exhibited for the binding of phosphate under physiological conditions" Gunning, P.T. *Org. Biomol. Chem.* **2005**, *3*, 3877-3879.

[8]. "Aspects of Weak Interactions" Williams, D. H., Westwell, M. S. Chem. *Soc. Rev.* **1998**, *27*, 57-64.

[9]. "On the Attribution and Additivity of Binding Energies" Jencks, W. P. *Proc. Natl. Acad. Sci. U.S.A*, **1981**, *78*, 4046-4050.

[10]. "An Enthalpic Component in Cooperativity: The Relationship Between Enthalpy, Entropy, and Noncovalent Structure in Weak Associations" Calderone, C. T.; Williams, D. H. *J. Am. Chem. Soc.* **2001**, *123*, 6262-6267.

[11]. "On the Nature of the Multivalency Effect: A Thermodynamic Model" Kitov, P. I.; Bundle, D. R. *J. Am. Chem. Soc.* **2003**, *125*, 16271-16284.

[12]. "The Cluster Glycoside Effect" Lundquist, J. J.; Toone, E. J. *Chem. Rev.* **2002**, *102*, 555-578.

[13]. "Carbohydrate-Protein Interactions: Basis of Glycobiology" Lee, Y. C.; Lee, R. T. *Acc. Chem. Res.* **1995**, 321-327.

[14]. "The Design of Molecular Hosts, Guests, and Their Complexes" Cram, D. J. *Science*, **1988**, *240*, 760-767.

[15]. "Supramolecular Chemistry-Scope and Perspectives Molecules, Supermolecules, and Molecular Devices" Lehn, J. –M. *Angew. Chem. Int. Edit.* **1988**, *27*, 89-112.

[16]. "Experimental and Computational Approaches to Estimate Solubility and Permeability in Drug Discovery and Development Settings" Lipinski, C. A.; Lombardo, F.; Dominy, B. W.; Feeney, P. J. *Adv. Drug Del. Rev.* **2001**, *46*, 3-26.

[17]. "Thermodynamic Aspects of Dicarboxylate Recognition by Simple Artificial Receptors" Linton, B. R., Goodman, M. S., Fan, E., Van Arman, S. A., Hamilton, A. D. *J. Org. Chem.* **2001**, *66*, 7313-7319.

[18]. "Enantioselectivity Measurements of Copper(II) Amino Acid Complexes Using Isothermal Titration Calorimetry" De Bruin, T. J. M., Marcelis, A. T. M., Zuilof, H., Sudholter, E.J. R. *Langmuir*, **2000**, *16*, 8270-8275.

[19]. "Expression of Electrostatic Binding Cooperativity in the Recognition of Cell-wall Peptide Analogues by Vancomycin Groups Antibiotics" Groves, P., Searle, M. S., Westwell, M. S., Williams, D. H. *J. Chem. Soc., Chem. Commun.* **1994**, 1519-1520.

[20]. "Burial of Hydrocarbon Causes Cooperative Enhancement of Electrostatic Binding" Sharman, G. J., Searle, M. S., Benhamu, B., Groves, P., Williams, D. H. *Angew. Chem.* **1995**, *34*, 1483-1485.

[21]. "Very Strong Binding of Appropriate Substrates by Cyclodextrin Dimers" Breslow, R., Greenspoon, N., Guo, T., Zarzycki, R. *J. Am. Chem. Soc.* **1989**, *111*, 8296-8297.

[22]. "Design, Synthesis, and Characterization of a High-Affinity Trivalent System Derived from Vancomycin and L-Lys-D-Ala-D-Ala" Rao, J., Lahiri, J., Wies, R. M., Whitesides, G. M. *J. Am. Chem. Soc.* **2000**, *122*, 2698-2710.

[23]. "An Alcohol Recognition Motif: Clear Evidence of Binding Site Cooperativity in the Complexation of Cyclohexanediols by Neutral Polyaza-Clefts" Bell, D. A., Diaz, S. G., Lynch, V. M., Anslyn, E. V. *Tetrahedron Lett.* **1995**, *36*, 4155-4158.

[24]. "Host-Guest Complexation. 35. Spherands, the First Completely Preorganized Ligand Systems" Cram, D. J., Kaneda, T., Helgeson, R. C., Brown, S. B., Knobler, C. B., Maverick, E., Trueblood, K. N. *J. Am. Chem. Soc.* **1985**, *107*, 3645-3657.

[25]. "Cu(I) and Cu(II) complexes of a pyridine-based pincer ligand" Verdernikov, A. N., Wu, P., Huffman, J. C., Caulton, K. G. *Inorganica Chimica Acta*. **2002**, *330*, 103-110.

[26]. Martell, A. E., Hancock, R.D (1996) in *Metal Complexes in Aqueous Solutions*, ed. Fackler, J. P. (Plenum Press: New York) pp. 58, 83.

[27]. Evidence for coordination is linked to the lesser increase in absorbance upon dicarboxylate binding compared with acetate binding even though dicarboxylate binding is stronger. Coordination at the axial site of copper is known to lower the *d-d* energy. The weakness of the axial site is such that the second coordination event may be more accurately described as an ion-pairing event.

[28]. D. M. Perreault, Ph. D. thesis, University of Texas, Austin, TX (USA), **1997**.

[29]. Connors, K. (1987) in *Binding Constants: The Measurement of Molecular Complex Stability*, (Wiley, New York), pp 147-149.

[30]. "Rapid measurement of binding constants and heats of binding using a new titration calorimeter" Wiseman, T., Williston, S., Brandts, J. F., Lin, L. –N. *Anal. Biochem.* **1989**, *179*, 131-137.

[31]. "On the Value of *c*: Can Low Affinity Systems Be Studied by Isothermal Titration Calorimetry?" Turnbull, W. B., Daranas, A. H. *J. Am. Chem. Soc.* **2003**, *125*, 14859-14866.

[32]. "Two Faces of Water" Chandler, D. *Nature*, **2002**, *417*, 491.

[33]. Martell, A. E., Hancock, R.D (1996) in *Metal Complexes in Aqueous Solutions*, ed. Fackler, J. P. (Plenum Press: New York) pp. 58, 83.

[34]. Evidence for coordination is linked to the lesser increase in absorbance upon dicarboxylate binding compared with acetate binding even though dicarboxylate binding is stronger. Coordination at the axial site of copper is known to lower the *d-d* energy. The weakness of the axial site is such that the second coordination event may be more accurately described as an ion-pairing event.

[35]. "Ion-Pairing Molecular Recognition in Water: Aggregation at Low Concentration that is Entropy Driven" Rekharsky, M., Inoue, Y., Tobey, S., Metzger, A., Anslyn, E. V. *J. Am. Chem. Soc.* **2002**, *124*, 14959-14967.

[36]. Grime, J.K. (1985) in *Analytical Solution Calorimetry*, ed. Grime, J.K. (John Wiley & Sons, New York), pp. 314.

[37]. (2005) in *Lange's Handbook of Chemistry*, ed Speight, J.G. (McGraw-Hill, Chicago), pp 2.620-2.669.

[38]. Skoog, D. A., Holler, F. J., Nieman, T. A. (1998) in *Principles of Instrumental Analysis, fifth edition.* (Brooks/Cole: United States) pp. 12.

[39]. "Do Zwitterions contribute to the ionic strength of a solution?" Stellwagen, E., Prantner, J. D., Stellwagen, N. C. *Anal. Biochem.* **2008**, *373*, 407-409.

[40]. "Thermodynamic Analysis of Receptors based on Guanidinium/Boronic Acid Groups for the Complexation of carboxylates, α-hydroxycarboxylates, and Diols: Driving Force for Binding and Cooperativity" Wiskur, S. L., Lavigne, J. J., Metzger, A., Tobey, S. L., Lynch, V., Anslyn, E. V. *Chem. Eur. J.* **2004**, *10*, 3792-3804.

Chapter 3. A Minimally Differential Array Sensor: The Detection and Differentiation of Nitrated Explosives Using Fluorescence Quenching and the Hydrophobic Effect.

3.1 Introduction

When multiple sensors are employed simultaneously but discretely this is called a sensor array. The field of molecular sensing has historically focused upon the design and synthesis of sensors that are sensitive and selective for a single analyte. Cross-reactive sensor molecules, those showing sensitivity for both the analyte of interest and for other molecules of the same class, have generally been considered unsuccessful designs. It has been shown, however, that cross-reactive sensors employed in an array format will generate unique response patterns that can be used to identify specific analytes.[1] The utility of cross-reactive sensors is complemented by the facility of their design and synthesis in comparison to highly selective sensors. The Anslyn group is interested in the limit of cross reactivity between sensors in an array format.

Our approach was to design and implement an array using highly promiscuous sensors to detect minimally differentiated analytes. To this end, we report a differential array of micelle-solubilized fluorophores for the detection and identification of small nitrated explosive analytes. The quenching ability of the analytes can be used to correlate their analyte identity, wherein the quenching patterns generated from the differential array are used in linear discriminant analysis (LDA). LDA results in a well-clustered two-dimensional plot, and a jack-knife analysis of the data suggests that this system can be used to identify unknown samples of analyte with 96% accuracy and with a detection limit of 19 μM.

3.1.1 A brief history of array sensing using supramolecular techiniques

Much of the early work on array sensing has been inspired by the mammalian senses of taste and smell. Just as the tongue uses only a few types of sensors in the form of taste buds to differentiate an effectively limitless number of flavors, so too have researchers endeavored to identify numerous analytes using a single device. One of these

"electronic tongues" was the result of a collaborative effort at The University of Texas at Austin. The array consists of micrometer sized polymer beads that reside in micro machined wells that control fluid exposure of the bead. The beads have various appended chemical functionalities that have been specifically chosen,[2] or are the result of strategic combinatorial syntheses.[3] Both on-bead signaling systems have been used, as well as extensive variations of indicator displacement assay (IDA) protocol.[2] The basic setup of the electronic tongue is shown in Figure 3.25.

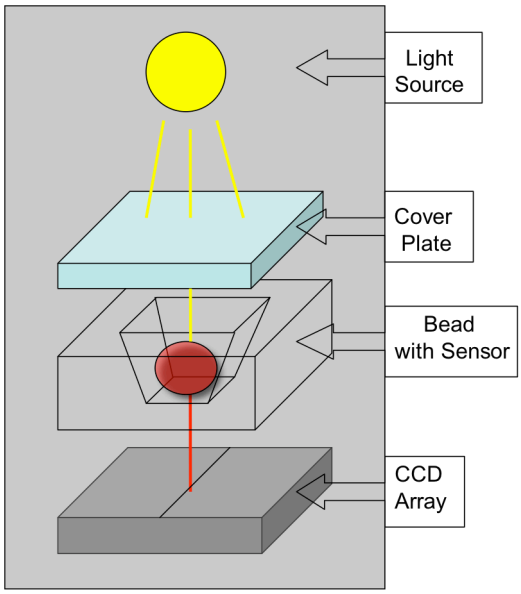

Figure 3.25 ***The Electronic Tongue.*** Light is passed through a bead that has been treated with an analyte solution and is recorded by CCD camera. The spectral qualities of the light are dissected according to attenuation of red, green and blue and coverted to data for use in pattern recognition protocols.

A few of the applications for which the electronic tongue proved effective were the discrimination of proteins and tripeptides (Figure 3.26).[3,4] In fact, array sensors have proven effective for a number of protein, peptide and amino acid analytes.[5] In another example from the Anslyn group, a 96-well plate array of three hosts and three indicators in different combinations was sufficient to discriminate five hydrophobic amino acids from each other and from their enantiomers for total of ten analytes (Figure 3.27).[6]

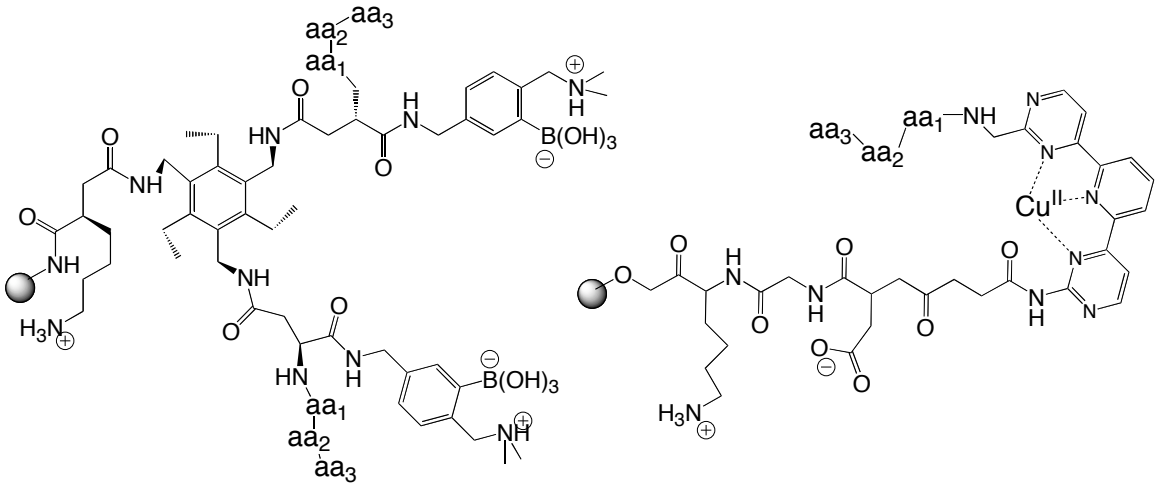

3.1 **3.2**

Figure 3.26 ***Bead mounted receptors used in the UT electronic tongue.*** Libraries of these receptors were generated by combinatorial synthesis of the tripeptide arms. The library on the left was able to differentiate a series of proteins while the Cu^{II}-containing library on the right was able to distinguish between tripeptides.

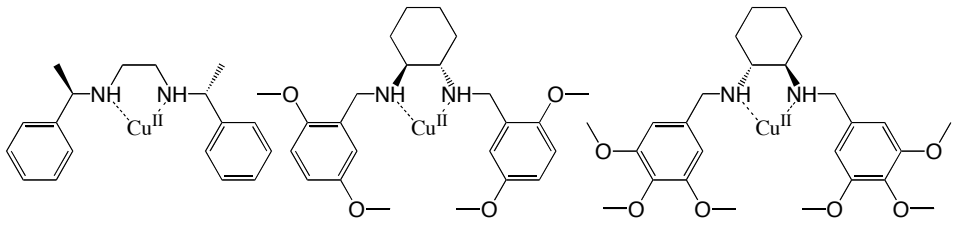

3.3 **3.4** **3.5**

Figure 3.27 ***Copper (II) complexes that enantiomerically distinguish amino acids.*** These complexes were used in combination with the indicators pyrocatechol violet, chromaxane cyanin R, and chrome azurole S to create an IDA style array.

The patterns generated by the array were submitted to principle components analysis (PCA), and one of the most interesting observations of this work was the clear differentiation of the axes of the PCA. The amino acids were sorted along the primary axis according to binding affinity, while the secondary axis served to demarcate the L- and D-amino acids.

Another array system for the detection of proteins, which provided much inspiration for the work in this chapter, came from the Thayumanavan group. They have

shown that polyanionic polymeric surfactants with pendant fluorophores form fluorescent micelles in water that are quenched to different degrees by a variety of metalloproteins (Figure 3.28).[7] Expanding upon this work, the Thayumanavan group used a similar polyelectrolyte that did not have a covalently attached fluorophore and co-dissolved a series of fluorophores, which bound the micelle interior. When metalloproteins analytes were added, they migrated to the exterior of the anionic polymer and quenched the fluorescence of the bound fluorophore. The array of bound fluorophores was shown to generate patterns diagnostic of each analyte.[8]

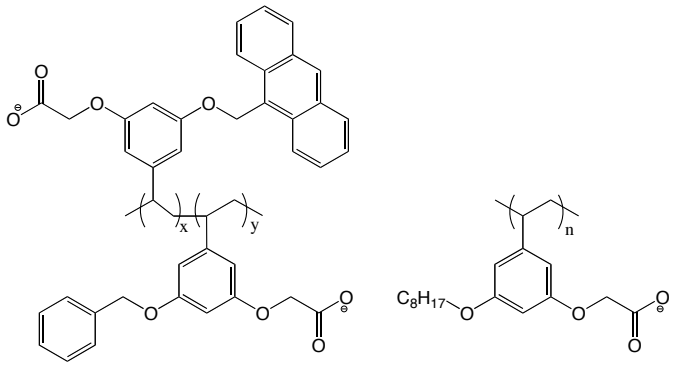

3.6 **3.7**

Figure 3.28 ***Polyelectrolyte amphiphiles.*** Micellar formations of these polymers in water have been shown to sense and differentiate metalloproteins. The polymer on the left has a covalently attached fluorophore while the polymer on the right was used in conjunction with a series of co-dissolved fluorophores.

Molecularly imprinted polymers (MIP) are polymeric matrices synthesized in the presence of a template molecule, which is then removed to leave a cavity that is shape specific for the template (Scheme 3.17). The rapidity of this process and the modest selectivity of the resultant sensors makes it ideal for the generation of differential arrays. Shimizu *et al.* have proven this concept by using an MIP generated IDA array to differentiate between six templated amines and a seventh amine that was not templated for but which nonetheless was sensed and differentiated by the array.[9] This study is an excellent example of an array that tested the limits of cross-reactivity, much in keeping with the spirit of this chapter.

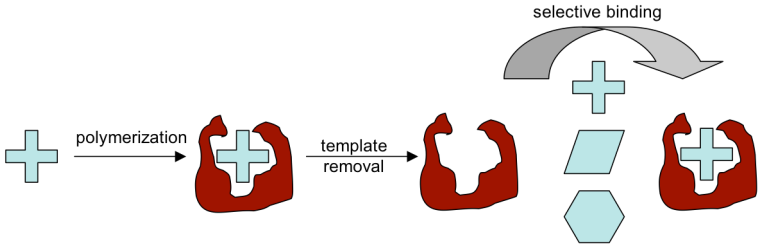

Scheme 3.17 ***Molecularly imprinted polymers.*** Polymerization in the presence of a template molecule imparts selectivity for that molecule.

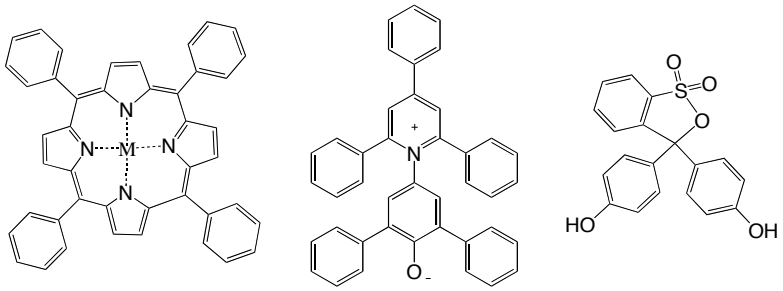

3.8 **3.9** **3.10**

Figure 3.29 ***Simple dyes from the Suslick array.*** Metalloporphyrins, **3.8**, solvatochromic dyes (Reichert's is shown, **3.9**) and pH indicators (phenol red shown, **3.10**)

A final array that also demonstrates the power of minimally discriminatory agents when employed *en masse* comes from the Suslick group.[10] Various Lewis basic metalloporphyrins, solvatochromic dyes, and acid and base sensitive pH indicators were arrayed on a commercially available hydrophobic surface (Figure 3.29). When exposed to amines, aromatic amines, thiols and a few different types of oxygen containing compounds in water the array displays diagnostic patterns. The pattern recognition algorithm of choice for this study was hierarchical cluster analysis (HCA). HCA expresses relationships between samples in a dendrograms, and indeed the group classifications in the Suslick study were highly ordered according to functional group. The same array was also quite adept at identifying complex mixtures as evidenced by the differentiation of twelve commercially available soft drinks.[10] The use of array sensing and pattern recognition protocols to translate supramolecular sensor output into qualitative and quantitative chemical information has become routine in recent years,

with numerous examples from our own group, and from the supramolecular community at large.[5,11,12]

3.2 The Detection and Differentiation of Nitrated Explosives

3.2.1 Background and significance

Despite useful roles in construction and demolition, nitrated explosives are most notorious for their use in military capacities and in terrorism campaigns. The presence of nitrated aromatic compounds such as tetryl (**3.11**) and TNT (**3.12**), and nitramines such as RDX (**3.14**) and HMX (**3.15**), is directly correlated with criminal intent or the presence of ordinances such as unexploded landmines or cluster bombs. The desire for sensitive, robust and inexpensive techniques for sensing nitrated explosives has driven research in this field.

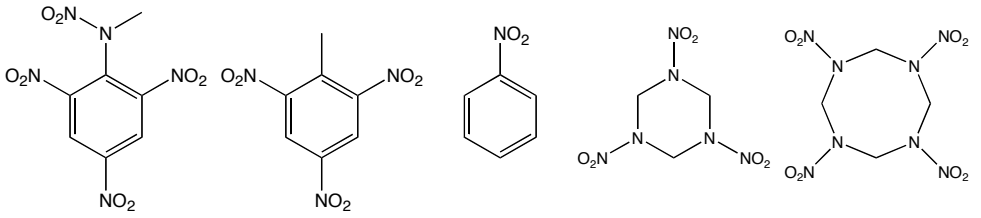

Tetryl 3.11 **TNT 3.12** **Nitrobenzene 3.13** **RDX 3.14** **HMX 3.15**

Numerous analytical methods for explosives detection have been developed[13] including chromatographic methods using UV,[14,15] indirect fluorescence,[16,17] and amperometric detection methods.[18] A biomimetic system was recently reported for the detection of dinitrotoluene,[19] and various mass spectrometry methods[20,21,22] for the detection of nitrated analytes are known. Additionally, the use of fluorescence quenching in numerous polymers[23,24,25] and other solid-state media[26,27] has been extensively investigated. Many of these systems have been well refined and are quite powerful. Swager *et al.* have reported a series of pentiptycene polymers that are particularly sensitive to nitroaromatics (Figure 3.30).[28,29] The special fluorescence properties of these polymers are believed to derive from the disruption of π-stacking in the solid state by the

pentiptycene moiety.[30] The porosity of the resulting polymer minimizes self-quenching and presents a high surface area to incoming fluorescence quenching analytes. A thin film flow cell variant of this technology has been commercialized.[31]

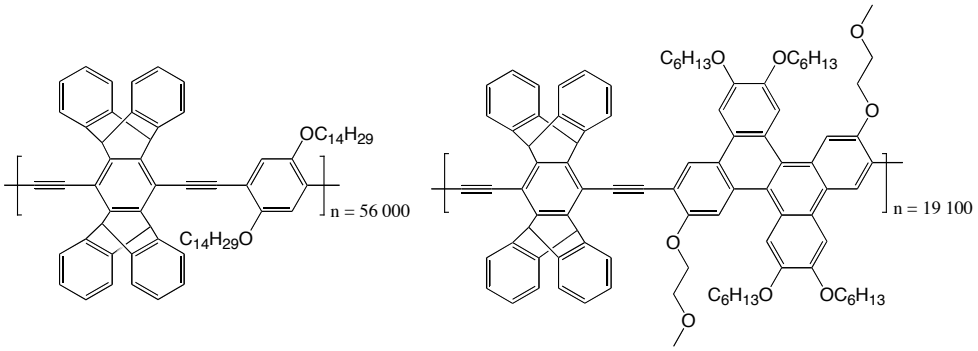

3.16 **3.17**

Figure 3.30 ***Polymeric pentriptycene TNT sensors.*** Developed by the Swager group, these polymers exhibit excellent fluorescence quenching in the presence of nitrated aromatics like TNT.

Fewer studies have probed the non-chromatographic, spectrophotometric detection and differentiation of non-aromatic nitrated explosives. Andrew and Swager recently reported an impressive turn-on system for the fluorescence detection of RDX and PETN that also differentiates the two compounds.[32] Their system relies on the photooxidation of a zinc-coordinated acridine dye to a fluorescent acridinium species in the presence of RDX or PETN, but not TNT (Scheme 3.18). Using this method, RDX and PETN were detectable at 70 μM and 130 μM concentrations respectively. This system is one of the few examples of the direct detection of nitrated analytes.

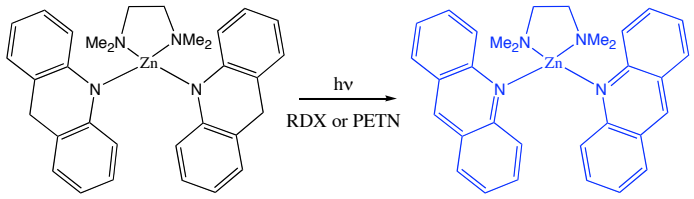

3.18

weakly fluorescent

strongly fluorescent

Scheme 3.18 ***A turn-on fluorescent sensor for RDX and PETN.*** Photoreaction of the zinc-acridine on the left in the presence of RDX or PETN generates the more fluorescent acridinium species.

Nitroaromatic and nitramine explosives such as TNT and RDX generally lack the basic and acidic functionalities that serve as "handles" in the design of selective supramolecular sensors. However, these compounds are known to quench the fluorescence of pyrene (**3.19**) as well as other polyaromatic hydrocarbons (PAHs), and this quenching ability differs among compounds.[16] Therefore, by monitoring pyrene fluorescence it is possible to sense the presence of nitrated explosives. To enhance this quenching and hence the sensitivity of a quenching based detection assay, we thought that it would be possible to sequester the pyrene in micelles in order to promote interaction between the micelle bound pyrene and the hydrophobic explosives. An analogous concept is a well-established method for determining the mean aggregation number of micelles,[33] though to our knowledge no one has pursued this idea as part of a sensing array.

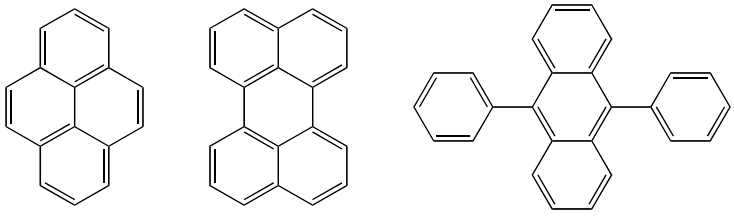

Pyrene
3.19

Perylene
3.20

DPA
3.21

A micellar solution was used to concentrate the analytes in the hydrophobic portion of the solution (inside the micelle), and thereby provide three advantages to our sensing

assay. First, the sensitivity of the assay should be improved because the analyte is more likely to reside in the micelle than in the bulk aqueous solution, and it is therefore more available to quench pyrene than its nominal concentration in the bulk surfactant solution would indicate. Second, while the pyrene is hydrophobic enough to be dissolved almost exclusively in the interior of the micelles,[34] the small, nitrated explosives are present to some degree in the aqueous medium. The differential hydrophobicity of the analytes implies that they will partition to different degrees between the micellar interior and the aqueous medium. This partitioning affects their ability to quench pyrene, and acts as another variable by which the analytes can be differentiated. Finally, pyrene is strongly quenched by molecular oxygen, an attribute that plagues its use in many sensing applications.[35] In the interior of a micelle, however, pyrene is known to be relatively insensitive to O_2,[34] making this micellar sensing assay amenable to routine bench top use without stringent methods to exclude O_2. With these postulates, we set forth to design an array for the detection and differentiation of the explosives and to thereby test the limits of non-selectivity in array sensing.

3.3 Results and Discussion

3.3.1 Design criteria

The ability of nitrated compounds to quench the fluorescence of PAHs lessens as one goes from nitroaromatics to nitramines to nitroaliphatics. While the difference in quenching ability between classes is quite large, the differences within a class are subtler. To differentiate closely related species such as TNT, tetryl, and nitrobenzene (**3.13**), or RDX and HMX, we applied our micelle/fluorophore system in an array format. By using solutions of pyrene, pyrene excimer, a pyrene-perylene (**3.20**) fluorescence resonance energy transfer (FRET) pair, and a diphenylanthracene (DPA, **3.21**) solution, we created an array of fluorophores dissolved in an aqueous solution of the commercial, nonionic, polysorbate surfactant Tween 80.

In designing our sensor array it was important to maintain the simplicity of the system while generating patterns of sufficient complexity to unequivocally identify the

analytes. Pyrene was chosen because of its ability to be quenched by nitrated species. DPA is not well quenched by nitrated species, but its high quantum efficiency means that any excitation light intercepted by the UV absorbing nitroaromatics will result in an attenuation of DPA fluorescence. Such absorption is far outmatched by quenching in the case of pyrene. Beyond simple solutions of pyrene or DPA, a higher concentration excimer emitting solution of pyrene was also used as well as a pyrene to perylene fluorescence resonance energy transfer (FRET) system. The logic behind the selection of the last two-fluorophore systems is discussed later.

Different nitrated analytes produce distinct patterns of fluorescence quenching that are diagnostic for the presence of that particular explosive. These quenching patterns can be translated into 2-dimensional plots using linear discriminant analysis (LDA) or principle component analysis (PCA). PCA is an unsupervised technique and is used to detect relationship between analytes. It is sufficient to determine if an array setup is working. LDA, on the other hand, is a supervised technique that permits the classification of analytes. The location of an unknown analyte on an LDA plot reveals its chemical identity.

3.3.1.1 Practical considerations when designing a 96-well array for sensing

When designing an array sensor one should begin by assuming that variance between 96-well plates will exceed variance within a 96-well plate. The point of this assumption is to avoid false positives due to apparent between-plate differences that one may attribute to interactions between sensor solutions and analytes. An example is shown in FIGURE. The example on the left shows the proper configuration of analyte to host or variable. Each plate includes both analytes, so the analyte differences with respect to each of the hosts/variables are not conflated with between plate differences. In this way false positives are minimized. If logistics force the experimenter to test different analytes on different plates then a control should be run: run the experiment without adding any analytes and see if the blank solutions are differentiated by plate using pattern recognition. If so, this differentiation should be dwarfed by differentiations generated in the presence of analyte.

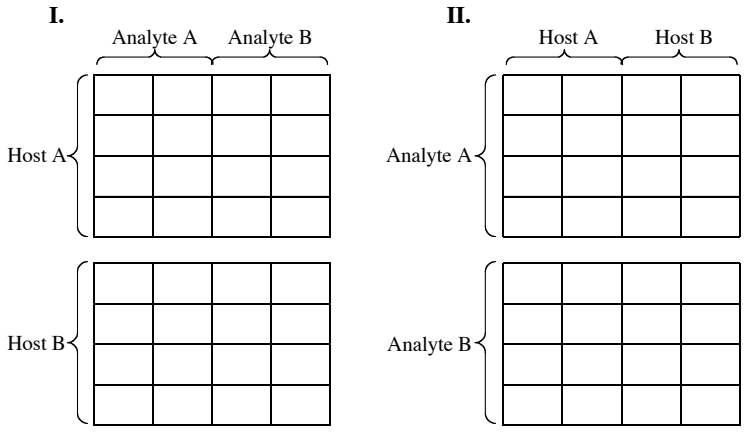

Figure 3.31 ***Two ways to design an array plate.*** Array design I. avoids between plate variability which could create false positives in novel system. Array design II. can create the impression that the analytes are being differentiated when in fact the host A and host B solutions are responding to small differences in plate preparation, a sensitivity that is difficult to predict *a priori*.

3.3.2 The role of micelles

Before creating the sensor array it was important to confirm the principle that a micellar solution of fluorophore is indeed more sensitive to quenching by the nitrated analytes than an equivalent concentration of fluorophore in an organic solvent. To this end two analogous solutions of pyrene (20 μM) were titrated with TNT (4.4 mM in MeCN). In one case the pyrene was dissolved in MeCN while in the other the pyrene was dissolved in an aqueous 2 mM solution of the nonionic polysorbate surfactant Tween 80. While the absolute fluorescence and hence the absolute change in fluorescence were higher for pyrene in MeCN (Figure 3.32), Stern-Volmer data clearly show a higher quenching efficiency in the micellar solution (Figure 3.33). The non-linearity of the Stern-Volmer plot in the micellar solution implies that a static quenching is occurring; therefore, a complex is forming between TNT and pyrene prior to photoexcitation. This complex is believed to result from pyrene's exclusive residency in the micelles, and the analyte's propensity to gather there as well, creating a high effective concentration of the quencher near the fluorophore.

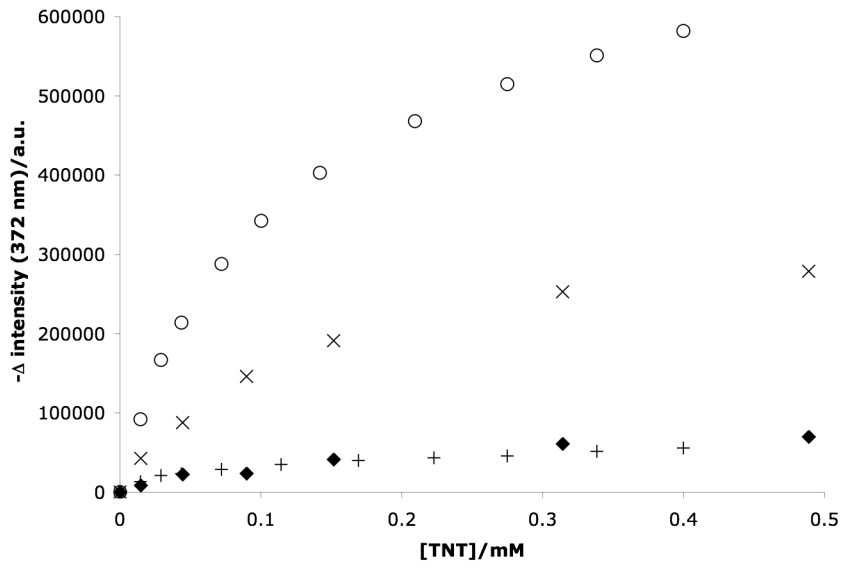

Figure 3.32 ***Quenching of pyrene monomer emission.*** Excitation λ_{max} 336 nm. ○, TNT into pyrene (20 μM) in MeCN (anaerobic);×, TNT into pyrene (20 μM) in Tween 80 (2 mM) in water; ＋, TNT into pyrene (20 μM) in MeCN (aerobic); ◆, MeCN into pyrene (20 μM) in Tween 80 (2 mM) in water. TNT was added as a solution of MeCN, therefore MeCN was added neat as a control. The *y*-axis is presented as –Δ intensity. a.u. = arbitrary units.

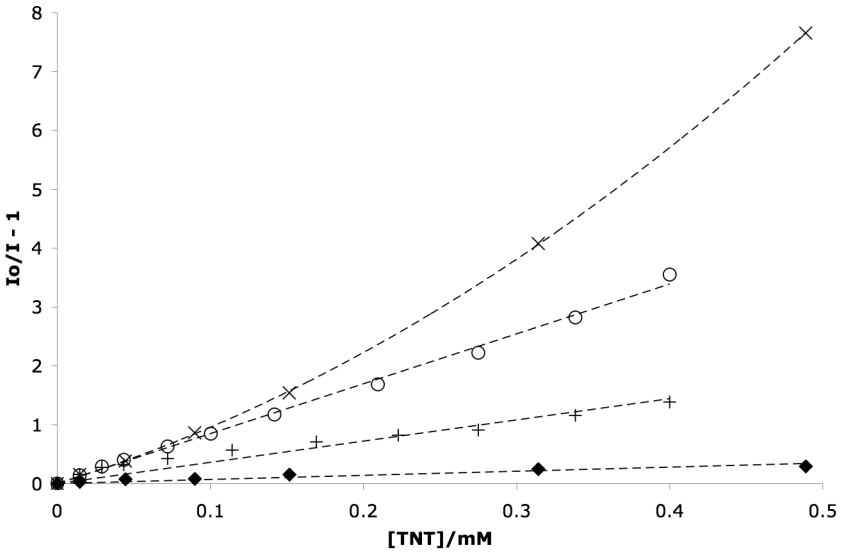

Figure 3.33 ***Stern-Volmer plots of the titration data from*** **Figure 3.32.** The symbols are unchanged from Figure 3.32. I_o/I is the ratio of the original intensity over the intensity after the addition of quencher. The linear plots indicate dynamic quenching behavior while the curved plots indicate static quenching.

Evidence of a similar assembly phenomenon is found in the pyrene surfactant solution itself. According to published values, the concentration of micelles in a 2 mM Tween 80 solution is 34 μM[36] indicating a ratio of 0.59 pyrene molecules per micelle when pyrene is at 20 μM. Indeed, at this concentration some pyrene excimer emission is already apparent, and at higher pyrene concentrations in the 2 mM Tween 80 solution, pyrene monomer emission continues to give way to excimer emission (Figure 3.34), a phenomenon not seen in MeCN until pyrene concentration reaches ~ 1 mM.[37] The low concentration excimer formation is further evidence of the small habitable volume for hydrophobes in the micellar solution. It should be pointed out that while pyrene resides in the hydrophobic interior of the micelle, smaller compounds such as TNT and RDX are expected to exist primarily at the micelle-water interface, migrating inward only as their concentration increases.[34] Despite the different micellar solvation modes, the pyrene and nitrated explosives are proximal and quenching is promoted in the micellar solutions as evidenced by the Stern-Volmer plot.

Besides enhanced quenching, a second advantage of micellar solutions of pyrene is the protection of pyrene from quenching by adventitious oxygen. When TNT is added to pyrene in MeCN in the presence of oxygen (Figure 3.33), the Stern-Volmer plot indicates a markedly weaker sensitivity to the presence of the nitroaromatic analyte. Figure 3.35 illustrates the rapidity with which a rigorously anaerobic solution of pyrene in MeCN can become quenched by atmospheric oxygen. Differential O_2 exposure across a 96-well plate during assay preparation would skew quenching profiles for the nitrated analytes, thus making pattern recognition impossible.

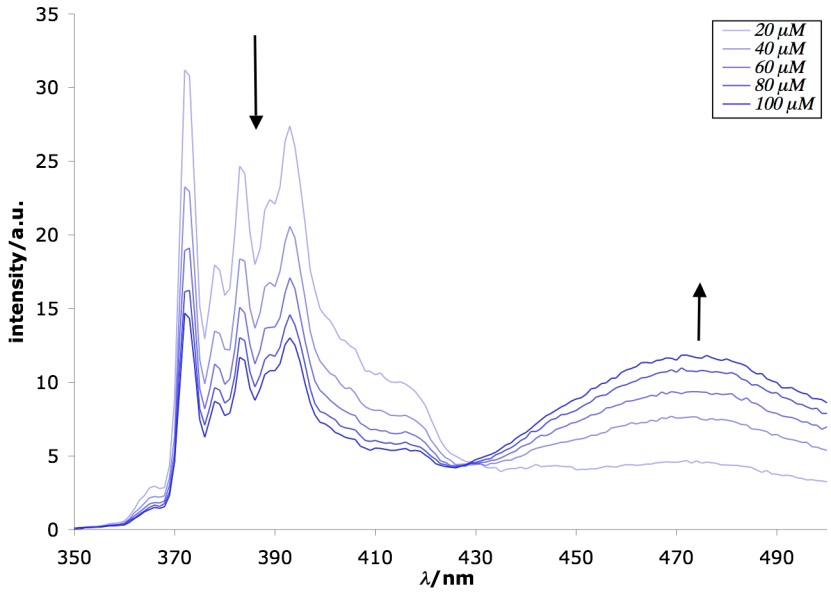

Figure 3.34 ***Pyrene excimer formation.*** The pyrene excimer grows in at lower concentrations in Tween 80 (2 mM) in water than in organic solvents. The excitation λ_{max} becomes longer as pyrene becomes more concentrated, from λ_{max} (20 μM)/336 nm to λ_{max} (100 μM)/342 nm.

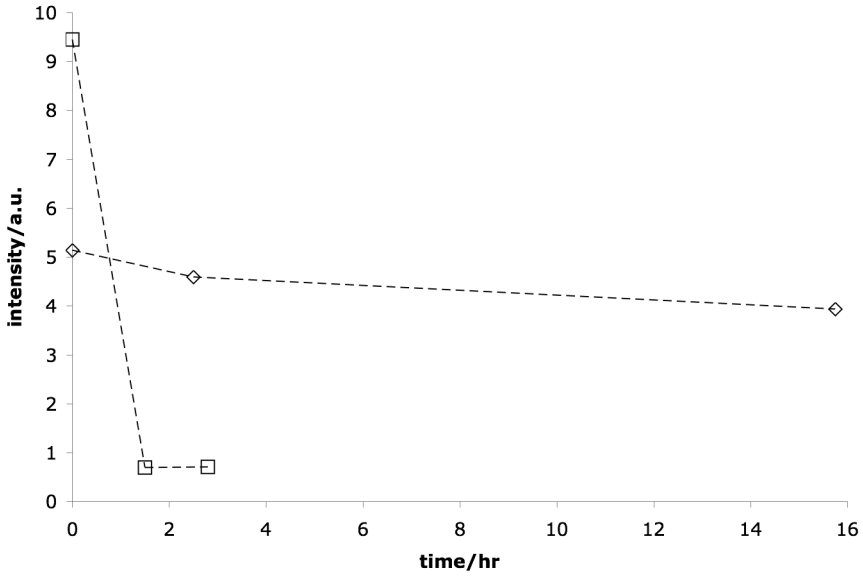

Figure 3.35 ***The quenching of pyrene by atmospheric oxygen.*** The quenching of pyrene emission (20 μM, λ_{max} 372 nm) upon exposure to O_2 is solvent dependent. □, MeCN; ◇, Tween 80 (2 mM) in water.

3.3.3 Pyrene response

Figure 3.36 shows differential quenching of pyrene by a series of nitrated compounds. Nitroaromatics are distinctly better quenchers of pyrene fluorescence than the nitramine compounds, and it is possible to differentiate singly, triply and quadruply nitrated aromatics (nitrobenzene, TNT and tetryl) at the ~0.1 mM point of the titration. RDX and HMX, however, are hardly distinguishable from each other even late in the titration data. In fact, at the micromolar concentrations at which an effective explosives sensor must operate, all of the analytes show highly similar signals. Therefore, the fluorescence modulation of a pyrene-micelle solution alone is insufficient to reliably sense and differentiate the explosive compounds at low concentrations. Stern-Volmer plots (Figure 3.37), however, reveal the fundamental differences in the quenching behavior of these nitrated species. It is these differences that are amplified by the use of subtly different fluorophore solution when applied in array format.

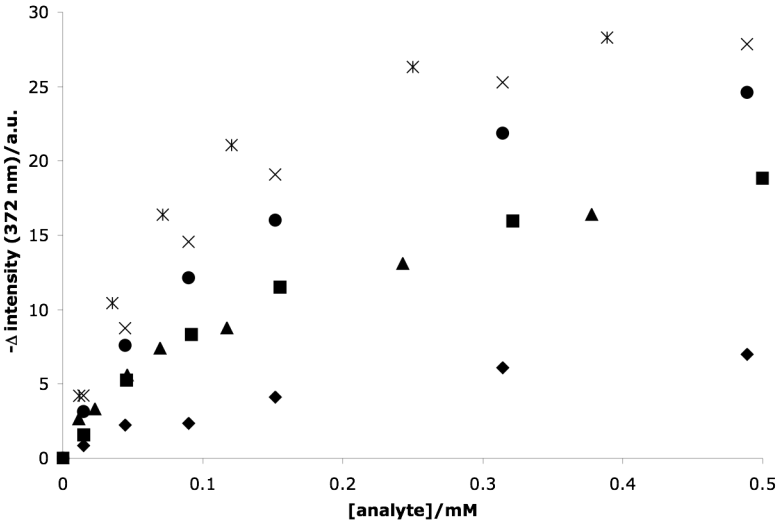

Figure 3.36 ***The quenching of pyrene in Tween 80 by nitrated analytes.*** Pyrene (20 μM) in Tween 80 (2 μM) in water was titrated with: ✳, tetryl; ×, TNT; ●, nitrobenzene; ■, RDX; ▲, HMX; ◆, MeCN. The *y*-axis is presented as –Δ intensity. a.u. = arbitrary units.

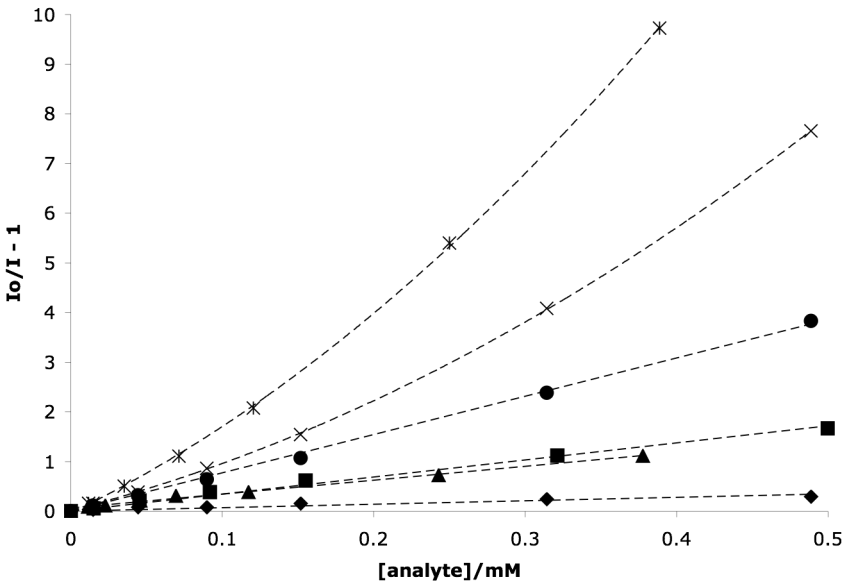

Figure 3.37 ***Stern-Volmer plots of the Titration Data from*** **Figure 3.36.** Pyrene (20 μM) in Tween 80 (2 μM) in water was titrated with: ✳, tetryl; ×, TNT; ●, nitrobenzene; ■, RDX; ▲, HMX; ◆, MeCN. I_o/I is the ratio of the original intensity over the intensity after the addition of quencher. The linear plots indicate dynamic quenching behavior while the curved plots indicate static quenching.

3.3.4 Pyrene excimer response

According to Focsaneanu and Scaiano, pyrene monomer emission and pyrene excimer emission are quenched in different ratios by different nitrated species in MeCN.[37] We confirmed that this is also the case in Tween 80 micelle solution. RDX and TNT show diverging ratios of monomer and excimer emission as their concentrations increase (Figure 3.38). Such ratiometric quenching is detectable in the 96-well plate reader by reading emissions through two separate filters. The sample (fluorophore solution in the presence of analyte) is excited by light passed through a 340/11 nm bandwidth filter, then emission readings are taken from a 380/20 nm filter and a 460/40 nm filter, bandwidths corresponding roughly to pyrene monomer and excimer emissions (Figure 3.39). Along with an analyte's ability to quench pyrene monomer fluorescence as a function of concentration, the array also includes the diagnostic ratio of monomer

and excimer emission. Clearly, the addition of this data will aid in further separation of TNT and RDX.

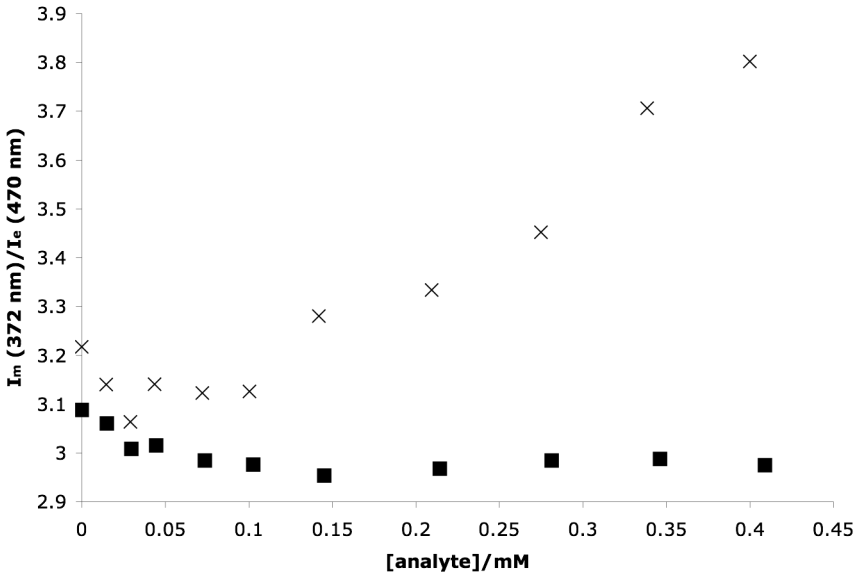

Figure 3.38 ***The ratio of pyrene monomer to excimer emission.*** Pyrene (20 μM) in Tween 80 (2 mM) in water. The ratio of monomer to excimer emission intensity increases as TNT (×) is titrated into the system, while staying effectively the same as RDX (■) is added.

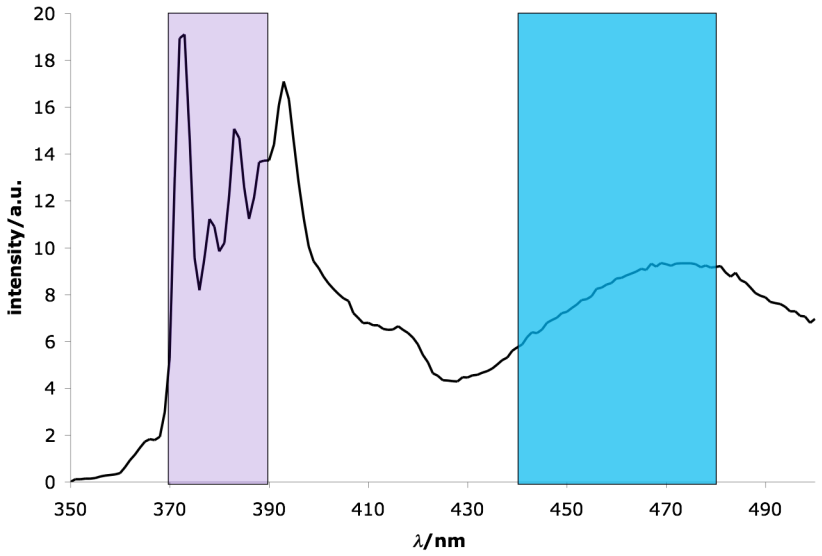

Figure 3.39 ***Bandwidths of emission filters in the 96-well plate reader.*** The spectrum of pyrene (60 μM) in Tween 80 (2 mM) in water is shown. The emission filters are aligned with the UV emission of the pyrene monomer and the visible blue emission of the excimer. The ratio of these emission areas is in some cases diagnostic of the identity of the quenching species.

3.3.5 The pyrene/perylene FRET pair

We were inspired by the ratiometric quenching of pyrene monomer and excimer emission, and thereby lead to explore an analogous system of dual emission using a pyrene-perylene FRET pair. When pyrene and perylene are co-dissolved in a micellar solution, excitation of pyrene results in some relaxation *via* emission of pyrene monomer along with some FRET to excite perylene which then relaxes *via* its own emission (Figure 3.40, topmost spectrum). Titration studies of this system revealed that while the ratio of pyrene and perylene emission does change as the two signals are quenched by a nitrated analyte, this change in ratio was the same for RDX and HMX. Although the FRET system did not display ratiometric quenching, it does represent an efficient transformation of data from the ultraviolet to the visible region because of the high perylene emission within the 460/40 nm bandwidth, and therefore opens the possibility

for future naked eye detection systems. The FRET system was therefore included in the 96-well array sensor.

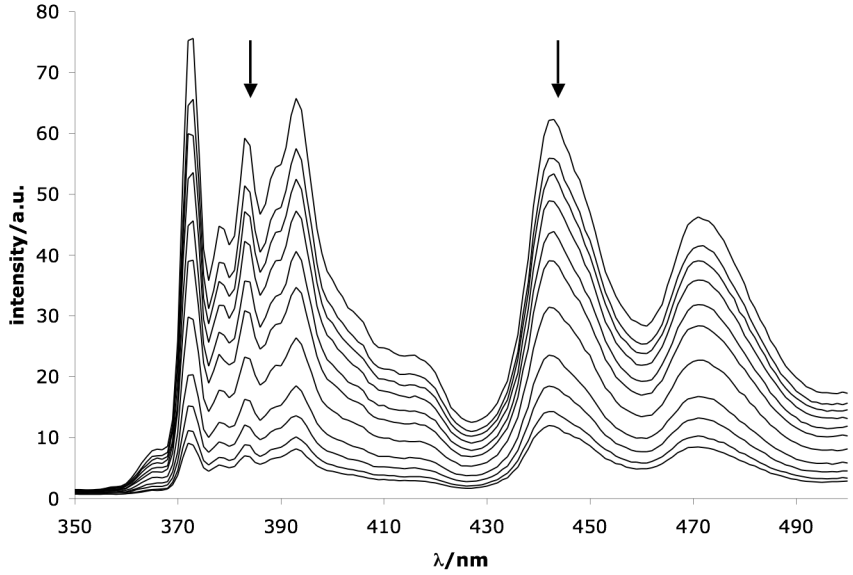

Figure 3.40 ***Emission spectra of FRET-pairing pyrene and perylene.*** The emission spectra as TNT (0 mM to 0.4 mM) was added to pyrene (20 μM) and perylene (20 μM) in Tween 80 (2 mM) in water (excitation λ_{max} 336 nm).

3.3.6 Diphenylanthracene response

By far the simplest of the fluorophore systems we used is that containing diphenylanthracene. Attenuation of the DPA signal upon addition of TNT is nearly linear (not shown), and is therefore due to simple absorption of excitation light by TNT in the UV. While one may argue that it would be much easier to measure TNT's absorbance directly, the sensitivity of fluorescence measurements is inherently higher than that of absorbance. Additionally, as mentioned previously in the case of perylene, transformation of ultraviolet absorbance information into the visible spectrum (emission λ_{max} (DPA)/ 411 nm) holds potential for future naked eye detection systems.

3.3.7 The sensor array

The sensor array consists of a series of 2 mM Tween 80 solutions with varying fluorophores that all undergo fluorescence attenuation when exposed to nitrated analytes. Those solutions are: a low concentration pyrene solution (20 μM) exhibiting predominately monomer fluorescence, a more concentrated pyrene solution (60 μM) with marked excimer fluorescence, a FRET displaying pyrene (20 μM) and perylene (20 μM) solution, and a DPA (20 μM) solution whose fluorescence attenuation is linked to the absorption of incident light by the nitroaromatics. These four solutions were treated with nitrated analytes and their fluorescence emissions observed over the two bandwidths discussed previously. In the case of the DPA solution only the 460/40 bandwidth filter was useful, and so a total of seven variables were submitted to linear discriminant analysis. The data is presented in Figure 3.41. The four variables on the left of the plot were gathered with the wider bandwidth emission filter and are therefore much large in absolute intensity. When rescaled so that the relatively unquenched acetonitrile blank corresponds to 100, the quenching sensitivity of the various methods as observed *via* the plate reader is better resolved (Figure 3.42). The five variables that directly correlate to the pyrene emission (B, C-G) demonstrate a 25% drop in fluorescence between the blank and the most heavily nitrated species, tetryl. It is also interesting to note that the DPA fluorescence persists except in the cases of TNT and tetryl, as expected. The quenching data was normalized using a mean centering protocol so that LDA should weight all of the variables equally (Figure 3.43). Using this method, 48 samples were correctly classified as belonging to one of six classes at a final analyte concentration of 19 μM. Cross-validation, or jack-knife analysis, was 96% accurate in predicting the identity of initially omitted observations. Figure 3.44 shows analyte clustering and the 95% confidence ellipse for each grouping. Similar 96-well assays with analyte concentrations of 1.9 μM were markedly less successful at sensing and differentiating the nitrated compounds, and therefore 19 μM was considered to be the limit of detection.

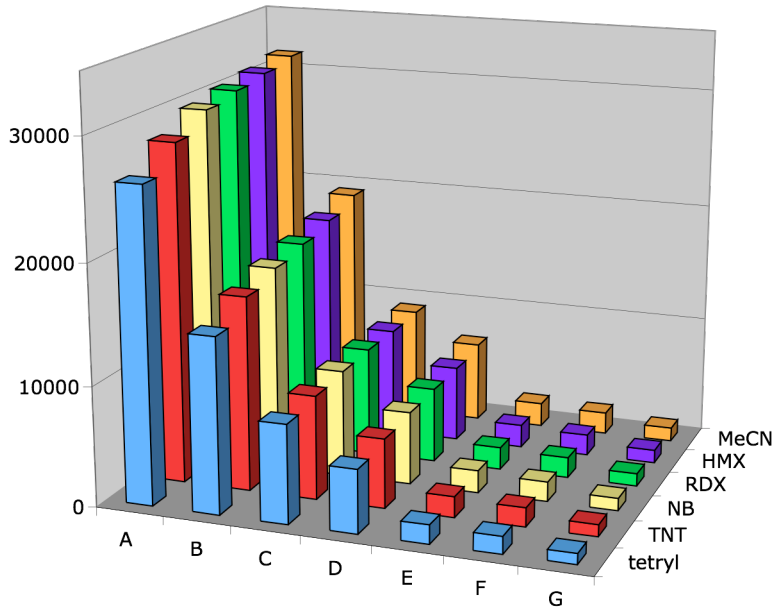

Figure 3.41 ***Raw data from 96-well plate fluorescence experiments.*** Fluorophore systems were dissolved in Tween 80 (2 mM) in water. Intensity data collected using 460/40 nm fluorescence emission filter: **A**, 20 μM pyrene/20 μM perylene; **B**, 60 μM pyrene; **C**, 20 μM DPA; **D**, 20 μM pyrene. Intensity data collected using 380/20 nm fluorescence emission filter: **E**, 20 μM pyrene/20 μM perylene; **F**, 60 μM pyrene; **G**, 20 μM pyrene.

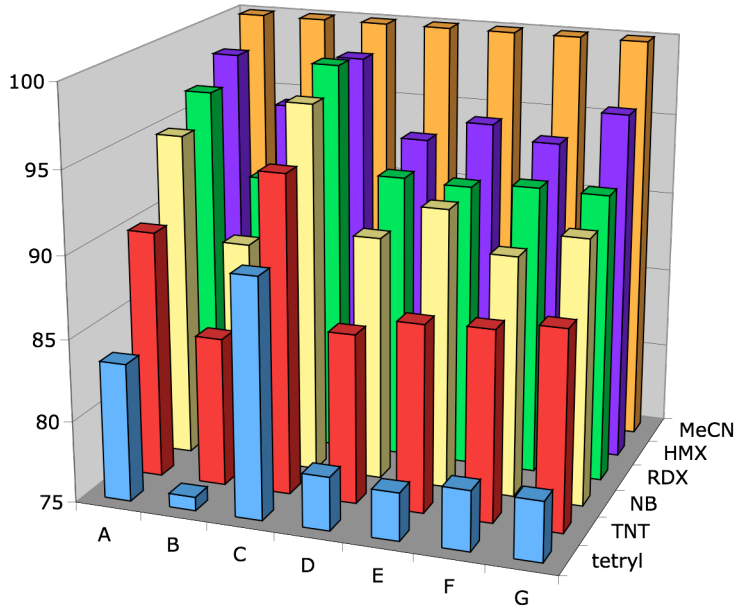

Figure 3.42 ***Data from*** **Figure 3.41** ***standardized according to the MeCN blank.***

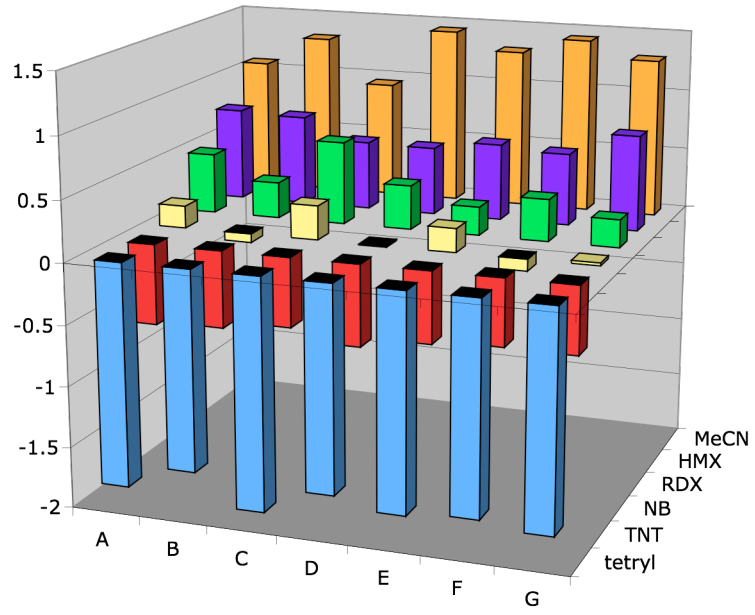

Figure 3.43 ***Mean centered data used in the LDA plots.***

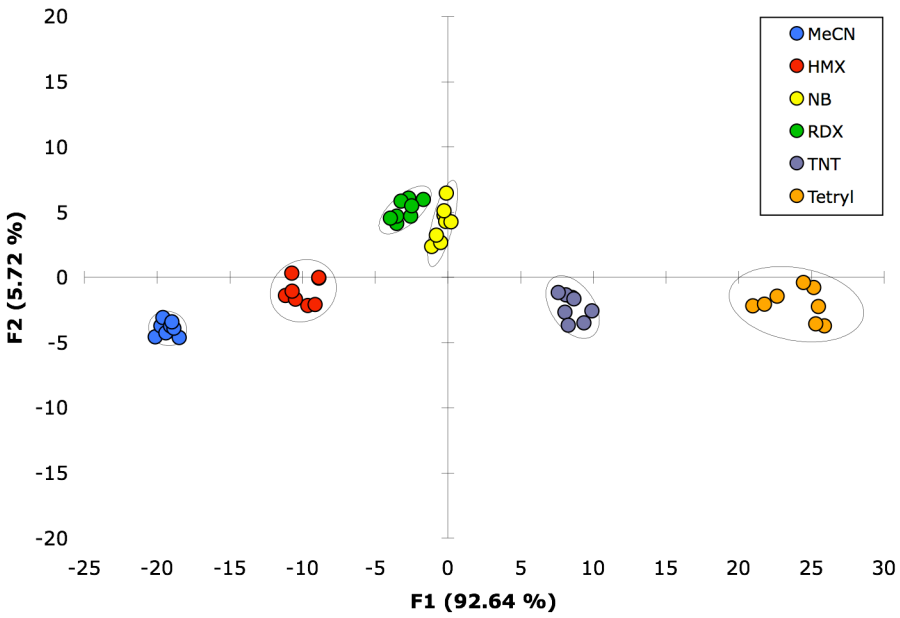

Figure 3.44 ***LDA plot of 96-well assay.*** The explosives shown were all at 19 μM concentration. MeCN served as the blank.

3.4 Conclusions

We have presented a powerful and relatively inexpensive sensor design for nitrated organic explosives. The well-known ability of these analytes to quench pyrene fluorescence was parlayed into a series of similar systems including ratiometric sensing using the pyrene excimer, a pyrene-perylene FRET pair, and a simple DPA signal attenuation due to UV absorption by aromatic analytes. Combining these fluorophore solutions in an array, and examining the fluorescence over two bandwidths resulted in a "fingerprint" for each analyte that allowed it to be classified according to its molecular identity using LDA. The sensor detects these explosive compounds with good sensitivity (19 μM), and also differentiates between highly similar structures such as RDX and HMX. The modular nature of this array means that it is expandable as alternative surfactants and fluorophores are considered for this application, and we are pursuing this line of research to enhance the scope and sensitivity of this method.

3.5 Experimental Details for Chapter 3

3.5.1 General

The chemicals were obtained from Acros Organics, Sigma-Aldrich and Fisher Scientific, and used without further purification. The exception was MeCN (Optima grade) which was obtained from Fisher Scientific and degassed prior to use *via* bubbling N_2 for 1 hr. TNT (4.40 mM), Tetryl (3.48 mM), RDX (4.50 mM) and HMX (3.38 mM) were all obtained as 1000 μg/mL MeCN solutions in sealed glass vials from Ultra Scientific. Water was distilled, deionized and filtered prior to use.

Single-cuvette fluorescence measurements were made using a Photon Technology International QuantaMaster spectrofluorimeter. 96-well plate fluorescence intensity data was gathered using a Biotek Synergy 2 Multi-detection Microplate Reader.

3.5.2 Fluorescence titrations

Fluorophores were dissolved in DMSO near their solubility limits (pyrene, 200 mM; perylene, 20mM DPA, 10 mM) and added to 2 mM Tween 80 in water to affect a the desired final concentration of fluorophore.

A sample titration is described. A cuvette was prepared with 3 mL of an aqueous solution of pyrene (20 μM) in Tween 80 (2 mM). This solution was excited with 336 nm light (pyrene excitation wavelength varied with solvent but emission maxima were consistently observed at 372 nm) and an emission spectrum recorded. An aliquot of TNT (4.4 mM) in MeCN was added, and after thorough mixing the emission spectrum at 336 nm excitation was again recorded. This was repeated until 0.3 mL of the MeCN solution had been added. The fluorescence at the emission maximum (372 nm) for each spectrum was then plotted against the corresponding TNT concentration.

3.5.3 96-well plate experiments

Two 96-well assay plates (Costar, #3632) having 8 rows and 12 columns were used to develop the plot seen in Figure 8. Each of the four Tween 80/fluorophore solutions detailed earlier was added to four contiguous rows of a plate resulting in two plates each of which contained two types of fluorophore solution. The wells of a plate were filled to 300 μL with three 100 μL aliquots of fluorophore solution using a Biotek Precision Microplate Pipetting System.

The five nitrated analyte solutions and the MeCN blank were added to the columns of the plate so that each analyte resided in two of the 12 columns. In this way, eight samples of each analyte existed for each of the fluorophore solutions. The nitrated analyte solutions were made by adding 3 μmol of analyte dissolved in MeCN (1000 μg/mL; neat MeCN in the case of the blank) to a 10 mL volumetric flask, and then adding MeCN to standardize the MeCN volume in each solution at 1 mL. The volumetric flask was then filled to 10 mL with an aqueous 2 mM Tween 80 solution for an analyte concentration of 0.3 mM. Using the microplate pipetting system, the nitrated analyte

solutions were added in a single 20 μL aliquot to the wells for a final in-well analyte concentration of 19 μM.

The 96-well assay plate was then submitted to measurements of fluorescence intensity. The fluorophore solutions were excited using a tungsten light source with a 340/11 bandwidth filter. Two readings of the emission radiation were taken: (1) the emission radiation was passed through a 380/20 bandwidth filter and read from a top 50% optics position with a sensitivity of 45, and (2) the emission radiation was passed through a 460/40 bandwidth filter and read from a top 400 nm optics position with a sensitivity of 45. In the case of the DPA solution only the 460/40 nm filter was used.

3.5.4 Data processing

Data processing was done using XLSTAT (version 2007.6). Fluorescence intensity data was transformed by standardization using unbiased standard deviation (n-1). The transformed data was then processed using linear discriminant analysis (LDA) to produce Figure 8. Cross-validation was performed using the leave-one-out method commonly known as the jack-knife method.

3.6 References for Chapter 3

1. "Sensing A Paradigm Shift in the Field of Molecular Recognition: From Selective to Differential Receptors" Lavigne, J. J.; Anslyn, E. V. *Angew. Chem. Int. Ed.* **2001**, *40*, 3118-3130.

2. (a) "Solution-Based Analysis of Multiple Analytes by a Sensor Array: Toward the Development of an "Electronic Tongue"" Lavigne, J. J.; Savoy, S.; Clevenger, M. B.; Ritchie, J. E.; McDoniel, B.; Yoo, S. –J.; Anslyn, E. V.; McDevitt, J. T.; Shear, J. B.; Neikirk, D. *J. Am. Chem. Soc.* **1998**, *120*, 6429-6430. (b) "Development of Multianalyte Sensor Arrays composed of Chemically Derivatized Polymeric Microspheres Localized in Micromachined Cavities" Goodey, A.; Lavigne, J. J.; Savoy, S.; Rodriguez, M. D.; Curey, T.; Tsao, A.; Simmons, G.; Wright, J.; Yoo, S. –J.; Sohn, Y.; Anslyn, E. V.; Shear, J. B.; Neikirk, D.; McDevitt, J. T. *J. Am. Chem. Soc.* **2001**, *123*, 2559-2570.

3. "Differential Receptors Create Patterns That Distinguish Various Proteins" Wright, A. T.; Giffin, M. J.; Zhong, Z.; McClesky, S. C.; Anslyn, E. V. *Angew. Chem. Int. Ed.* **2005**, *44*, 6375-6378.

4. "A Differential Array of Metalated Synthetic Receptors for the Analysis of Tripeptide Mixtures" Wright, A. T.; Anslyn, E. V.; McDevitt, J. T. *J. Am. Chem. Soc.* **2005**, *127*, 17405-17411.

5. "Pattern-Based Peptide Recognition" Collins, B. E.; Anslyn, E. V. *Chem. Eur. J.* **2007**, *13,* 4700-4708.

6. "Pattern-Based Discrimination of Enantiomeric and Structurally Similar Amino Acids: An Optical Mimic of the Mammalian Taste Response" Folmer-Anderson, J. F.; Kitamura, M.; Anslyn, E. V. *J. Am. Chem. Soc.* **2006**, *128*, 5652-5653.

7. "Selective Sensing of Metalloproteins from Nonselective Binding Using a Fluorogenic Amphiphilic Polymer" Sandanaraj, B. S.; Demont, R.; Aathimanikandan, S. V.; Savariar, E. N.; Thayumanavan, S. *J. Am. Chem. Soc.* **2006**, *128*, 10686-10687.

8. "Generating Patterns for Sensing Using a Single Receptor Scaffold" Sandanaraj, B. S.; Demont, R.; Thayumanavan, S. *J. Am. Chem. Soc.* **2007**, *129*, 3506-3507.

9. "Colorimetric Molecularly Imprinted Polymer Sensor Array using Dye Displacement" Greene, N. T.; Shimizu, K. D. *J. Am. Chem. Soc.* **2005**, *127*, 5695-5700.

10. "A Colorimetric Sensor Array for Organics in Water" Zhang, C.; Suslick, K. S. *J. Am. Chem. Soc.* **2005**, *127*, 11548-11549.

11. "Supramolecular Analytical Chemistry" Anslyn, E. V. *J. Org. Chem.* **2007**, *72*, 687-699.

12. "Array-Based Sensing of Proteins Using Conjugated Polymers" Miranda, O. R.; You, C. –C.; Phillips, R.; Kim, I. –B.; Ghosh, P. S.; Bunz, U. H. F.; Rotello, V. M. *J. Am. Chem. Soc.* **2007**, *129*, 9856-9857.

13. "Sensors—An effective approach for the detection of explosives" Singh, S. *J. Haz. Mater.* **2007**, *144*, 15-28.

14. *Nitroaromatics and Nitramines by High Performance Liquid Chromatography (HPLC)*; Report No.: SW-846 Update III, Method 8330; U.S. Environmental Protection Agency: Washington, DC, 1994.

15. "Practical modifications to U.S. EPA method 8330 for the analysis of explosives by HPLC" Weisberg, C. A.; Ellickson, M. L. *Am. Lab.* **1998**, *30*, 32N-32V.

16. "Fluorescence Quenching as an Indirect Detection Method for Nitrated Explosives" Goodpaster, J. V.; McGuffin, V. L. *Anal. Chem.* **2001**, *73*, 2004-2011.

17. “Micellar electrokinetic capillary chromatography of high explosives utilising indirect fluorescence detection” Kennedy, S.; Caddy, B.; Douse, J. M. F. *J. Chromatogr.* **1996**, *726,* 211-222.

18. “In-line coupling capillary electrochromatography with amperometric detection for analysis of explosive compounds” Hilmi, A.; Luong, J. H. T. *Electrophoresis* **2000**, *21*, 1395-1404.

19. “Chemical sensing of DNT by engineered olfactory yeast strain” Radhika, V.; Proikas-Cezanne, T.; Jayaraman, M.; Onesime, D.; Ha, J. H.; Dhanasekaran, D. N. *Nat. Chem. Biol.* **2007**, *3*, 325-330.

20. “Sensitive determination of RDX, nitroso-RDX metabolites, and other munitions in ground water by solid-phase extraction and isotope dilution liquid chromatography–atmospheric pressure chemical ionization mass spectrometry” Cassada, D. A.; Monson, S. J.; Snow, D. D.; Spalding, R. F. *J. Chromatogr. A* **1999**, *844*, 87-95.

21. “Detection of explosives on skin using ambient ionization mass spectrometry” Justes, D.R.; Talaty, N.; Cotte-Rodriquez, I.; Cooks, R. G. *Chem. Commun.* **2007**, 2142-2144.

22. “Desorption Electrospray Ionization of Explosives on Surfaces: Sensitivity and Selectivity Enhancement by Reactive Desorption Electrospray Ionization” Cotte-Roderiquez, I.; Takats, Z.; Talaty, N.; Chen, H.; Cooks, R. G. *Anal. Chem.* **2005**, *77*, 6755-6764.

23. “Detection of trinitrotoluene in water by fluorescent ion-exchange resins” Heller, C. A.; McBride, R. R.; Ronning, M. A. *Anal. Chem.* **1977**, *49*, 2251-2253.

24. “Detection of Explosives with a Fluorescent Nanofibril Film” Naddo, T.; Che, Y.; Zhang, W.; Balakrishnan, K.; Yang, X.; Yen, M.; Zhao, J.; Moore, J. S.; Zang, L. *J. Am. Chem. Soc.* **2007**, *129*, 6978-6979.

25. “Polymer sensors for nitroaromatic explosives detection” Toal, S. J.; Trogler, W. C. *J. Mater. Chem.* **2006**, *16*, 2871-2883.

26. “High-Speed Fluorescence Detection of Explosives-like Vapors” Albert, K. J.; Walt, D. R. *Anal. Chem.* **2000**, *72*, 1947-1955.

27. “Effect of Polycyclic Aromatic Hydrocarbons on Detection Sensitivity of Ultratrace Nitroaromatic Compounds” Zhang, H. –X.; Chen, Q.; Wen, R.; Hu, J. –S.; Wan, L. –J. *Anal. Chem.* **2007**, *79*, 2179-2183.

28. “Porous Shape Persistent Fluorescent Polymer Films: An Approach to TNT Sensory Materials” Yang, J. –S.; Swager, T. M. *J. Am. Chem. Soc.* **1998**, *120*, 5321-5322.

29. “Oxidative Cyclization of Bis(biaryl)acetylenes: Synthesis and Photophysics of Dibenzo[*g,p*]chrysene-Based Fluorescent Polymers” Yamaguchi, S.; Swager, T. M. *J. Am. Chem. Soc.* **2001**, *123*, 12087-12088.

30. “Fluorescent Porous Polymer Films as TNT Chemosensors: Electronic and Structural Effects” Yang, J. –S.; Swager, T. M. *J. Am. Chem. Soc.* **1998**, *120*, 11864-11873.

31. www.icxt.com/products/icx-detection/explosives/fido/

32. “A Fluorescence Turn-On Mechanism to Detect High Explosives RDX and PETN” Andrew, T. L.; Swager, T. M. *J. Am. Chem. Soc.* **2007**, *129(23)*, 7254 - 7255.

33. “Luminescent probes for detergent solutions. A simple procedure for determination of the mean aggregation number of micelles” Turro, N. J.; Yekta, A. *J. Am. Chem. Soc.* **1978**, *100*, 5951 – 5952.

34. “Absorption and emission studies of solubilization in micelles. Part 1.—Pyrene in long-chain cationic micelles” Dorrance, R. C.; Hunter, T. F. *J. Chem. Soc., Faraday Trans. 1* **1972**, *68*, 1312-1321.

35. Vullev, V. I.; Jiang, H.; Jones, G. II, in *Topics in Fluorescence Spectroscopy*, ed. C. D. Geddes and J. R. Lacowicz, Springer, New York, 2005, vol. 10, ch. 7, pp. 216.

36. Bhairi, S. M. *Detergents: A guide to the properties and uses of detergents in biological systems*; Calbiochem-Novabiochem Corp.: La Jolla, CA, 2001; p 38.

37. “Potential analytical applications of differential fluorescence quenching: pyrene monomer and excimer emissions as sensors for electron deficient molecules” Focsaneanu, K. –S.; Scaiano, J. C. *Photochem. Photobiol. Sci.* **2005**, *4*, 817-821.

Chapter 4. The Determination of Enantiomeric Excess in α-Chiral Alcohols Using Supramolecular Chemistry. Part I. Toward the Development of an Indicator Displacement Assay Using Ti^{IV} Alkoxides Complexed with Chiral Diol Ligands.

4.1 The Determination of Enantiomeric Excess

The importance of chirality in biological systems has been repeatedly established. From the right-handed helix of DNA to the left handed power hitters of Major League Baseball, the fundamental difference between non-super-imposable mirror image type structures in nature can be profound. The synthetic chemist's pursuit of chiral purity stems from the enantiomerically pure natural products that he or she seeks to replicate and from the empirically disastrous effects of pharmaceutical racemates, the most famous being Thalidomide. The primary bottleneck in the pursuit of enantioselective methods is the analysis of the *ee* or chiral purity of the reaction products.[1]

The laboratory scale determination of *ee* is currently performed using chiral GC and HPLC methods, and high-throughput variants of these techniques as well as mass spectrometry and capillary electrophoresis are able to scan sample sets in the thousands per day.[1] An alternative method of *ee* determination is via spectrophotometry, including UV-visible, fluorescence, circular dichroism (CD) and IR. A number of spectrophotometric methods have been developed to determine the enantiomeric excess of a variety of functional groups. Spectrophotometric analysis of *ee* has two major advantages over chromatographic methods: (1) spectrophotometric hardware tends to be cheaper, more reliable, and easier to use than chromatographic systems, and (2) because retention time is a variable in chromatographic systems, these methods are inherently slower than spectrophotometric methods whose execution may require the observation of as little as a single wavelength of light. The difficulty of the spectrophotometric determination of *ee* lies in transducing chiral information into a measurable signal.

The only spectrophotometric method for the direct quantification of *ee* is CD, which is limited to use with analytes having chromogenically active groups near their chiral center. With all other spectrophotometric methods the observation of *ee* requires

the presence of a chiral bias and an optical transduction mechanism, and the most convenient method to fulfill these requirements is through supramolecular chemistry.

4.1.1 Supramolecular Analytical Systems for the Optical Determination of Enantiomeric Excess

The term chiral bias refers to the presence of a stereocenter in the, usually macromolecular, host that will lead to a diastereomeric complex upon binding of the host to either enantiomer of the analyte. For a given enantiomer of the host these complexes are non-degenerate in energy and will be formed to different extents according to their relative stabilities. An optical signaling system that reports the complexation of host and guest will therefore correlate directly to *ee* when the total concentration of analyte is known. Among the reported systems relying upon the thermodynamic stability of host-guest diastereomers, two signaling motifs are common: (1) structural or electronic changes in the host itself upon binding that result in a modulation of spectrophotometric properties, or (2) the displacement of a reversibly bound indicator from the host that results in a change in the properties of the indicator due to changes in the protonation state or solvatochromic environment, etc. A third type of system for the spectrophotometric determination of *ee*, which involves the kinetic resolution of pseudo-enantiomeric chiral indicators has also been demonstrated.[2]

4.1.1.1 Covalently attached signaling agents

The most common chiral reporters have been 1,1'-binaphthyl based compounds (Figure 4.45). The ability of the 1,1'-binaphthyl moiety to serve as the reporter and the source of chiral bias has been heavily exploited just as it has also found considerable utility in the development of enantioselective catalysis.[3] Irie *et al.* first reported differences in the quenching efficiency of (R)-(+)- and (S)-(-)-N,N-dimethyl-α-phenylethylamine with respect to (R)-(-)-1,1'-binaphthyl fluorescence in 1978.[4] The thrust of this work was formally to provide evidence of the role of specific geometry in

certain modes of fluorescence quenching, but it served as inspiration for a spate of binaphthyl-based chiral amine quenching assays to come.

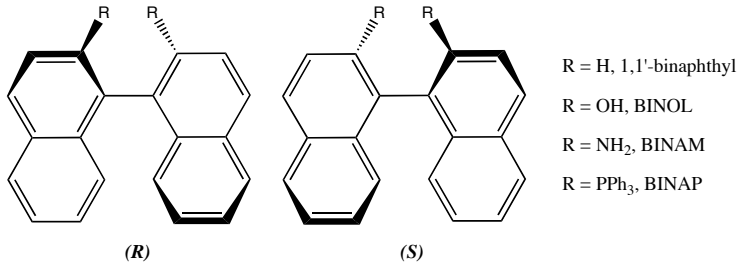

Figure 4.45 ***A series of common binaphthyl based compounds.*** The binaphthyl core has proven popular in enantioselective catalytic and sensing applications.

One of the first supramolecular systems to effect colorimetric detection of chirality came from the Kubo group. Their system relied on a calixarene tethered to an (*S*)-BINOL, and was shown to bind enantio-exclusively to the (*R*)-enantiomers of phenylglycinol, phenylalaninol and phenylglycine, while no binding to either enantiomer of phenylethyl amine was reported (Figure 4.46).[5] Although the BINOL group was present, binding was reported in terms of the absorbance shift of the host.

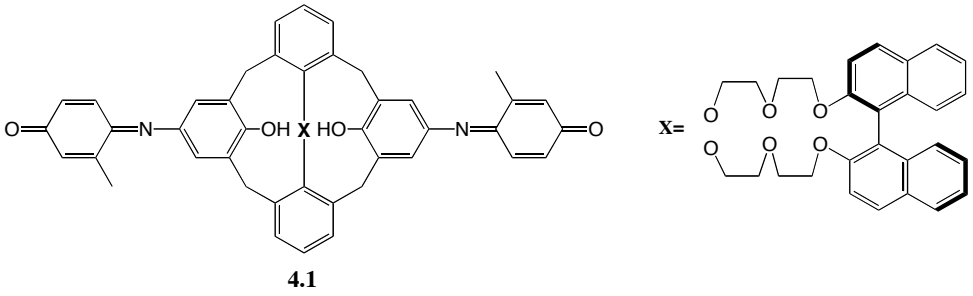

4.1

Figure 4.46 ***An early enantioselective design.*** Compound **4.1** selectively binds the (*R*)-enantiomers of phenylglycinol, phenylalaninol and phenylglycine in ethanol.

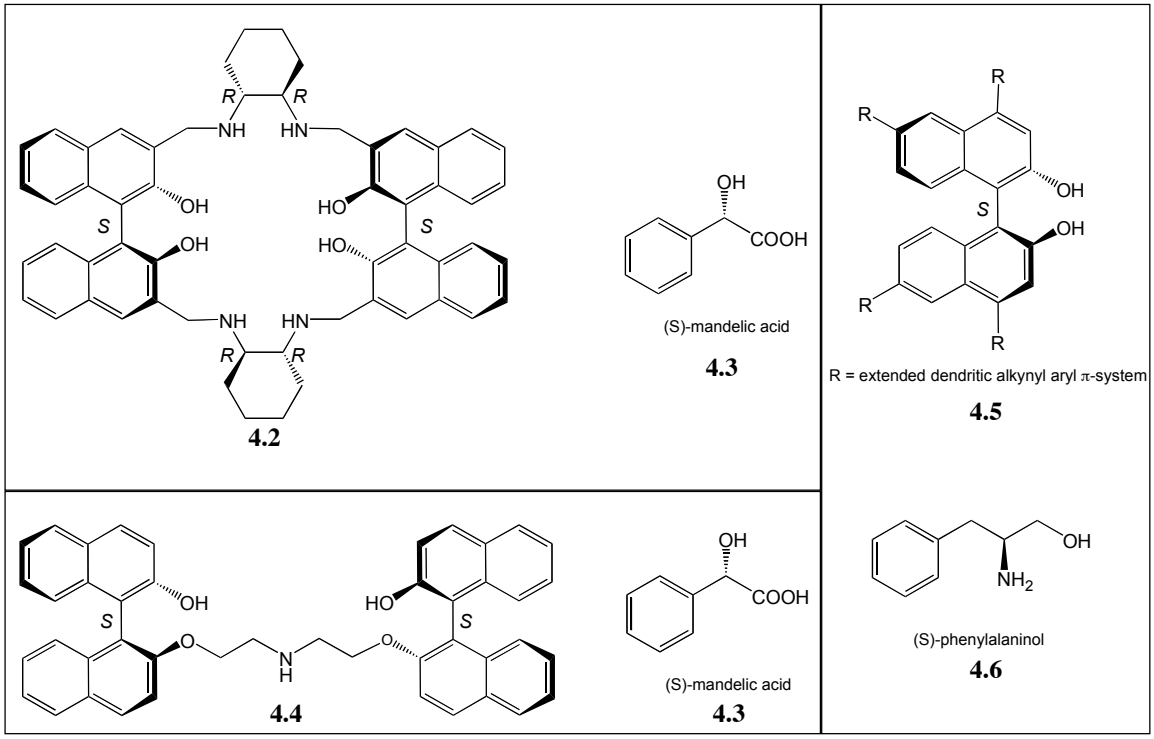

Figure 4.47 ***A series of fluorescent hosts from the Pu group.*** The hosts are pictured with the enantiomer of the analyte that they preferentially bind.

The Pu group especially has developed numerous sensors for the discrimination of not only chiral amines, but also amino alcohols and α-hydroxy carboxylic acids, all using the 1,1'-binaphthyl core to provide chiral bias and signal transduction for the determination of *ee* (Figure 4.47).[6]

The first reported chiral sensor having a C_3-symmetric binding environment was reported by the Ahn group (Figure 4.48). **4.7** displays an increase in fluorescence when binding chiral ammonium salts that was unexpected due to the lack of traditional fluorophores on the host. This off-on behavior was attributed to increase in rigidity that reduced the facility of non-radiative relaxation pathways for the host.

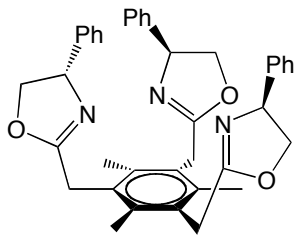

4.7

Figure 4.48 ***A C_3-symmetric sensor.*** This fluorescent sensor from the Ahn group exhibits off-on signaling and is enantioselective for (*R*)-methylbenzyl ammonium.

4.1.1.1 Enantioselective indicator displacement assays

The first enantioselective IDA was reported by the Anslyn group for the discrimination of α-hydroxyacids (Scheme 4.19). Operating in aqueous methanol, this system relied upon reversible covalent boronic ester formation to effect indicator and analyte binding. The degree of indicator displacement by the chiral analytes is determined by the stability of the resultant host-analyte diastereomer. In the case of **4.8** binding to phenyllactic acid, the indicator displace signaled a steric preference for D-phenyllactic acid by (*R,R*)-**4.8** and L-phenyllactic acid by (*S,S*)-**4.8**.[7] Another application of chiral IDA's that has been reported by the Anslyn group is the enantioselective discrimination of α- chiral amino acids (Scheme 4.20).[8] This system was later used in an array sensing protocol that was described in Chapter 3.

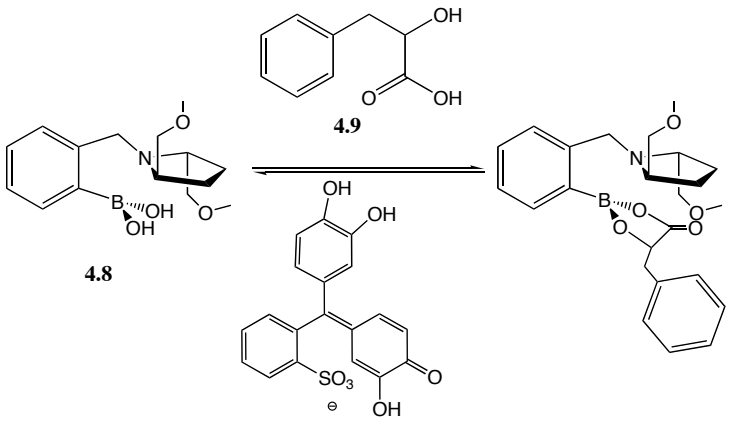

4.9

4.8

4.10

Scheme 4.19 *The first chiral IDA.* The simple boronic acid host **4.8** showed enantioselective binding to α-hydroxyacids.

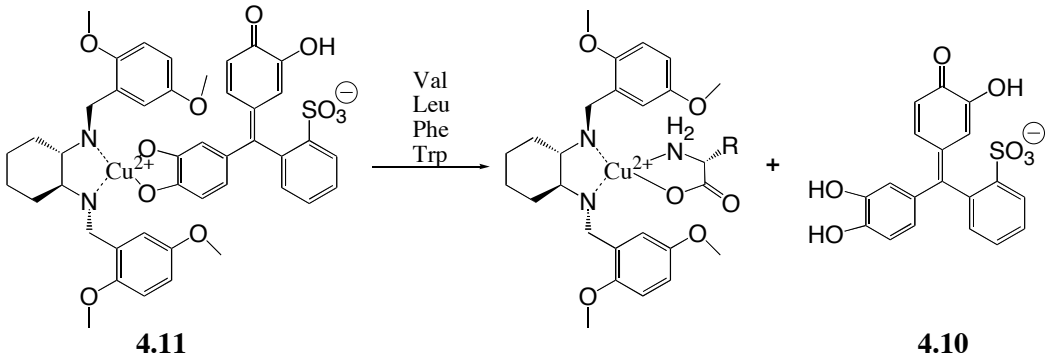

4.11 **4.10**

Scheme 4.20 ***An IDA for chiral amino acids.*** Host **4.11** was enantioselective for the D-enantiomer of the hydrophobic amino acids shown.

4.1.2 The Supramolecular Chemistry of Mono-alcohols

Supramolecular sensing has seen great success in developing sensing protocols for a number of functional groups, but one class that has proven to be continually elusive however is simple alcohols. Alcohols exhibit some H-bond donor/acceptor activity,[9] but only minimal metal coordination in their neutral state. One of the only examples of differential binding between simple alcohols comes from the Yoshida group who covalently attached a naphthyl group to β-cyclodextrin to create a sensor for cycloalkanols in water. The alcohols were discriminated based upon the size of the aliphatic group, which caused a change in the molar ellipticity of the host upon binding

the alcohol (Scheme 4.21).[10] To sense alcohols in water is an impressive feat, however binding in the Yoshida system is driven hydrophobically and not by the alcohol moiety, so it is unclear how selective their system is for the class, alcohols, despite being able to differentiate between members of the class. It is well known that cyclodextrins can bind hydrophilic molecules in water and therefore it's difficult to determine the relevance of this study in terms of alcohol binding. This example illustrates just how elusive a true sensor for simple alcohols remains.

The difficulty of developing an alcohol sensor lies in the weakness of monodentate alcohol coordination. In order to offset the weakness of a single hydroxyl group as functional binding handle it is necessary to use extremely oxophilic Lewis acids, which are found mostly among the transition metals of the early *d*-block. The oxophilicity of such species results also in extreme sensitivity to adventitious water either as a route to decomposition, *e.g.* hydrolysis of Ti^{IV} compounds to TiO_2, or simply as a competitor of analyte alcohols for coordination sites. The problem of sensing and differentiating simple alcohols is at its most extreme when it is desired to differentiate between the two enantiomers of a given structure. We chose to focus on converting the Sharpless epoxidation catalyst to an enantioselective sensor of simple alcohols, despite the sensitivity of Ti^{IV} to water, because it has shown utility in differentiating secondary allylic alcohols.[11]

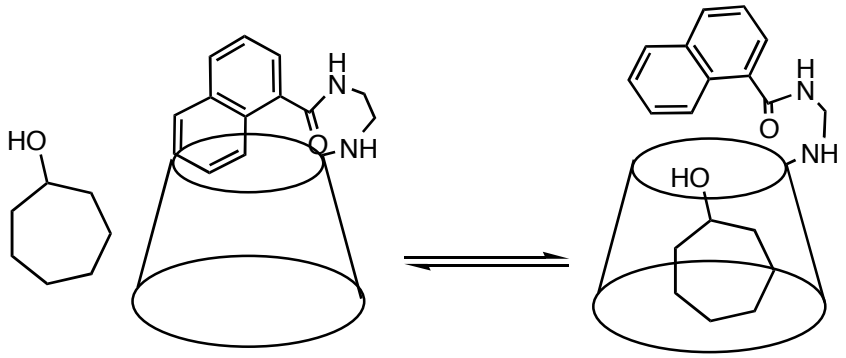

4.11 **4.12**

Scheme 4.21 ***The Yoshida β-CD alcohol sensor.*** Bulky aliphatic alcohols enter the β-CD cavity and perturb the molar ellipticity of the naphthyl moiety.

4.2 Modifying the Sharpless Epoxidation System for Use in Organometallic Indicator Displacement Assays

The Sharpless epoxidation system for allylic alcohols is arguably the most well-known, widely applied and robust chiral transformation found in the synthetic literature.[12] The Sharpless system consists of a Ti^{IV} alkoxide made chiral *via* complexation with an ester of tartaric acid. These systems are normally used with *tert*-butylperoxide as the stoichiometric oxidizing agent. For a given allylic alcohol, the face that will be epoxidized is selected by the choice of tartrate ester enantiomer used (Scheme 4.22).[11] When it was first developed this system required stoichiometric amounts of Ti^{IV} and tartrate ester,[11,13] but the addition of molecular sieves led to the Sharpless system's general applicability with catalytic amounts of Ti^{IV}.[14,15] The active catalyst has been shown to be a Ti^{IV}:tartrate ester 2:2 dimer with epoxidation occurring at a single Ti^{IV} center (Figure 4.49).[16,17,18,19,20] The same Ti^{IV}/tartrate ester system has also proven effective for the kinetic resolution of racemic allylic alcohols.[15,21] As with the epoxidation of prochiral substrates, the allylic alcohol enantiomer that will be epoxidized more quickly can be determined by the choice of tartrate ester enantiomer used. It is this discrimination of chiral substrates prior to reaction that inspired us to try to convert the Sharpless epoxidation system to an indicator displacement assay for the determination of enantiomeric excess in simple alcohols.

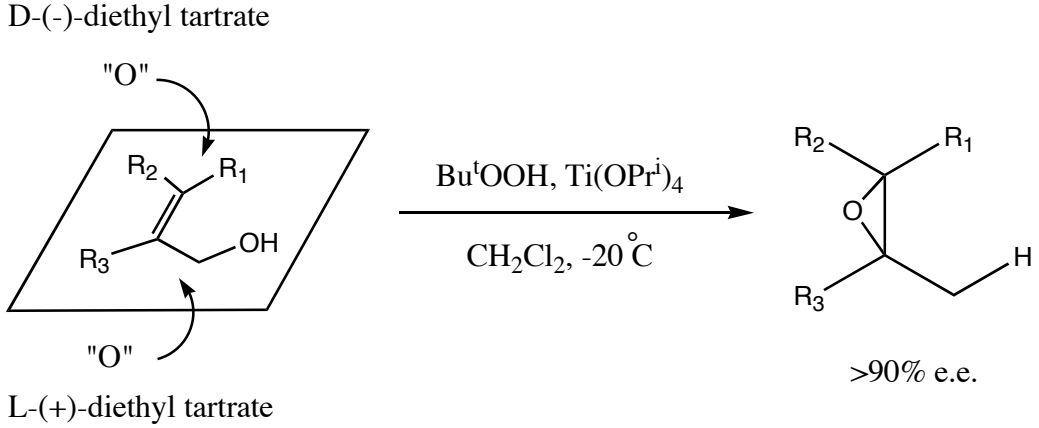

Scheme 4.22 ***The Sharpless epoxidation system.*** The face of the allylic alcohol that becomes epoxidized is dictated by the chirality of the tartrate ester.

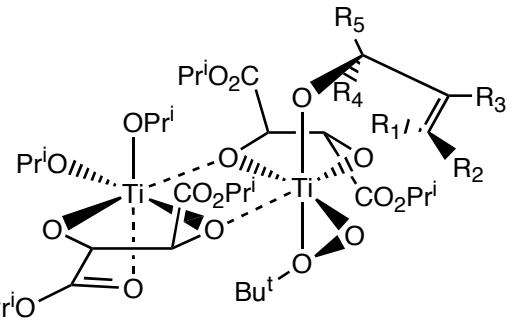

Figure 4.49 ***The active catalyst in the Sharpless epoxidation of allylic alcohols.*** The complex shown is generated from $Ti(OPr^i)_4$ and the diisopropyl tartrate ester, but a number of other alkoxides and esters are also common.

4.2.1 Strategy

We postulated that because the Ti^{IV}-tartrate ester complex of the Sharpless system can discriminate α-chiral alcohols in the transition state of the epoxidation reaction, it could therefore be optimized to act as a sterically sensitive host system for the spectrophotometric determination of *ee* by the incorporation of a signaling element. We chose to pursue an IDA style signaling system.

The binding sites available to indicators and alcohol analytes on the Ti:tartrate ester dimer are those positions occupied by residual alkoxides after chelation of the tartrate ester diol moieties. The titanium/tartrate ester complexes are shown in monomeric form in Scheme 4.23 because for the purposes of the argument at hand the binding stoichiometries of the monomer are the same as in the dimer, and the monomeric form is more clearly represented in two-dimensions. As shown, there is room for the coordination of a single bidentate chelating indicator (bromopyrogallol red) or potentially two monodentate coordinating indicators (*para*-nitrophenol, PNP, **4.14**). Preliminary qualitative attempts to displace these indicators using methanol indicated that it was possible to displace a phenolic indicator (PNP) with a simple alcohol, but not an indicator having a catechol functionality. The ability of the [Ti^{IV}(tartrate)] complex to bind multiple equivalents of a monodentate indicator leads to a larger series of possible complexes than is normally seen in an IDA.

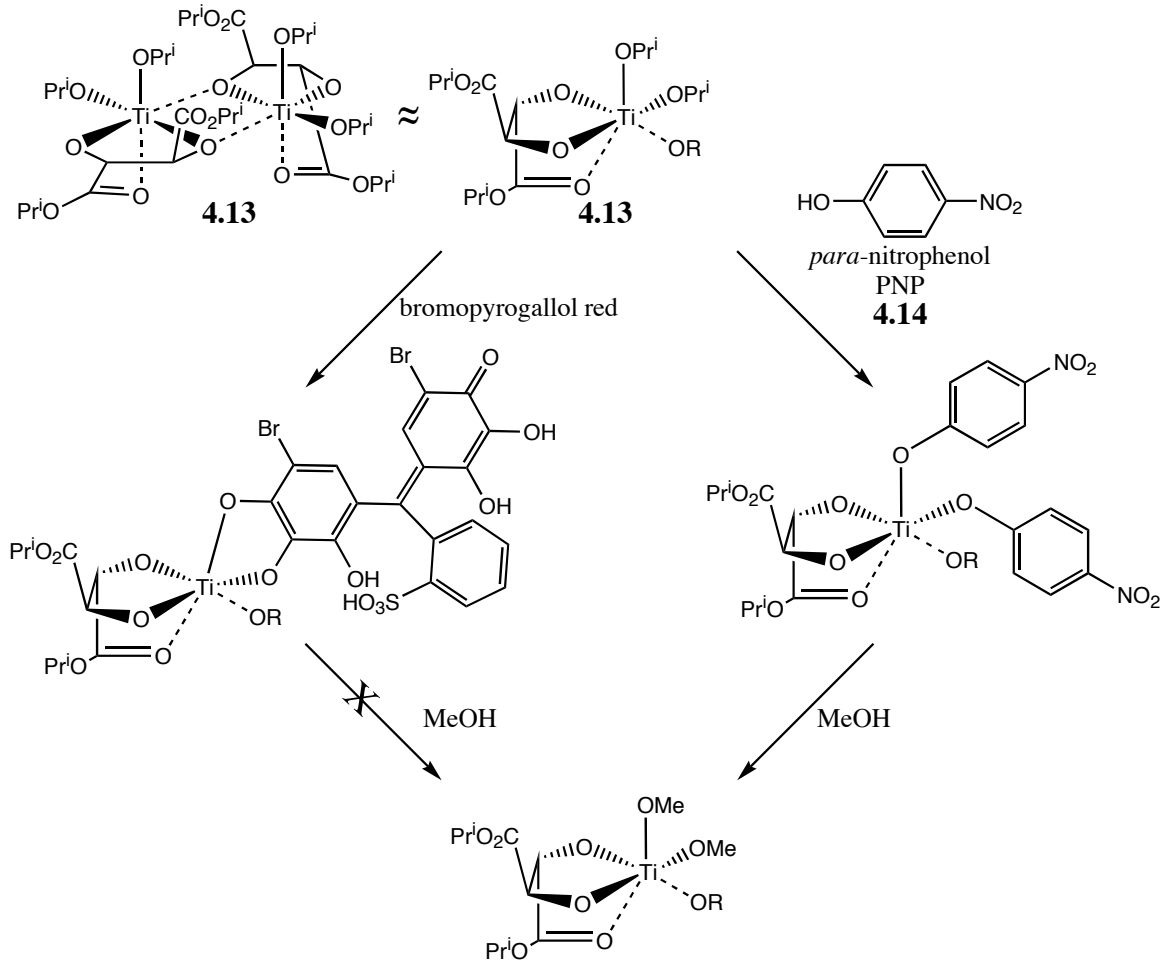

Scheme 4.23 ***Chelating and coordinating indicators binding to [Ti(OPr^i)$_2$(diisopropyltartrate)]*** **4.13.** In early qualitative experiments, methanol was able to effect color change in PNP treated solutions, but not those having bromopyrogallol red. The difference was attributed to stronger bidentate binding of the titanium center by bromopyrogallol red.

Scheme 4.24 shows the different modes of signaling that one could expect when Ti(OPr^i)$_4$ is treated with one equivalent of tartrate ester and one or two equivalents of a phenolic indicator, all of which could lead to a usable sensor, but not all of which are traditional IDAs. It is known that phenoxides will preferentially displace alkoxides from Ti^{IV},[22] so in reaction A in Scheme 4.24 it is assumed that coordinated isopropoxide will be displaced prior to displacement of the phenoxide indicator. It is possible that replacement of isopropoxide with an incoming aliphatic alcohol analyte could result in modulation of the absorption of the bound phenolic indicator, but such a modulation may

not be sufficiently large to use for sensing. It should be noted that one difficulty of using Ti/tartrate ester complexes made *in situ* for alcohol sensing is the presence of free isopropanol produced in the initial complex formation. The free isopropanol is a titanium-coordinating compound in competition with the analyte alcohol and results in an observed reduction in the binding affinity of the analyte alcohol to the titanium ^{IV} complex. However, because of the aforementioned preference of Ti^{IV} for phenoxide ligands, it was anticipated that excess alcohol analyte would be required to displace the phenoxide-based indicator anyway, thereby making competition effects from the isopropanol negligible. The titanium/tartrate ester complex can also be prepared from $Ti(OBu^t)_4$ to yield the less competitive *tert*-butanol as a side product.

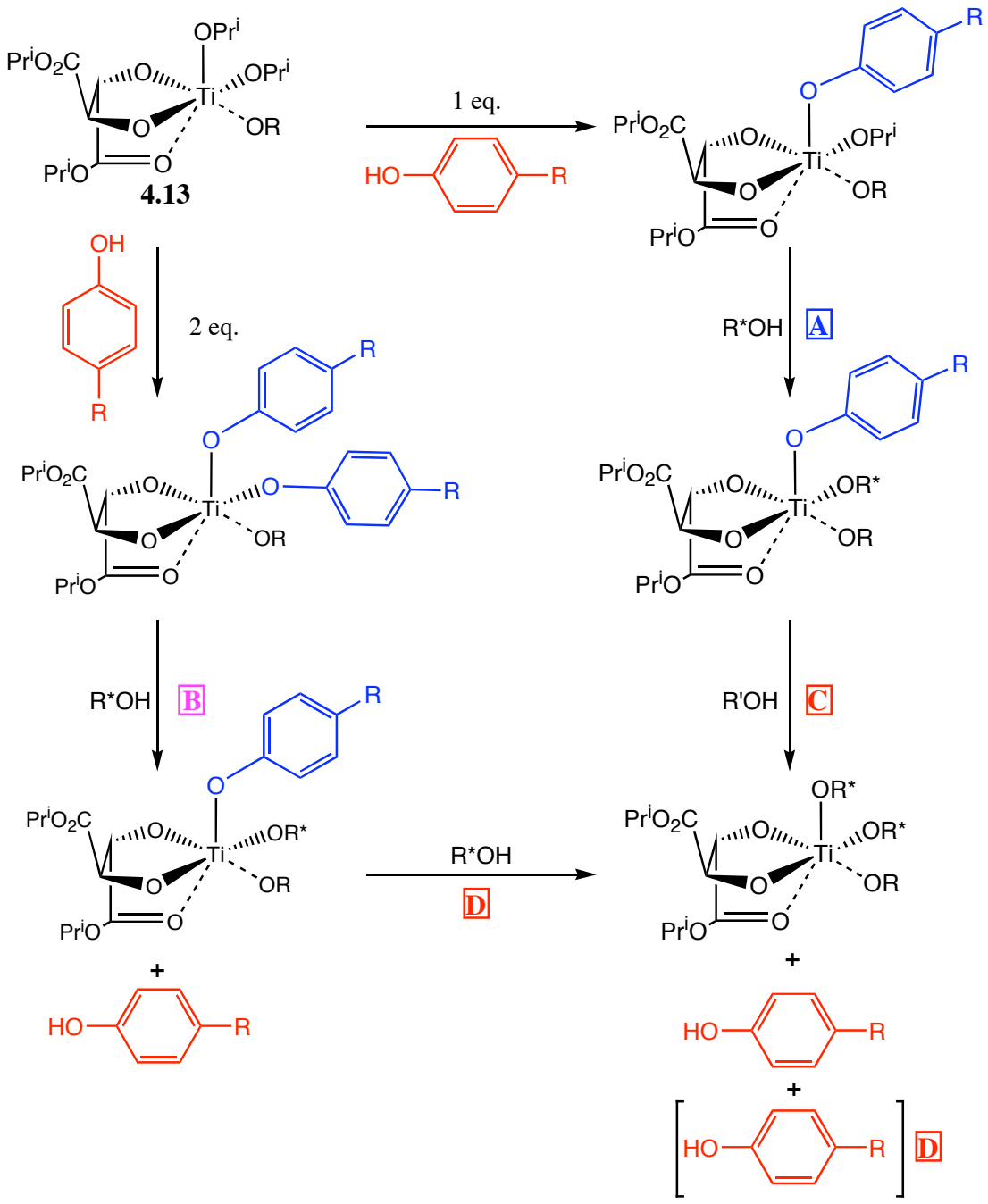

Scheme 4.24 ***Monodentate indicators allow multiple signaling possibilities.*** Modes of signaling that might be anticipated given the presence of two coordination sites on TiDET. Reaction A could conceivably generate a usable signal modulation while reactions B, C and D constitute traditional indicator displacement signaling.

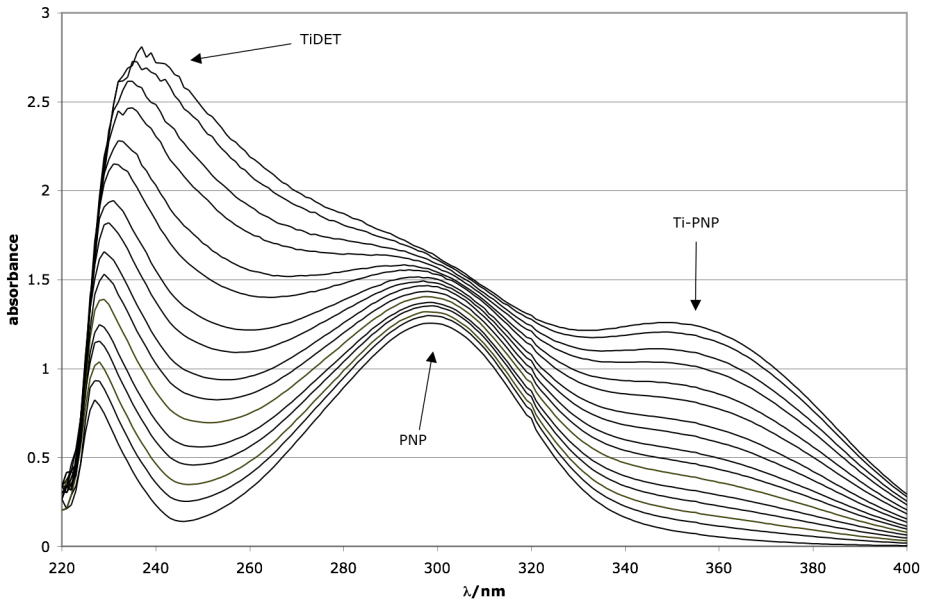

Figure 4.50 ***TiDET into PNP.*** Absorption spectra of PNP (100 μM) as Ti:DET (500 μM) is added. Interference by TiDET absorption obscures the developing Ti-PNP signal.

4.2.2 Finding an Indicator

Early results using PNP as an indicator were promising. PNP develops a yellow color upon addition of the Ti^{IV} tartrate ester complex and this solution becomes colorless upon the addition of excess methanol. This colorimetric shift is ostensibly due to the protonation of PNP upon displacement from the Ti^{IV} center by methanol. From this preliminary qualitative success came a UV-Vis titration study on the binding of PNP to a $Ti(OPr^{i})_4$:L-diethyltartrate complex (TiDET). Titrations were carried out in DCM at -20 °C in order to prevent transesterification of the tartrate ester as prescribed in the literature.[11] Full experimental details are available at the end of the chapter. Attempts to determine a stoichiometry of binding and relevant affinities were thwarted by an overlap in the absorbance of PNP with that of the added TiDET (Figure 4.50), which yielded binding isotherms unsuitable for fitting analysis. Therefore, other monodentate indicators with longer wavelength absorptions were screened for binding to TiDET.

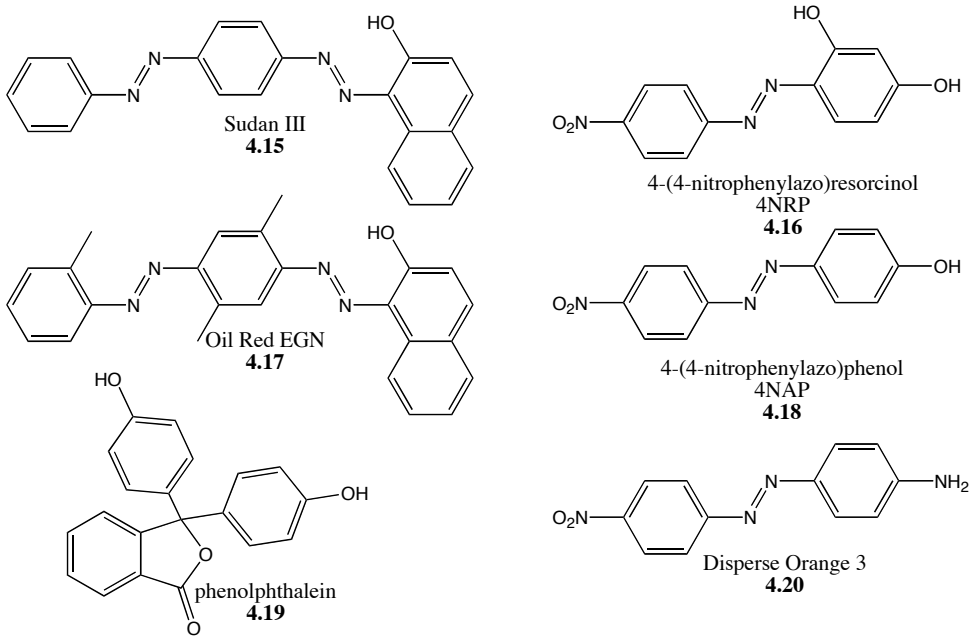

Figure 4.51 ***Phenolic and anilinic indicators.*** Indicators that were screened for binding to TiDET.

One anilinic and five phenolic indicators (Figure 4.51) were assessed for binding to TiDET. Among these six indicators, only 4-(4-nitrophenylazo)phenol (4NAP, **4.18**) and 4-(4-nitrophenylazo)resorcinol (4NRP, **4.16**) changed color upon addition of TiDET (Figure 4.52 and Figure 4.53). Despite the presence of what appears to be an isosbestic point, the titration with 4NAP did not yield a usable binding isotherm for the determination of binding stoichiometry and affinity apparently due to unexpectedly slow kinetics of indicator coordination (Figure 4.54). The titration isotherm for 4NRP looked similar to that for 4NAP, and the simplicity of a single phenolic group on 4NAP led us to focus our efforts on this compound.

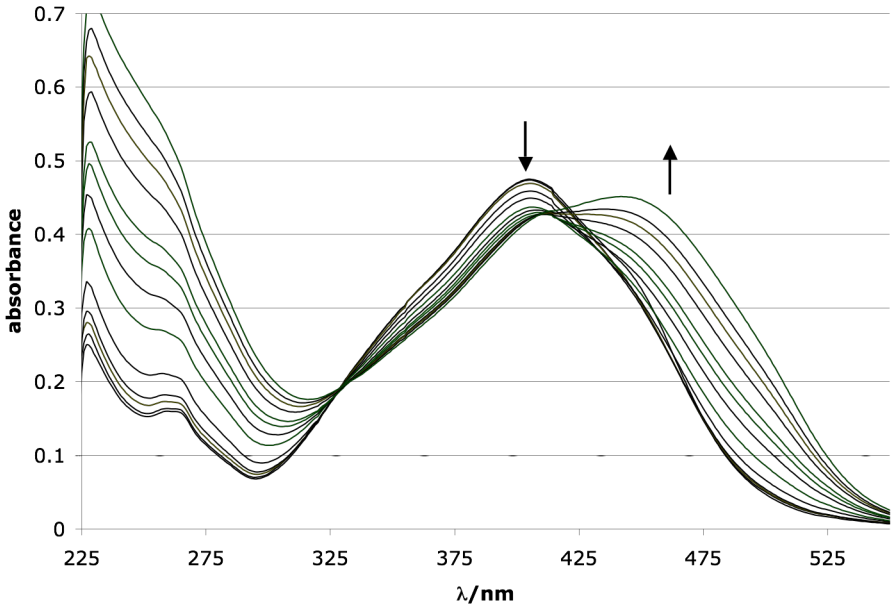

Figure 4.52 ***4NRP color change upon addition of TiDET.*** Titration of Ti:DET (100 μM) into 4NRP (20 μM).

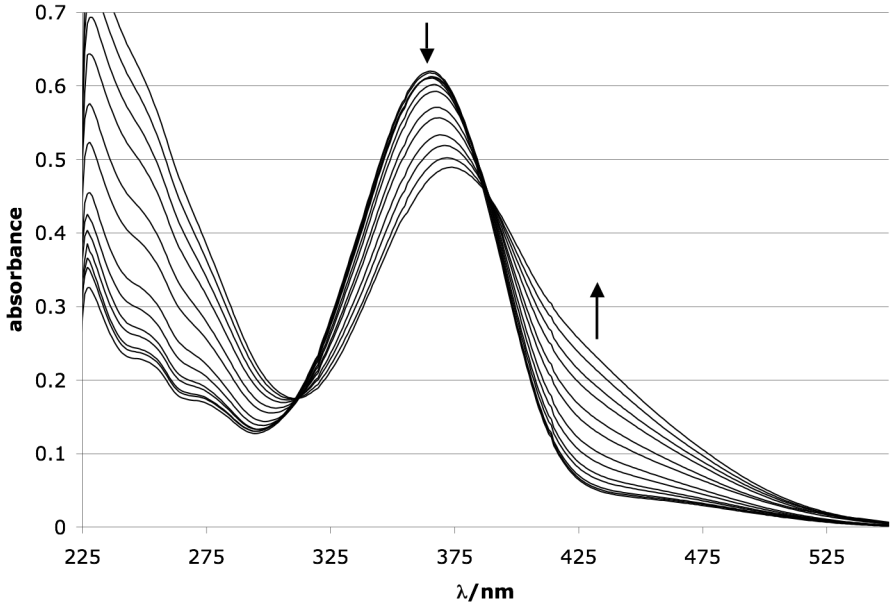

Figure 4.53 ***4NAP color change upon addition of TiDET.*** Titration of Ti:DET (100 μM) into 4NAP (20 μM).

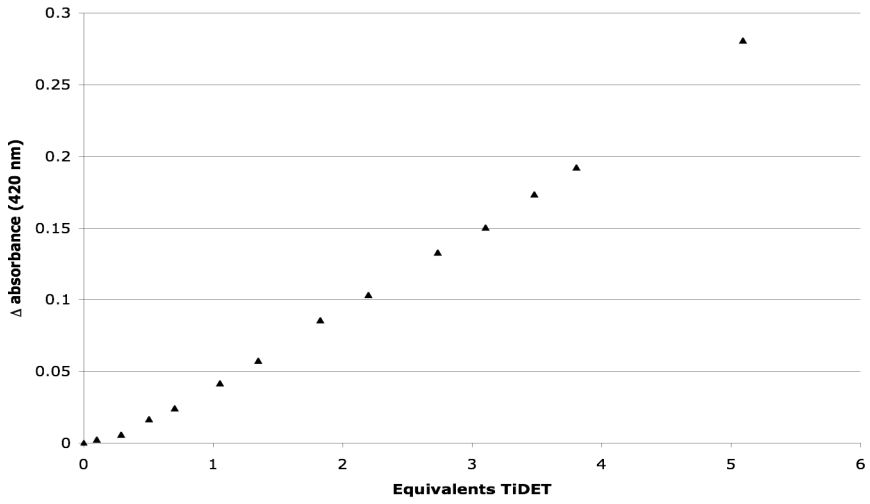

Figure 4.54 ***Plot of change in absorbance of 4NAP at 420 nm in*** **Figure 4.53.** Addition of TiDET to 4NAP (20 μM) yields an unusable isotherm when given insufficient time to react.

Because of the slow kinetics of indicator coordination, the isotherm of TiDET binding to 4NAP was developed using a series of separate samples in which 4NAP and various concentrations of TiDET were premixed and let to sit for 0.5 h before spectra were recorded. These solutions resulted in a reasonable binding isotherm that was spectrophotometrically stable for 4 h after the initial 0.5 h priming period (Figure 4.55). The binding isotherm indicates a weak association, which consequently presented no evidence of 1:2 TiDET:4NAP like that proposed in Scheme 4.24. The saturation of the isotherm appears to support that 4NAP is coordinating to the Ti^{IV} center, but the stoichiometry is unclear from this data. With a usable indicator in 4NAP, but a system that was difficult to interpret by UV-Vis, we decided to study the Ti^{IV}:ligand:indicator system by NMR.

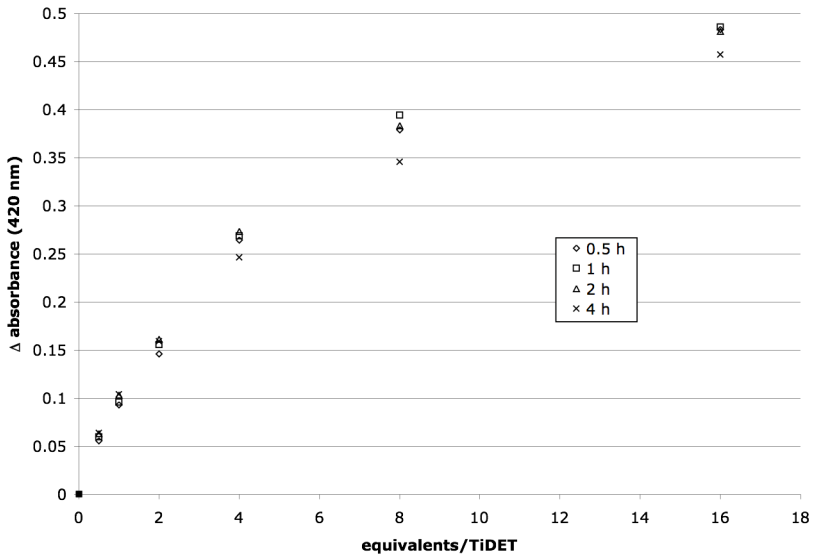

Figure 4.55 ***Titration of TiDET into 4NAP.*** Six samples all having 4NAP (20 μM) and different concentrations of TiDET in DCM were kept at -20 °C for 4 hours. During this time their spectra were collected at the times indicated. Changes in the plotted isotherm were minimal over this time period.

We also chose to change from the tartrate ester chiral ligand to ether diols (Figure 4.56). The literature indicates that Ti^{IV}:ether diol complexes are more stable to nucleophilic attack and show analogous behavior to tartrate esters in their propensity to form 2:2 Ti^{IV}:diol complexes.[23,24,25,26] While diol ethers perform poorly in enantioselective epoxidation, they are nonetheless capable of creating a chiral binding pocket for enantiomeric alcohols as they are known to form a stable complex with Ti^{IV} alkoxides at room temperature.[23,24] Transitioning from -20 °C to room temperature also greatly improves the ease with which experiments may be carried out, especially in light of the sensitivity of Ti^{IV} to moisture because working at room temperature allowed for titration solutions to be prepared in a glove box. The downside to working at room temperature is that DCM evaporation becomes a problem and solution concentrations are difficult to maintain as evaporation causes the solutions to concentrate. For this reason, and because they are known to be compatible with the Sharpless catalyst, the solvents of choice became toluene for the UV-Vis studies and d_6-benzene for NMR studies.

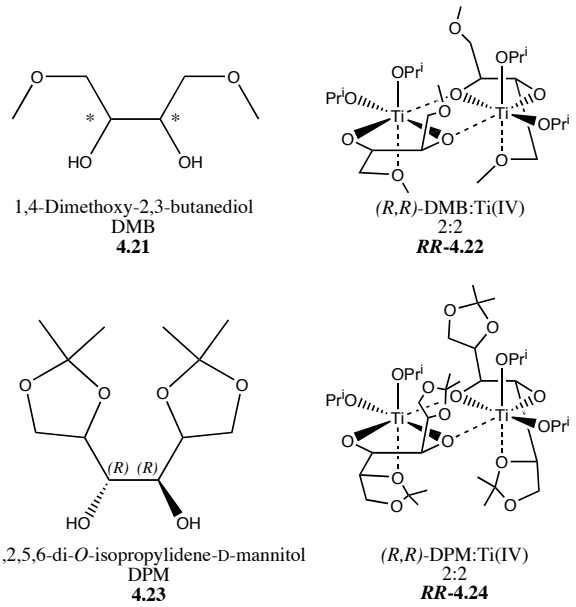

Figure 4.56 ***Chiral ether diol ligands.*** The necessity of working at -20 °C made the tartrate ester ligands burdensome to work with and therefore the chiral modifier of choice became diol ethers. Unlike tartrate esters, diol ethers are stable against nucleophilic attack at room temperature.

4.2.3 NMR Studies of Ti^{IV}-Based Host-Guest and Indicator Complexes.

The binding of the $Ti(OPr^i)_4$:DPM complex (TiDPM, **4.24**, Figure 4.56) to 4NAP was studied by H^1 NMR at a constant total concentration of 20 mM ([TiDPM] + [4NAP]) in hopes of producing a Job plot for the determination of the host/indicator binding stoichiometry. Interpretation of a Job plot using NMR requires the observation of a signal that is unique to the bound complex, and which should therefore be maximized at a host/guest concentration ratio that corresponds to the stoichiometry of the complex. Unfortunately, no peaks conclusively belonging to the TiDPM:4NAP complex were identified in the busy spectra. Instead of a Job plot, however, other evidence of a 1:2 TiDPM:4NAP complex analogous to that proposed in Scheme 4.24 was observed. First, the 4NAP was incompletely dissolved in the presence of fewer than 0.5 equivalents of TiDPM, above which it appeared to dissolve completely, possibly because it was pulled into solution upon coordination to the Ti^{IV} (Table 4.8). Additional evidence of the 1:2 complex was found by comparing the B protons of 4NAP (Figure 4.57) to the methyne

proton of free isopropanol (Scheme 4.25). The ratio of isopropanol to 4NAP protons (B) was calculated assuming 1:2, 1:1 and no binding scenarios between TiDPM and 4NAP (Table 4.9). The observed peak integration ratios most closely resemble the 1:2 binding scenario in which 4NAP is able to displace two equivalents of isopropoxide from the Ti^{IV} center (Figure 4.58). This result confirms the earlier interpretation of UV-Vis data that the color change observed upon addition of Ti^{IV}:ligand complex to 4NAP is indeed due to coordination of 4NAP to the Ti^{IV} center at the expense of bound alkoxide. Hence, we undertook a second NMR study to determine if an incoming secondary alcohol could similarly expel the bound isopropoxide.

Sample	[TiDPM] /mM	[4NAP] /mM	[4NAP]/ [TiDPM]	4NAP dissolved?
1	0	20	-	no
2	2.5	17.5	7	no
3	5	15	3	no
4	7.5	12.5	1.66	yes
5	10	10	1	yes
6	12.5	7.5	.60	yes
7	15	5	.33	yes
8	17.5	2.5	.14	yes
9	20	0	0	-

Table 4.8 ***4NAP solubility with respect to TiDPM equivalents.*** 4NAP becomes soluble in the presence of over 0.5 equivalents of TiDPM.

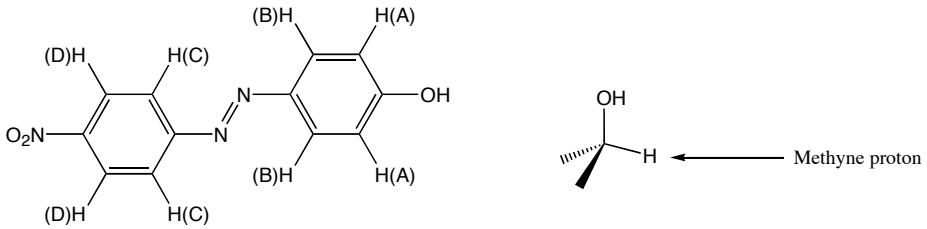

4NAP
4.14

isopropanol

Figure 4.57 ***The protons of 4NAP and isopropanol.*** In NMR experiments the "B" protons of 4NAP and the methyne proton of isopropanol could be integrated with minimal interference from surrounding peaks.

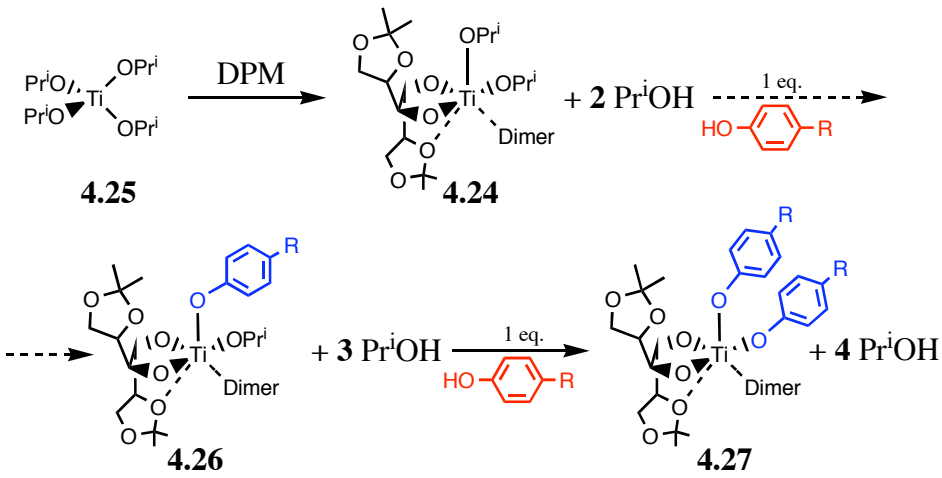

Scheme 4.25 ***The displacement of isopropoxide to form isopropanol.*** Complex **4.24** is shown as one half of the dimer seen in Figure 4.56. Each equivalent of bound 4NAP generates an equivalent of free isopropanol.

	Concentration of 4NAP and subsequent amount of "B" protons		*Concentration of TiDPM and attending two equivalents of isopropanol. This is the isopropanol concentration if no binding occurs*		*Concentration of isopropanol released if 4NAP binds once to TiDPM and resultant total concentration of isopropanol*		*Concentration of isopropanol released if 4NAP binds twice to TiDPM and resultant total concentration of isopropanol*		*Ratio of 4NAP "B" protons over isopropyl methyne protons at different binding stoichiometries*		
Sample	[4NAP] /mM	4NAP "B" protons	[TiDPM] /mM	Initial H PriOH	Released H PriOH (1:1)	Total H PriOH (1:1)	Released H PriOH (1:2)	Total H PriOH (1:2)	no binding	1:1	1:2
4	12.5	25	7.5	15	7.5	22.5	7.5 + 5	27.5	1.67	1.11	0.91
5	10	20	10	20	10	30	10	30	1.00	0.67	0.67
6	7.5	15	12.5	25	7.5	32.5	7.5	32.5	0.60	0.46	0.46
7	5	10	15	30	5	35	5	35	0.33	0.29	0.29
8	2.5	5	17.5	35	2.5	37.5	2.5	37.5	0.14	0.13	0.13

Table 4.9 ***The determination of theoretical ratios of isopropanol to 4NAP.*** The concentration of isopropanol in solution is the sum of that which is liberated upon 4NAP binding and the two equivalents generated during the initial formation of TiDPM from $Ti(OPr^i)_4$.

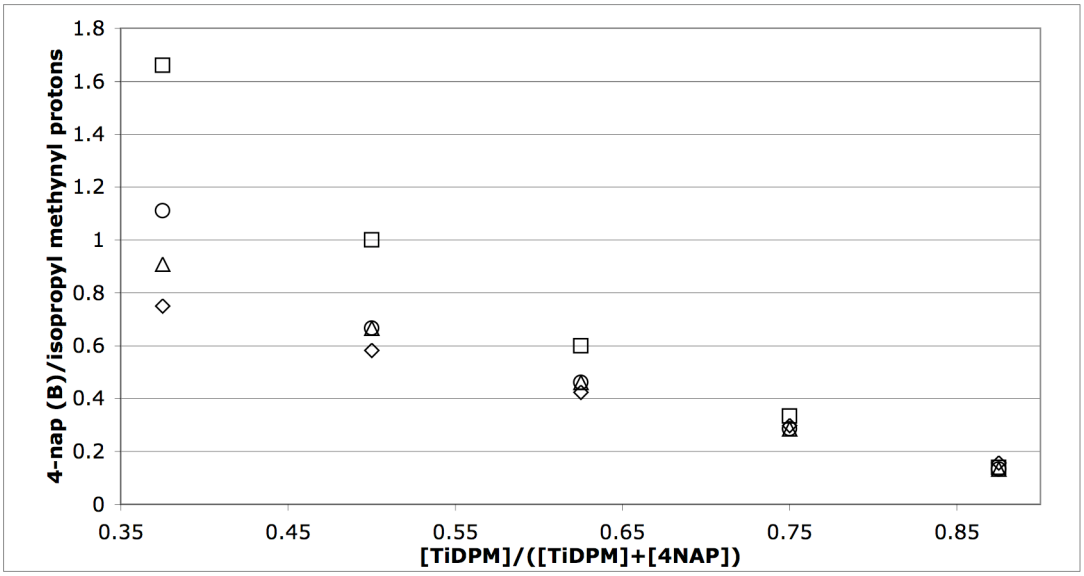

Figure 4.58 ***Observed and calculated ratios of 4-nap (B) to isopropyl methyne protons.*** The x-axis is the TiDPM fraction of total guest concentration. ◇, observed; △, calculated for 1:2 TiDPM:4NAP; ○, calculated for 1:1 TiDPM:4NAP; □, calculated for a scenario in which no binding occurs.

Equivalents of 1PhEtOH / TiDPM	Calculated concentrations with no binding		Calculated concentrations with 1:1 binding		Calculated concentrations with 1:2		Ratios			
	A	B	A'	B'	A''	B''	0	1:1	1:2	Obs
	1PhEtOH (mM)	Pr^iOH (mM)	1PhEtOH (mM)	Pr^iOH (mM)	1PhEtOH (mM)	Pr^iOH (mM)	A/B	A'/B'	A''/B''	
1.56	31.1	40	11.1	60	0	71.1	0.778	0.185	0.000	N/A
5.19	103.7	40	83.65	60	63.65	80	2.591	**1.394**	0.796	1.712
10.35	207	40	187	60	167	80	5.175	3.117	**2.088**	2.695

Table 4.10 ***Free isopropanol as an indicator of 1-phenylethanol binding.*** At a set concentration of TiDPM (20 mM), the relative concentration of free isopropanol was monitored with respect to added 1-phenylethanol (1PhEtOH).

The addition of the secondary benzyl alcohol, 1-phenylethanol, to the TiDPM complex was monitored using the ratio of isopropanol to 1-phenylethanol, as had been done using 4NAP. Binding was monitored again by the relative ratio of the methyne proton of displaced isopropanol to, in this case, the methyne proton of 1-phenylethanol in its unbound form. Table 4.10 details expected peak ratios in circumstances of binding zero, one or two equivalents of 1-phenylethanol to the Ti^{IV} center. At 31.1 mM of added

1-phenylethanol, the signal of free 1-phenylethanol was insufficiently resolved tointegrate. At 103.7 mM and 207.3 mM (respectively about 5 and 10 equivalents of guest with respect to Ti^{IV}) the integration ratios between 1-phenylethanol and free isopropanol indicate addition of less than one and then between one and two equivalents of 1-phenylethoxide. When 103.7 mM of 1-phenylethanol is available to bind 20 mM TiDPM, less than one equivalent of the guest is in the bound form, therefore a rough K_{eq} value for the binding of the first equivalent of 1-phenylethanol can be estimated using Eq. 1.

$$K_{eq} = \frac{[HG][\mathrm{Pr}^{i}OH]}{[H][G]} \tag{1}$$

Where [H] is [TiDPM], [G] is [1-phenylethanol], [HG] is the concentration of the TiDPM:1-phenylethanol complex. Using the total concentrations of host and guest (H_{tot} and G_{tot}) and the ratio of unbound 1-phenylethanol [G] to unbound isopropanol [$Pr^{i}OH$] it is possible to determine [HG], [$Pr^{i}OH$], [H] and [G] in order to solve for K_{eq}.

$$[G] = [G]_i - [HG] \tag{2}$$

$$[H] = [H]_i - [HG] \tag{3}$$

$$\frac{[G]}{[\mathrm{Pr}^{i}OH]} = \frac{([G]_i - [HG])}{[\mathrm{Pr}^{i}OH]} \tag{4}$$

Two equivalents of isopropanol are formed concomitantly with TiDPM and an additional equivalent is formed with every instance of host/guest coordination, therefore:

$$[Pr^{i}OH] = 2H_{tot} + [HG] \tag{5}$$

Substituting Eq. 5 into Eq. 4 and taking [G]/[$Pr^{i}OH$], $[G]_i$ and $[H]_i$ from Table 4.10 yields:

$$1.712 = \left(\frac{103.6mM - [HG]}{(2 * 20mM) + [HG]} \right) \quad (6)$$

Solving Eq. 6, [HG] = 12.95 mM which in turn allows Eqs. 2, 3 and 5 to be solved: [G] = 90.65 mM, [H] = 7.05 mM and [Pr^{i}OH] = 52.95 mM. Eq. 1 is then solved as follows:

$$K_{eq} = \frac{12.95mM * 52.95mM}{7.05mM * 90.65mM}$$

$$K_{eq} = 1.07$$

It must noted that this calculated value for K_{eq} is from a single experiment with no error calculated and that the result is close enough to 1 as to be extremely spurious; however, a $K_{eq} > 1$ is interesting because the steric difference between 1-phenylethanol and isopropanol, a phenyl group (*A* value = 2.8) versus a methyl group (*A* value = 1.74),[27] would imply that isopropanol can coordinate Ti^{IV} with less steric strain than 1-phenylethanol. While too much conjecture about the results of a single experiment is ill advised, it is interesting to note a few points of support for this finding. First, both 1-phenylethanol and isopropanol appear to be much weaker ligands of Ti^{IV} than 4NAP. Addition of 4NAP to the TiDPM system results in stoichiometric displacement of both of the coordinated isopropoxides to yield two equivalents of isopropanol. The order of coordination affinity appears to be 4NAP >> 1-phenylethanol > isopropanol, and this trend correlates directly to the acidity of the hydroxyl group proton. The phenolic proton is distinctly more acidic than the aliphatic alcohols (for the analogous phenol PNP, pK_a = 7.2 in water),[28] and due to the difference in group electronegativities between phenyl and methyl substituents (3 versus 2.3; Pauling scale) 1-phenylethanol is expected to be more acidic than isopropanol.[27]

While the difference in acidities is most likely the primary cause of the observed K_{eq}, a second, subtler but more elegant steric effect could also be at work. Sharpless has reported an enzyme like specificity of fit in the kinetic resolution of *trans* olefins using

Ti^{IV}tartrate ester catalysts. Kinetic resolution is faster and more efficient as the steric bulk of the substrates is increased until at a critical bulkiness it becomes a hindrance. 1-Phenylethanol could excel at filling available space in the TiDPM cavity and in this way out compete isopropanol. By whatever means the apparent preference of TiDPM for 1-phenylethanol over isopropanol may be explained, the NMR experiments presented thus far have made clear that the titanium complex prefers to bind 4NAP over secondary alcohols.

A third series of NMR experiments was conducted to determine if 1-phenylethanol is at all capable of displacing 4NAP from TiDPM, but no evidence of displacement was forthcoming at NMR concentrations. Having learned more about the stoichiometry and relative coordinative affinity of the indicator and secondary alcohols to TiDPM, we were prepared to test new ether diol ligands and to adjust relative concentrations of host, indicator and guest in order to develop an operational IDA. The project at this point returned to the UV-Vis spectrophotometer.

4.2.4 UV-Vis Studies of 4NAP binding to Ti^{IV}: diol ether complexes

The discovery of systems for the determination of *ee* is often plagued with false positive results. Differences in concentration between *R*- and *S*-analyte, interfering impurities or experimental error could all contribute to a difference in response of an enantiomeric sensing system. In order to insure the fidelity of chirality sensing protocols, it is good practice to test the sensing system by assessing the chiral discrimination of both enantiomeric versions of the sensor. A true enantioselective sensor must exhibit cross-reactivity with respect to analyte chirality,[7,8] for example, should a *(S,S)*-DPM based system show a greater response to a certain *(S)*-alcohol than to the corresponding *(R)*-alcohol, then the *(R,R)*-DPM based system must respond more to the *(R)*-alcohol. However, because DPM (1,2,5,6-di-*O*-isopropylidene-D-mannitol) is a derivative of naturally occurring D-mannitol, its D enantiomer is cheap while the L enantiomer happens to not be commercially available. In anticipation of the necessary control reactions described above, the ligand 1,4-dimethoxy-2,3-butanediol (DMB, **4.21**) (Figure 4.56) was chosen because it is available in excellent purity in both the (*R,R*)- and (*S,S*)- enantiomer.

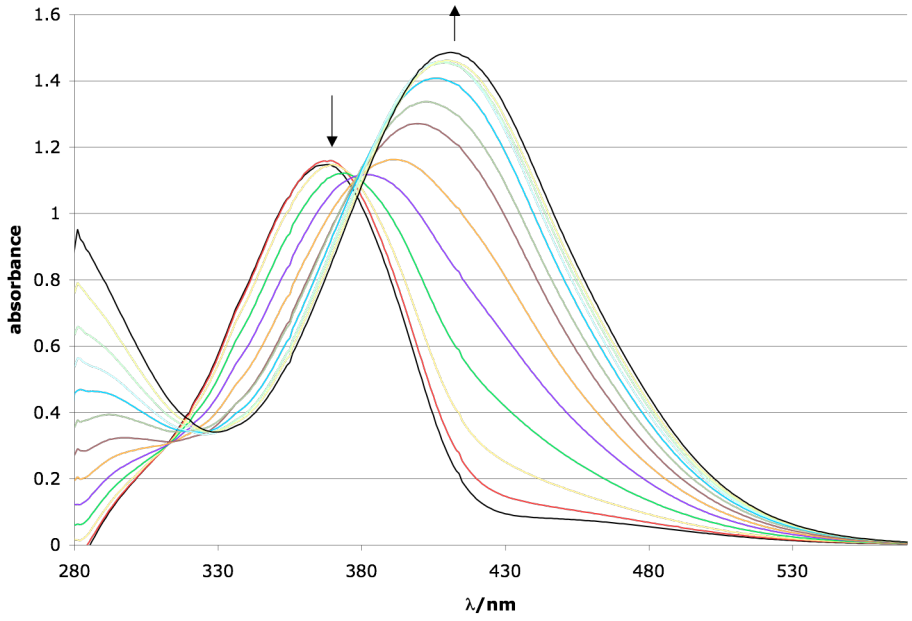

Figure 4.59 Titration of *S-TiDMP into 4NAP*. *S*-TiDMB (1 mM) into 4NAP (0.05 mM).

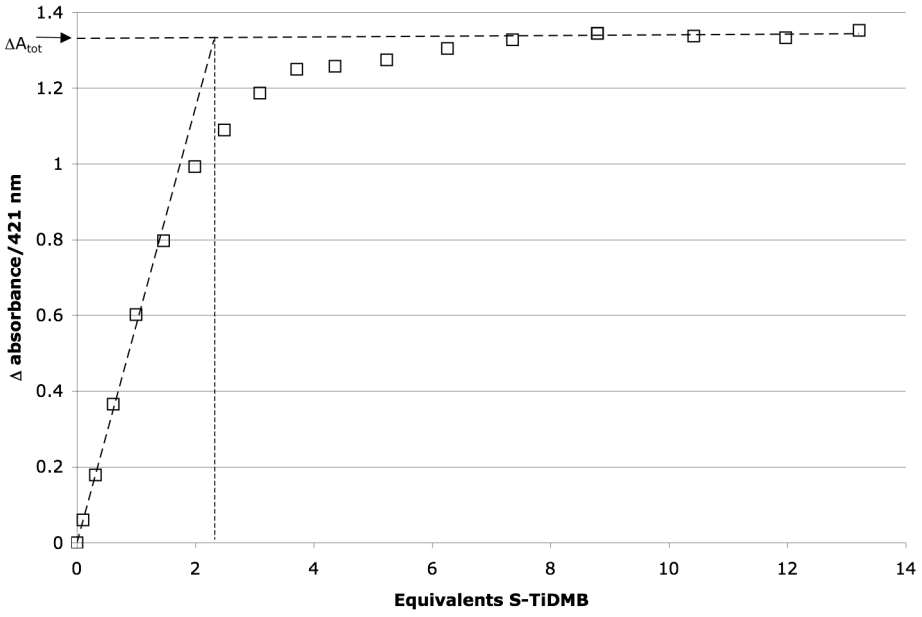

Figure 4.60 ***The binding isotherm of the titration of S-TiDBM into 4NAP seen in* Figure 4.59.** Change in the absorbance of 4NAP (0.05 mM) at 421 nm as function of *S*-TiDBM. The binding isotherm indicates a 2:1 *S*-TiDBM:4NAP saturation stoichiometry.

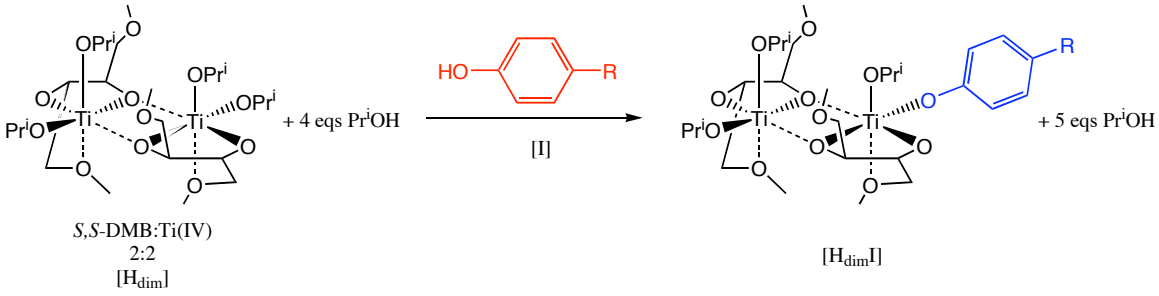

Scheme 4.26 ***4NAP binding to S-TiDMB dimer.*** A schematic of the reaction described by Eq. 7.

The (*S,S*)-DMB ligand and $Ti(OPr^i)_4$ complex (*S*-TiDMB) was titrated into a solution of 4NAP (Figure 4.59). The transition from unbound to bound 4NAP generates a pseudo-isosbestic point indicating that more than two species are absorbing in this region, but they are most likely similar to each other (i.e. mono-, di-, or oligomeric TiDMB species). Interestingly, the equilibrium isotherm plotted from the growing 421 nm peak indicated a 2:1 stoichiometry of *S*-TiDMB:4NAP (Figure 4.60). While this stoichiometry is ostensibly the opposite of the 1:2 stoichiometry observed for the TiDPM

system in the H^1-NMR studies, it was not possible using NMR to monitor the different complexes formed at high TiDPM concentration because all of the analyses were focused upon the isopropanol liberated upon coordination. When *S*-TiDMB is treated as a dimer (Scheme 4.26), the K_{eq} value can be solved using a nominal variation on Eq. 1, where I = 4NAP.

$$K_{eq} = \frac{[H_{\text{dim}}I][\text{Pr}^i OH]}{[H_{\text{dim}}][I]} \tag{7}$$

K_{eq} can be solved at given total concentrations of H_{dim} and I_{tot} by also determining the bound fraction of I_{tot} (β_I) as the change in absorbance (ΔA) divided by the total change in absorbance (ΔA_{tot}=1.331), which was defined as the y-intercept of the asymptotic trendline in Figure 4.60.

$$\beta_I = \frac{\Delta A}{\Delta A_{tot}} \tag{8}$$

Hence, [I], [H_{dim}I], [Pr^iOH], and [H_{dim}] are determinable.

$$[\text{I}] = \text{I}_{\text{tot}} (1 - \beta_\text{I}) \tag{9}$$

$$[\text{H}_{\text{dim}}\text{I}] = \text{I}_{\text{tot}} * \beta_\text{I} \tag{10}$$

$$[\text{Pr}^\text{i}\text{OH}] = 4\text{H}_{\text{dim}} + [\text{H}_{\text{dim}}\text{I}] \tag{11}$$

$$[\text{H}_{\text{dim}}] = \text{H}_{\text{dim}} - [\text{H}_{\text{dim}}\text{I}] \tag{12}$$

Substitution of Eqs. 9, 10, 11 and 12 into Eq. 7 yields Eq. 13.

$$K_{eq} = \frac{\beta_I (I_{tot} * \beta_I + 4H_{\text{dim}})}{H_{\text{dim}}(1 + \beta_I) - \beta_I (I_{tot} + I_{tot} * \beta_I)} \tag{13}$$

Sample	Equiv. TiDMB	Conc. dimer (μM)	ΔA	β_1	K_{eq}
A	2.49	62.3	1.089	0.818	2.24
B	3.09	77.2	1.187	0.892	2.23
C	3.72	92.9	1.250	0.939	2.22

Table 4.11 ***The calculation of K_{eq} at three points in the binding isotherm from*** **Figure 4.60.** The average K_{eq} is 2.23 for the reaction shown in Scheme 4.26.

Using Eq. 13, the K_{eq} values shown in Table 4.11 were determined at three data points near the inflection point in the titration. The average K_{eq} was 2.23. As suggested by the NMR data of the analogous TiDPM system, the displacement of isopropanol by 4NAP is quite facile. The absorbance of bound 4NAP does not saturate until two equivalents of Ti^{IV} have been added to the solution. This stoichiometry is intriguing because NMR studies indicate the existence of a 2:1 4NAP:TiDPM complex, which, if it exists at the lower concentrations of the UV-Vis experiments, must exhibit different absorption characteristics than the species observed upon saturation of the curve in Figure 4.60. A few hypotheses arise from these data. One possibility is that the 4NAP is binding at higher ratios in the presence of fewer than two equivalents of Ti^{IV}, but the ability of Ti^{IV} to withdraw electrons from 4NAP is minimized when multiple indicators are bound and donating charge to the metal center. In this case the bound 4NAP signal will appear to be "more" deprotonated as the TiDMB concentration increases. A second possibility is that phenoxide is acting as a bridging ligand in the 2:1 TiDMB:4NAP complex (Figure 4.61). Bridging is common in Ti^{IV} ligands as evidenced by the persistence of Ti^{IV} dimers in the presence of a wide variety of diol ligands.[18,24] In the first scenario a multi-stage process is expected, while in the bridging scenario, it is possible that the 2:1 complex is formed even as low concentrations of titanium and is therefore the only bound 4NAP species in solution. A third hypothesis is that the TiDMB complex actually dimerizes or otherwise aggregates around 0.1 mM and generates the active 4NAP binding species. If this mechanism is active then the apparent 1:2 stoichiometry is coincidental, and the TiDPM concentration at which the curve begins to saturate will be 0.1 mM regardless of 4NAP concentration.

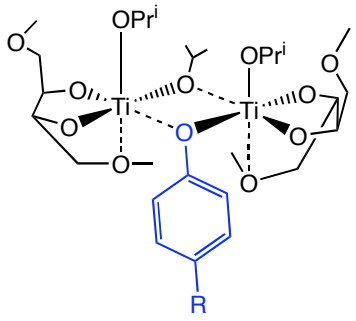

Figure 4.61 ***A bridging phenoxide ligand.*** 2:1 TiDMB:4NAP stoichiometry could result from a bridging mode of phenoxide coordination.

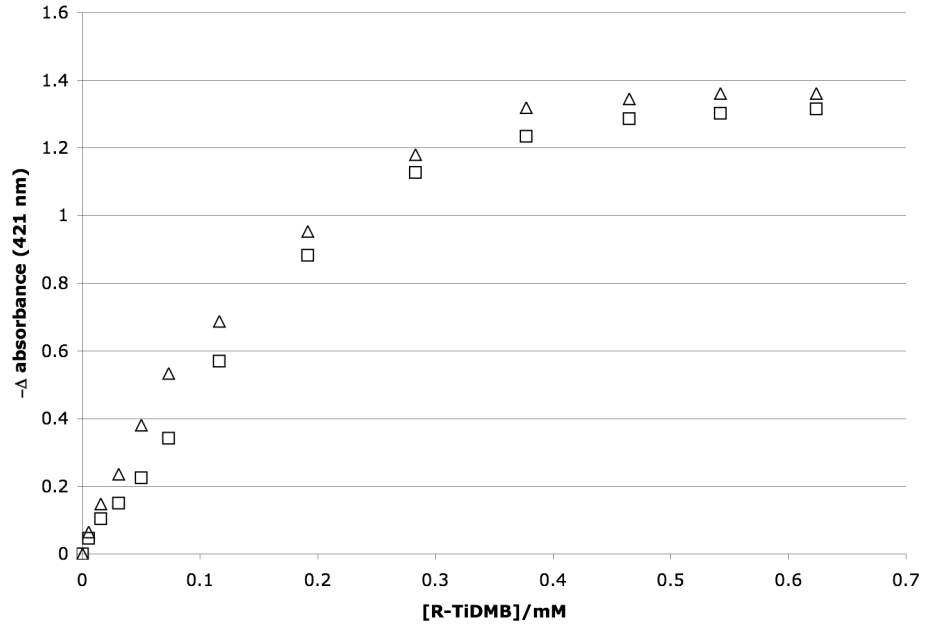

Figure 4.62 ***R-TiDMB complexes from different Ti^{IV} alkoxides.*** Titration of two R-TiDMB complexes differing by the parent Ti^{IV} alkoxide. The Δ absorbance is plotted as its absolute value (-Δ absorbance). □, derived from $Ti(OBu^t)_4$; △, derived from $Ti(OPr^i)_4$.

In order to better understand this process the 4NAP titration was repeated using (*R*)-DMB as the ligand, and also using *R*-TiDMB created using $Ti(OBu^t)_4$ (TiBuDMB).

Tangentially, using TiBuDMB also allowed us to screen a bulkier and therefore potentially more sterically discriminating host. *R*-TiDMB and *R*-TiBuDMB were titrated into 4NAP (Figure 4.62). The *R*-TiBuDMB isotherm reveals an apparent two step process with the first inflection point somewhere between 0.5 and 1 equivalents of Ti^{IV} (0.25 - 0.5 equivalents of dimer) corresponding perhaps to the indicator saturated titanium complex seen in the NMR studies. The second inflection occurs at around two equivalents of a Ti^{IV} (1 equivalent dimer) and is probably the same binding event described by the TiDMB curve in the case of $Ti(OPr^i)_4$ based hosts. Having evidence of a multistage process, the system was probed for aggregation activity on the part of Ti^{IV}DMB. It was found that the inflection points of the 4NAP binding isotherm are not actually a function of 4NAP concentration, but instead appear consistently at 0.05 mM and 0.1 mM of TiDMB indicating that the strong binding complex may be assembling in solution above 0.05 mM (Figure 4.63). A similar result is apparent when looking at $Ti(OPr^i)_4$ derived complexes at different concentrations of 4NAP. Although these titrations are not conspicuously bimodal they exhibit the later saturation event at 0.1 mM regardless of 4NAP concentration (Figure 4.64). The 4NAP concentration only influences the total change in absorbance. In light of evidence of Ti^{IV} aggregation, the Ti^{IV}DMB:4NAP system is more difficult to define, especially in terms of an indicator on/off paradigm. Despite stoichiometric confusion, the system does display interaction between Ti^{IV} and 4NAP in the presence of a chiral ligand. Any color change upon addition of a secondary alcohol might not constitute a true IDA, but if such a color change should prove repeatable and enantioselective then the system would be useful as a sensor whose mechanism could be worked out in time.

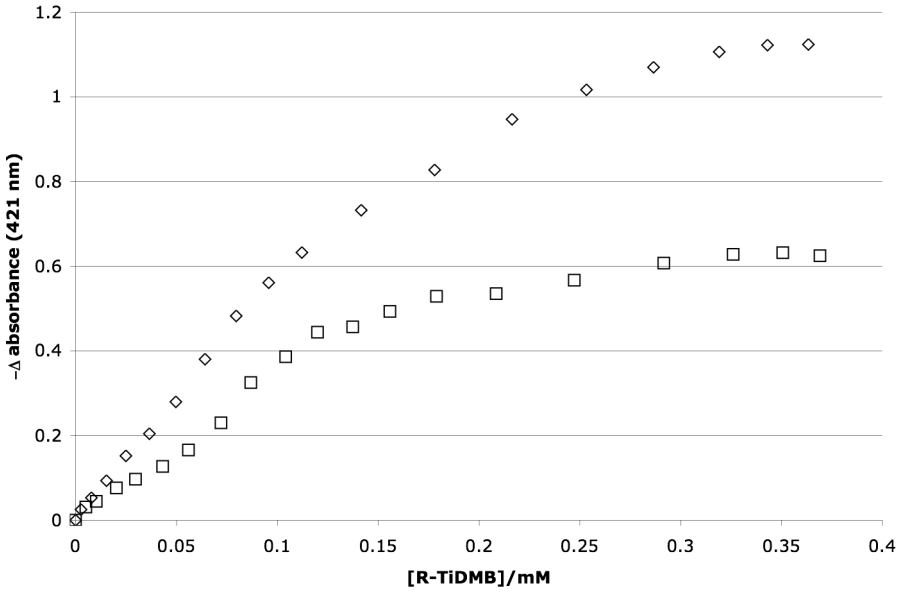

Figure 4.63 The titration of R-TiBuDMB (0.5 mM) into 4NAP at different concentrations. The Δ absorbance is plotted as its absolute value (-Δ absorbance). ☐, [4NAP] = 0.025 mM; ◇, [4NAP] = 0.05 mM.

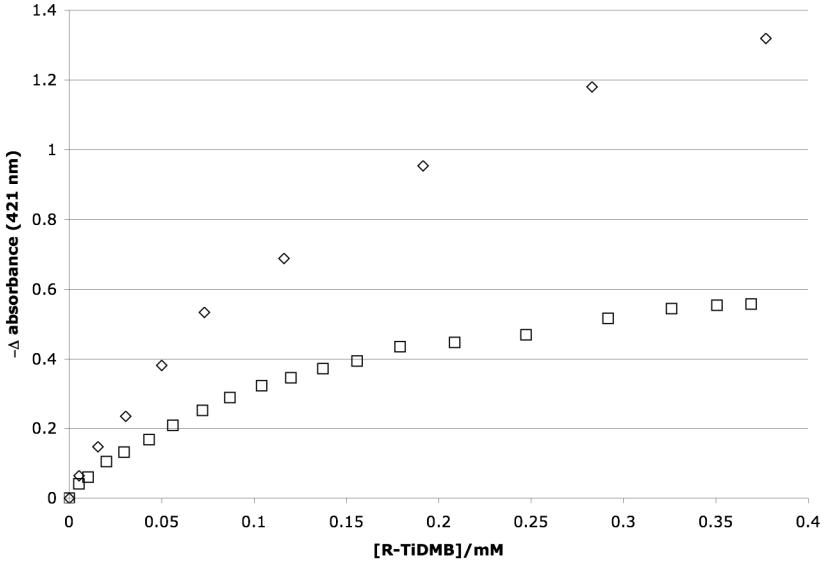

Figure 4.64 ***The titration of R-TiBuDMB into 4NAP.*** The Δ absorbance is plotted as its absolute value (-Δ absorbance). ☐, [4NAP] = 0.025 mM; ◇, [4NAP] = 0.05 mM.

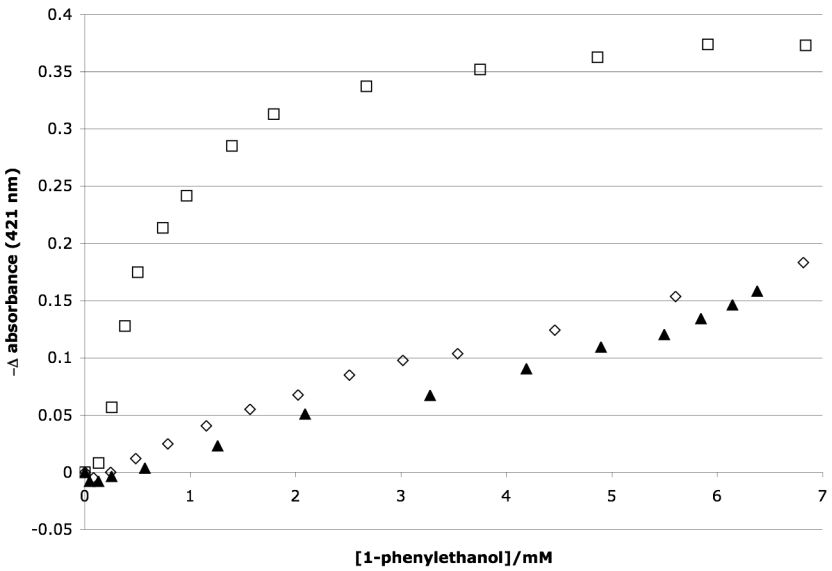

Figure 4.65 ***Titration of racemic 1-phenylethanol into TiDMB complexes bound with 4NAP.*** The Δ absorbance is plotted as its absolute value (-Δ absorbance). □, [S-TiBuDMB] = 0.2 mM, [4NAP] = 0.05 mM; ◇, [S-TiDMB] = 0.2 mM, [4NAP] = 0.05 mM; ▲, [S-TiDMB] = 0.1 mM, [4NAP] = 0.05 mM. Deriving the Ti^{IV} complex from $Ti(OBu^t)_4$ instead of $Ti(OPr^i)_4$ (□ vs ◇) creates a greater difference in response to 1-phenylethanol than does changing the TiDMB:4NAP ratio (◇ vs. ▲).

4.2.5 Displacement of the Indicator by Secondary Alcohol

Signal modulation of TiDMB:4NAP complexes of various stoichiometries was observed upon addition of very high concentrations of racemic 1-phenylethanol (Figure 4.65). The total TiDMB concentration was tested at 0.1 mM and 0.2 mM with a nominally greater response from the 0.2 mM system. The parent titanium alkoxide proved to be a more important variable than concentration, with TiBuDMB:4NAP complexes displaying almost twice as much change in absorbance over the same concentration range of 1-phenylethanol. The spectra corresponding to the titration of the TiBuDMB:4NAP system are shown juxtaposed with the spectrum of unbound 4NAP(Figure 4.66). Despite the saturation behavior of the change in absorbance in Figure 4.65, the 4NAP has not returned to its unbound form. The system is not a formal IDA, but does respond to incoming 1-phenylethanol, albeit at dozens of equivalents.

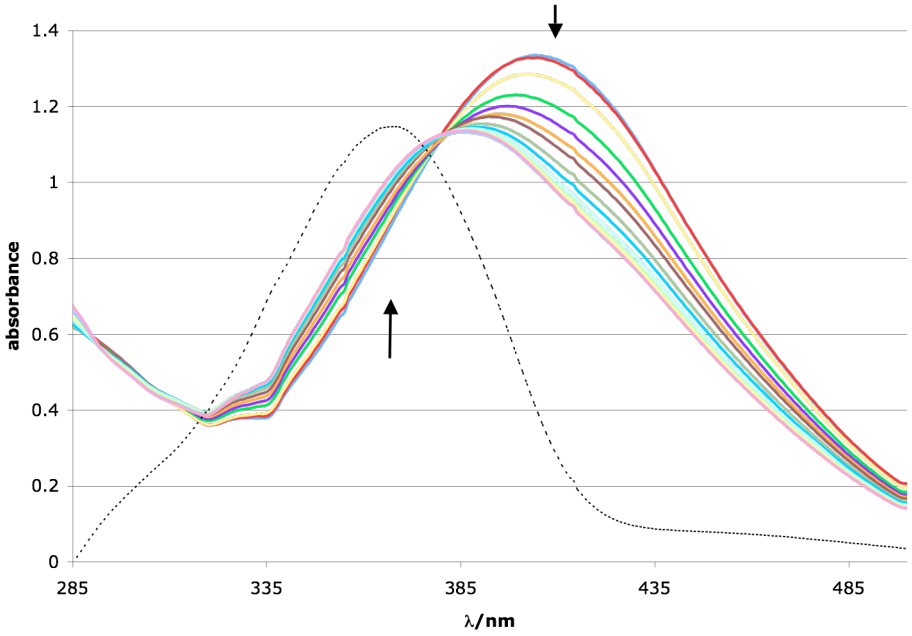

Figure 4.66 ***Spectral change induced by 1-phenylethanol addition to Ti^{IV} indicator complex.*** The colored spectra and arrows detail the change in absorbance of S-TiBuDMB and 4NAP (2 mM and 0.05 mM, respectively) upon addition of racemic 1-phenylethanol (Binding isotherm seen in Figure 4.65) in toluene. The spectrum of 4NAP at 0.05 mM in toluene is the black dotted line.

The system was tested for sensitivity to the chirality of 1-phenylethanol. The signal modulation upon addition of 1-phenylethanol differs according to the steric bulk of the parent titanium alkoxide. When $Ti(OPr^i)_4$ is used, the addition of *R*- or *S*-1-phenylethanol results in an initial increase in absorbance at 421 nm, but then followed by a more pronounced decrease (Figure 4.67). The fact that this effect is not as pronounced in the titration of racemic 1-phenylethanol (Figure 4.65) is probably due to batch differences. Repeatability is extremely difficult in dealing with highly water reactive Ti^{IV} and very hygroscopic hydroxylated compounds (alcoholic analytes and diol ligands).

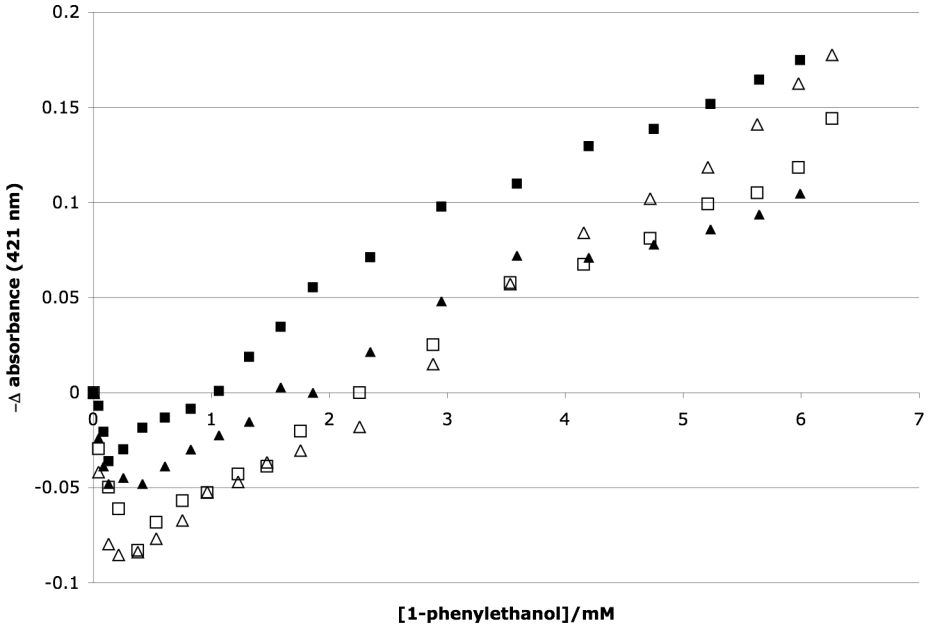

Figure 4.67 ***Change in absorbance at 421 nm of Ti(OPr^i)$_4$ derived TiDMB:4NAP (0.2 mM:0.05 mM) upon addition of 1-phenylethanol.*** The Δ absorbance is plotted as its absolute value (-Δ absorbance). Filled shapes refer to *S,S*-DMB while empty shapes refer to *R,R*-DMB, and triangles refer to incoming *S*-phenylethanol while squares refer to incoming *R*-phenylethanol. *e.g.* □, *R*-phenylethanol titrated into *R*-TiDMB.

The Ti(OBu^t)$_4$ derived systems resemble true binding isotherms superficially, but they never really saturate either (Figure 4.68). In light of the extreme reproducibility issues (notice the repeat titration of *S*-1-phenylethanol into *S*-TiBuDMB:4NAP in Figure 4.68) the nearly overlapping curves of Figure 4.68 (△, □ and ■) were regarded as sufficient evidence that this system was not worth pursuing any longer as an enantioselective sensor of secondary chiral alcohols.

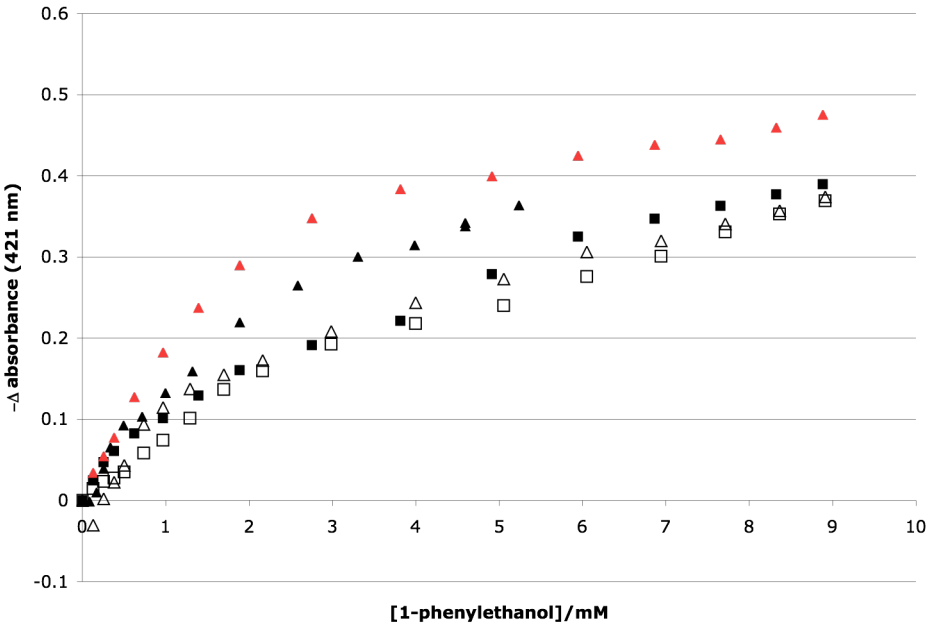

Figure 4.68 ***Change in absorbance at 421 nm of Ti(OBu^t)$_4$ derived TiDMB:4NAP (0.2 mM:0.05 mM) upon addition of 1-phenylethanol.*** The Δ absorbance is plotted as its absolute value (-Δ absorbance). Filled shapes refer to *S,S*-DMB while empty shapes refer to *R,R*-DMB, and triangles refer to incoming *S*-phenylethanol while squares refer to incoming *R*-phenylethanol. The red and black triangles represent repeat titrations of *S*-phenylethanol into *S*-TiDMB.

4.2.6 Conclusions: Sensitivity and Irreversibility

Reported above is the first attempt to use Ti^{IV} complexed with chiral diol ligands as a sensor for enantiomeric excess of chiral secondary alcohols. The Sharpless catalytic system for enantiomeric epoxidation that inspired this work is one of the most robust and widely used enantioselective transformations known. The promise of a Ti^{IV} based sensor for simple chiral alcohols lies in its oxophilicity, and ability to coordinate alcoholic monodentate ligands in such a way that the subtle steric differences of chirality are called into play, as seen in Sharpless catalysis. The problem so far in developing a Ti^{IV}-based IDA seems rooted in the determination of an appropriate indicator.

The use of 4NAP as an indicator was dictated by early qualitative results which showed that monodentate phenolic indicators were the only class tested to display color change upon binding to Ti^{IV} and apparent reversal of this change upon addition of

millimolar quantities of alcohol. Later experiments detailed that although color change was observable upon the addition of alcohol, true displacement of the phenolic indicator was not occurring. Correlations between the Brønsted acidity of the incoming alcohol or phenol and binding strength of the resultant alkoxide or phenoxide were observed, and for an indicator to be displaced it will most likely need to be much less acidic than 4NAP. It will be difficult to find an indicator whose acidity approaches that of simple alcohols, however, because good indicators have extended π-systems in conjugation with the site of deprotonation in order to effect color change upon deprotonation. This extended π-system inherently lowers the energy of the deprotonated anion and hence contributes to a more acidic parent hydroxy group. The conceptual difficulty of finding a truly displaceable indicator informed the decision to study in depth the current TiDMB:4NAP system, which displays a usable, but difficult to understand signal modulation upon the addition of 1-phenylethanol.

At millimolar concentrations, it is possible that the TiDMB:4NAP system is responding to solvent effects and not to coordination of the alcohol at the Ti^{IV} center. If the role of the alcohol were really non-specific then that would explain the apparent lack of enantioselectivity of the system because physical properties, such as the dielectric constant are independent of chirality. Yet the promise of this system remains when one observes the difference in response of analyte alcohols of the $Ti(OPr^{i})_4$ and $Ti(OBu^{t})_4$ derived complexes. The $Ti(OBu^{t})_4$ derived system shows nearly twice the response to 1-phenylethanol at 421 nm and this is ostensibly due to the single methyl group that differentiates *tert*-butoxide from isopropoxide. The appropriate chiral diol ligand might be able to generate a similar difference in response upon complexing different enantiomers of chiral alcohol. While viable and interesting avenues of research remain in the use of Ti^{IV} based sensors, our desire to develop the first enantioselective sensor for chiral alcohols led us to pursue a different sensing approach altogether. This approach is detailed in the next chapter.

4.3 Experimental Details for Chapter 4

4.3.1 General

The chemicals were obtained from Acros Organics, Aldrich, TCI America, and EM Science. Methylene chloride was distilled from calcium hydride and stored under argon. Toluene was distilled from calcium hydride and stored in the glove box. All glassware including volumetric flasks, cuvettes and most syringes was oven-dried overnight at 115 °C, then cooled under vacuum and stored in a desiccator or glove box. Syringes that could not tolerate such heat exposure were dried in the oven for 1 h and then cooled under vacuum.

This project underwent two phases, the first in which tartrate ester ligands were used and the second in which ether diol ligands were used. Experiments using tartrate esters were conducted in dichloromethane using Schlenk vacuum and argon line methodology in order that glassware could be partially submersed in a -20 °C ice/acetone bath. When etherdiols were used as the ligands, toluene or benzene was the solvent, and preparatory work was confined to an N_2 glove box in the presence of P_2O_5 atmospheric drying agent. All liquids entering the glove box were triply deoxygenated by the freeze/pump/thaw protocol. Titrations requiring sample manipulation outside of the glove box were conducted using argon balloons to maintain anhydrous atmospheres. Tartrate esters were all vacuum distilled and then stored under argon. Ti^{IV}alkoxides were vacuum distilled and then stored under argon during the tartrate ester studies. In the case of the etherdiol studies, the Ti^{IV}alkoxides were vacuum distilled into Schlenkware and then imported to the glovebox for storage. All solids including DPM and indicators were dried under vacuum overnight at 110 °C and then stored either under argon or in the glove box. The low-melting DMB ligands were stored in a desiccator and put under vacuum before being transferred to the glovebox.

4.3.2 NMR experiments

^{1}H NMR samples were prepared in the glove box using C_6D_6 that was distilled from sodium and benzophenone before being transferred to the glove box for storage.

Samples were protected from atmospheric moisture using electrician's tape, and ^{1}H NMR spectra were gathered as soon as possible after samples left the glove box.

4.3.3 UV-Visible titrations

A sample UV-Vis titration was conducted as follows. The UV-Vis was blanked with a cuvette of neat toluene. A cuvette was filled with 0.95 mL of a solution containing 4NAP (0.05 mM), $Ti(OPr^i)_4$ (0.1 mM) and (*S*)-DMB (0.1 mM) in toluene, and the spectrum of this solution was recorded. A second solution containing 1-phenylethanol (8.29 mM, racemic) and otherwise identical to the first solution was added in aliquots to the cuvette and spectra were recorded between each aliquot.

4.4 References for Chapter 4

1. "Combinatorial and Evolution-Based Methods in the Creation of Enantioselective catalysts" Reetz, M. T. *Angew. Chem. Int. Ed.* **2001**, *40*, 284-310.

2. "Reaction Microarrays: A Method for Rapidly Determining the Enantiomeric Excess of Thousands of Samples" Korbel, G. A.; Lalic, G.; Shair, M. D. *J. Am. Chem. Soc.* **2001**, *123*, 361-362.

3. "Modified BINOL Ligands in Asymmetric Catalysis" Chen, Y., Yekta, S. Yudin, A. K. *Chem. Rev.* **2003**, *103*, 3155.

4. "Steric Effect on Fluorescence Quenching of 1,1'-Binaphthyl by Chiral Amines" Irie, M.; Yorozu, T.; Hayashi, K. *J. Am. Chem. Soc.* **1978**, *100*, 2236-2237.

5. "Colorimetric Chiral Recognition by a Molecular Sensor" Kubo, Y.; Maeda, S.; Tokita, S.; Kubo, M. *Nature*, **1996**, *382*, 522-524.

6. (a) "Fluorescence of Organic Molecules in Chiral Recognition" Pu, L. *Chem. Rev.* **2004**, *104*, 1687-1716. (b) "A Cyclohexyl-1,2-diamine-Derived Bis(binaphthyl) Macrocycle: Enhanced Sensitivity and Enantioselectivity in the Fluorescent Recognition of Mandelic Acid" Li, Z. –B.; Lin, J.; Pu, L. *Angew. Chem. Int. Ed.* **2005**, *44*, 1690-1693. (c) "A Practical Enantioselective Fluorescent Sensor for Mandelic Acid" Jing, L.; Hu, Q. –S.; Xu, M. –H.; Pu, L. *J. Am. Chem. Soc.* **2002**, *124*, 2088-2089.

7. (a) "Facile Quantification of Enantiomeric Excess *and* Concentration with Indicator-Displacement Assays: An Example in the Analysis of α-Hydroxyacids" Zhu, L.; Anslyn, E. V. *J. Am. Chem. Soc.* **2004**, *126*, 3676-3677. (b) "Guidelines in Implementing Enantioselective Indicator-Displacement Assays for α-Hydroxycarboxylates and Diols" Zhu, L.; Zhong, Z.; Anslyn, E. V. *J. Am. Chem. Soc.* **2005**, *127*, 4260-4269.

8. "Colorimetric Enantiodiscrimination of α-Amino Acids in Protic Media" Folmer-Andersen, J. F.; Lynch, V. M.; Anslyn, E. V. *J. Am. Chem. Soc.,* **2005**, *127*, 7986-7987.

9. "An Alcohol Recognition Motif: Clear Evidence of Binding Site Cooperativity in the Complexation of Cyclohexanediols by Neutral Polyaza-Clefts" Bell, D. A., Diaz, S. G., Lynch, V. M., Anslyn, E. V. *Tetrahedron Lett.* **1995**, *36*, 4155-4158.

10. "Fluorescent amino-β-cyclodextrin derivatives as a receptor for various types of alcohols having cyclic and macrocyclic rings" Takenaka, Y.; Nakashima, H.; Yoshida, N. *J. Mol. Struct.*, **2007**, *871*, 149-155.

11. "The First Practical Method for Asymmetric Epoxidation" Katsuki, T.; Sharpless, K. B. *J. Am. Chem. Soc.* **1980**, *102*, 5974-5976.

12. "In the Arena of Enantioselective Synthesis, Titanium Complexes Wear the Laurel Wreath" Ramon, D. J.; Yus, M. *Chem. Rev.* **2006**, *106*, 2126-2208.

13. "Asymmetric Epoxidation Provides Shortest Routes to Four Chiral Epoxy Alcohols Which Are Key Intermediates in Syntheses of Methymycin, Erythromycin, Leukotriene C-1 and Disparlure" Rossiter, B. E.; Katsuki, T.; Sharpless, B. T. *J. Am. Chem. Soc.* **1981**, *103*, 464-465.

14. "Procedure for the Catalytic Asymmetric Epoxidation of Allylic Alcohols in the Presence of Molecular Sieves" Hanson, R. M.; Sharpless, K. B.; *J. Org. Chem.* **1986**, *51*, 1922-1925.

15. "Catalytic Asymmetric Epoxidation and Kinetic Resolution: Modified Procedures Including in Situ Derivatization" Gao, Y.; Hanson, R. M.; Klunder, J. M.; Ko, S. Y.; Masamune, H.; Sharpless, K. B. *J. Am. Soc. Chem.* **1987**, *109*, 5765-5780.

16. "On the Mechanism of Titanium-Tartrate Catalyzed Asymmetric Epoxidation" Sharpless, K. B.; Woodard, S. S.; Finn, M. G. *Pure & Appl. Chem.* **1983**, *55*, 1823-1836.

17. "Crystal Structures of Two Titanium Tartrate Asymmetric Epoxidation Catalysts" Williams, I. D.; Pedersen, S. F.; Sharpless, K. B.; Lippard, S. J. *J. Am. Chem. Soc.* **1984**, *106*, 6430-6431.

18. "On the Mechanism of Asymmetric Epoxidation with Titanium-Tartrate Catalysts" Finn, M. G.; Sharpless, K. B. In *Asymmetric Synthesis*; Morrison, J. D., Ed.; Academic Press: New York, 1985; Vol. 5, Chapter 8.

19. "Mechanism of Asymmetric Epoxidation. 1. Kinetics" Woodard, S. S.; Finn, M. G.; Sharpless, K. B. *J. Am. Chem. Soc.* **1991**, *113*, 106-113.

20. "Mechanism of Asymmetric Epoxidation. 2. Catalyst Structure" Finn, M. G.; Sharpless, K. B. *J. Am. Chem. Soc.* **1991**, *113*, 113-126.

21. "Kinetic Resolution of Racemic Allylic Alcohols by Enantioselective Epoxidation. A Route to Substances of Absolute Enantiomeric Purity" Martin, V. S. Woodard, S. S., Katsuki, T.; Yamada, Y.; Ikeda, M.; Sharpless, K. B. *J. Am. Chem. Soc.* **1981**, *103*, 6237-6240.

22. "o-Aminophenoxytitanium complexes" Lafuente, M.; Royo, P. *Transition Met. Chem.* **1989**, *14*, 237.

23. "Solution Structures of Sharpless Epoxidation Catalysts" Potvin, P. G.; Kwong, P. C. C.; Brook, M. A. *J. Chem. Soc., Chem. Commun.* **1988**, 773-775.

24. "The solution structures of chiral Ti^{4+} alkoxides" Potvin, P. G.; Gau, R.; Kwong, P. C. C.; Bianchet, S. *Can. J. Chem.* **1989**, *67*, 1523-1537.

25. "The solution structures of chiral Ti^{4+} alkoxides. II. the roles of diolate basicity and side-chain binding group polarity" Bianchet, S.; Potvin, P. G. *Can. J. Chem.* **1992**, *70*, 2256-2265.

26. "An NMR study of mixed, tartrate-containing Ti^{IV} complexes" Potvin, P. G.; Fieldhouse, B. G. *Can. J. Chem.* **1995**, *73*, 401-413.

27. Anslyn, E. V.; Dougherty, D. A. *Modern Physical Organic Chemistry, 1st Ed.* (University Science Books, 2004) ch. 2.

28. "Hammett Substituent Constants for Electron-withdrawing Substituents: Dissociation of Phenols, Anilinium Ions and Dimethylanilinium Ions" Fickling, M. M.; Fischer, A.; Mann, B. R.; Packer, J. Vaughan, J. *J. Am. Chem. Soc.* **1959**, *81*, 4226-4230.

Chapter 5. The determination of enantiomeric excess in α-chiral alcohols using supramolecular chemistry. Part II. Derivitizing chiral alcohols to create C_2-symmetric and asymmetric ligands of greater binding affinity than the parent alcohols.

5.1 A Derivatizaton Strategy for the Sensing of Enantiomeric Excess in Simple Chiral Alcohols

The difficulties of sensing simple alcohols were explored in the last chapter, both in their historical context and in the specific case of developing the Sharpless catalyst into an enantioselective sensor. The chiral diol modified Ti^{IV} indicator system from Chapter 4 was not well defined in terms of structure or signal transduction because the monodentate alcohol was too weak a ligand to displace the phenolic indicator. In order to develop an indicator displacement assay (IDA) for the determination of *ee* in alcohols it was necessary to improve the competitiveness of simple alcohols with indicators for coordination sites around the metal center of an organometallic host. For experimental convenience, we also desired to move away from the rigorously anhydrous experimental conditions that the Ti^{IV} system required. We hypothesized that performing a simple derivatization of the alcohols could convert them to strong polydentate ligands for hydrolytically stable metal ions such as Cu^{II} and Zn^{II}, while preserving their chiral information for an *ee*-sensitive IDA. The ideal derivatization would require little to no purification, and would position the chiral centers of the former alcohol for maximal interaction with the chiral bias of the host. With these parameters in mind the system in Scheme 5.27 was proposed.

The bis-ether methyl pyridine derivative (BOMP) has a pyridine core and two ethers positioned to create a tridentate ligand for binding the metal center of an organometallic host. Pyridine is a decidedly stronger ligand than an alcohol according to differences between pyridine and water along the spectrochemical series.[1] Therefore, the pyridine core is the most important part of the BOMP derivative in terms of binding affinity. The ethereal arms will aid in binding the metal, but their primary purpose is to

position the chiral information contained in the arms of the BOMP around the metal center close to the chiral information of the host complex.

A. Derivatization

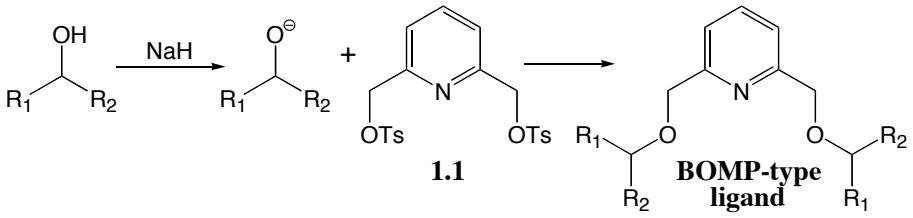

B. IDA

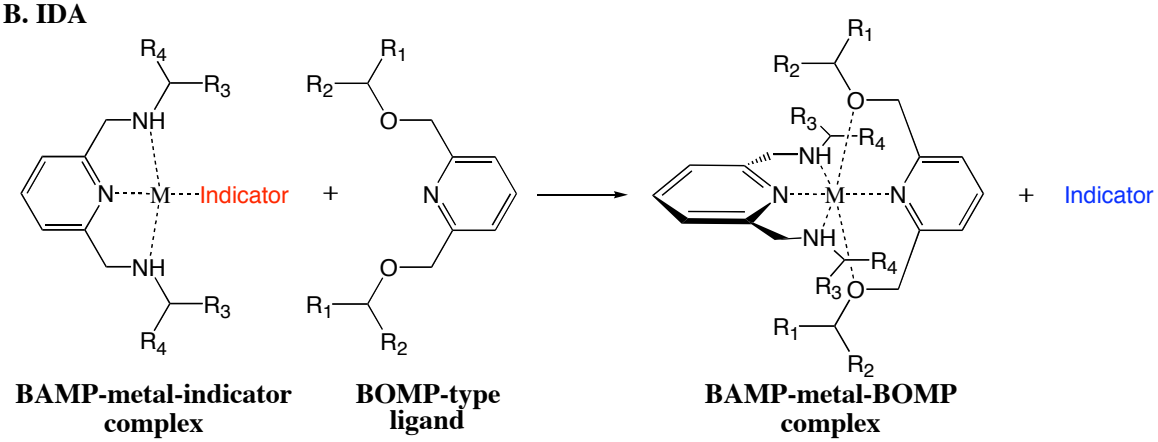

Scheme 5.27 ***Derivatization of a secondary alcohol to create a stronger ligand.*** (A) Converting alcohols to tridentate pyridine ligands will improve their binding affinity to metals, and (B) derivatization could create a ligand competitive enough to displace an indicator, whose chiral ether moieties would be forced to interact with the chiral arms of the BAMP ligand.

The ligand of the host complex must have a greater affinity for the metal than the BOMP ligand or the indicator in order to enforce chirality around the metal binding site and to avoid stripping of the metal by either the BOMP guest or the indicator. The bis-aminomethyl pyridine host ligand (BAMP) was chosen because it has secondary amines that will coordinate transition metal ions better than the BOMP ethers, and also because modeling studies with Cu^{II} indicate good interaction between the arms of the BOMP guest and the arms of the $[Cu^{II}(BAMP\ )]^{2+}$ host (Figure 5.69). For convenience in the modeling study, the BOMP guest was a methanol derivative and although it is not chiral, the chiral bias of the BAMP ligand is seen to influence the positioning of the methyl

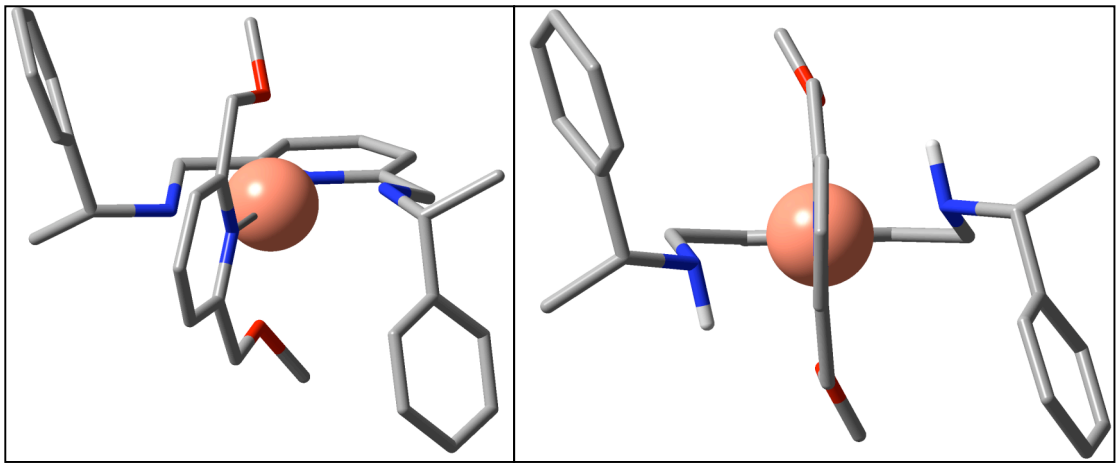

Figure 5.69 ***Energy minimized BOMP-Cu(II)BAMP complex.*** The methyl arms of the BOMP ligand are induced to exhibit a clockwise rotation. Hydrogen atoms have been omitted for clarity

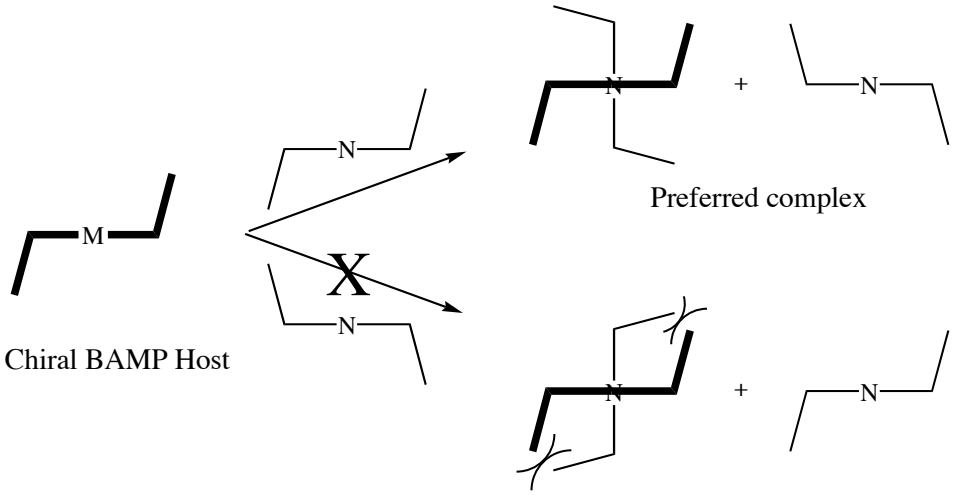

Scheme 5.28 ***A chiral metal-BAMP host should preferentially bind one enantiomer of BOMP guest.*** If the two pyridine groups in the BAMP-metal-BOMP complex are considered axial ligands (Figure 5.69), the secondary amine and ether oxygens inhabit an equatorial region which is modeled in this scheme.

groups of the BOMP. If, instead of methanol, the BOMP ligand were synthesized from an enantiomerically pure α-chiral alcohol, then it would be expected that a chiral BAMP-metal host would bind preferentially to one of the enantiomers of BOMP (Scheme 5.28). If this preferential binding can be translated to an indicator displacement event, then an enantioselective IDA for BOMP, and by extension simple chiral alcohols, will result.

The relationship between the *ee* of an α-chiral alcohol and the *ee* of its BOMP derivative could be complicated. Each equivalent of BOMP generated from the ditosylate **5.1** consumes two equivalents of alcohol. If the alcohol is α-chiral and the sample is not enantiopure then its reaction with **5.1** will yield three products: the (*R,R*)-, (*S,S*)- and (*R,S*)-*meso*-BOMP. Three possibilities exist for the yield of *meso*-BOMP from a mixture of enantiomers of a given alcohol. If the formation of the first ether arm has no effect upon the formation of the second then the yield of *meso*-BOMP will be statistical; however, if the formation of the first predisposes the second arm to react with one or the other enantiomer of alkoxide then the *meso*-BOMP will be formed in either greater than statistical yield (if the first ether arm promotes reaction with its enantiomer), or less than statistical yield (if the first ether arm promotes reaction with alkoxides of its own stereochemistry). The implications of *meso*-BOMP formation, statistical or not, are not entirely clear, although it is interesting to note that *meso*- and homochiral BAMP are diastereomers and could theoretically be differentiated using an achiral sensing assay. At the beginning of this study, however, it was only necessary to recognize that *meso*-BOMP formation would require that *ee* calibration curves must always be determined from the derivatized α-chiral alcohol solution and cannot be approximated by enantiopure mixtures of (*R,R*)- and (*S,S*)-BOMP derivatives. The first priority was to synthesize *(R,R*)- and (*S,S*)-BOMP and BAMP compounds to confirm the viability of our approach.

5.2 Results and Discussion

5.2.1 Synthesis of BAMP ligands and BOMP guests

The interaction between BOMP and BAMP ligands around a metal center was expected to be enantioselective. From a practical standpoint BOMP and BAMP are convenient choices of derivatized guest and host ligand as they may both be synthesized from ditosylate **5.1**, a compound with which our group has previous experience.[B2] In order to test the hypothesis that enantiomeric BOMP ligands can be differentiated by a

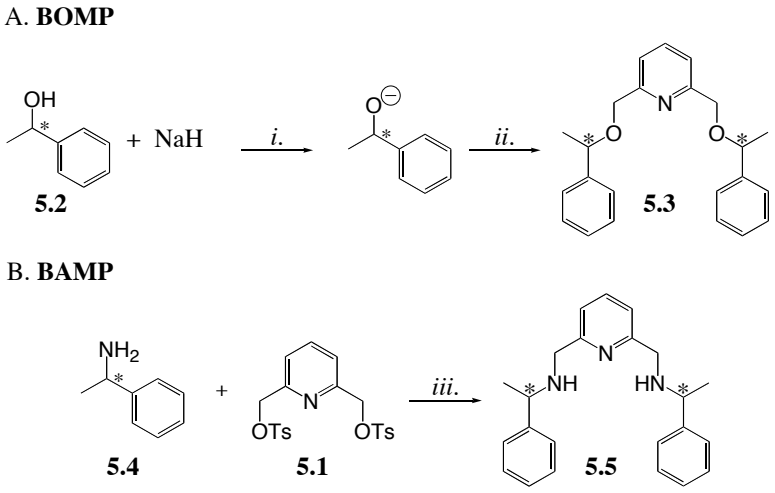

Scheme 5.29 ***Synthesis of methylbenzyl BOMP and BAMP.*** The *(R,R)*- and *(S,S)*-enantiomers of methylbenzyl BOMP and methylbenzyl BAMP were all generated. Reagents, conditions and yields: (*i.*) DMF, 0 °C, 15 min (*ii.*) **5.1**, rt, overnight, 54 % (*iii.*) MeCN, Hünigs base, 50 °C, 2 h, 45 %.

BAMP-based IDA, prototype BOMP and BAMP compounds were synthesized using 1-phenylethanol **5.2** and 1-phenylethylamine **5.4** respectively (Scheme 5.29).

(R,R)- and *(S,S)*-methylbenzyl BOMP were synthesized by first abstracting the hydroxide proton of alcohol **5.2** with sodium hydride followed by addition of ditosylate **5.1**. The optimization of the BOMP synthesis is necessary in order to develop a practical method for the determination of *ee* in α-chiral alcohols *via* BOMP derivatization; therefore it was gratifying that the methylbenzyl BOMP **5.3** could be purified by filteration through silica gel (see Experimental section). The BAMP enantiomers, (*R*)- and (*S*)-**5.5** were also prepared by nucleophilic substitution of **5.1**, in this case with amine **5.4**. The next step in our study was to screen metals for binding to **5.5** to form the organometallic host complex.

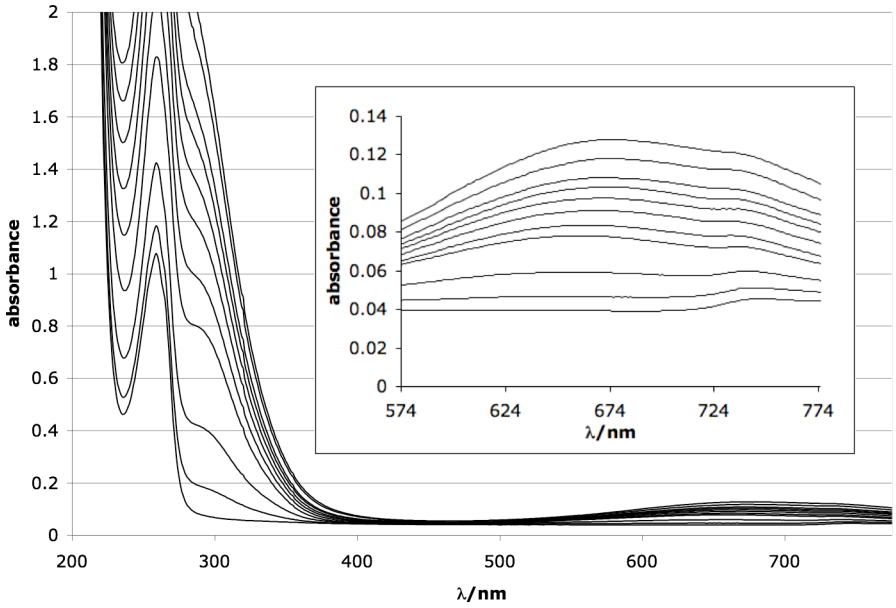

Figure 5.70 ***Absorbance spectra as Cu^{II} triflate is added to (S,S)-5.5.*** $Cu^{II}(OTf)_2$ was added to *(S,S)*-**5.5** (0.25 mM) in 1:1 water:methanol with HEPES buffer (50 mM) at pH 7. Absorbance increases in the UV-region correspond to changes in **5.5** absorbance upon chelation to Cu^{II} while the *d-d* transition of Cu^{II} in the visible region (inset) is also effected by the chelation event.

5.2.2 BAMP-ligand to metal binding studies using UV-Vis.

Metal binding to (*S,S*)-**5.5** was assessed by UV-Vis titration. **5.5** absorbs in the UV region (λ_{max} = 259 nm) and this absorbance band is perturbed when **5.5** chelates to a metal. The exact nature and degree of the perturbation seems to vary with the metal used, but in all cases an inflection point was observed at a metal concentration equal to the concentration of **5.5** (i.e. 1 equivalent). This method is demonstrated by the titration with Cu^{II}, an ion that is known to exhibit strong binding to BAMP-type ligands, and whose *d-d* transitions are correlated to the coordination state of the metal ion. Upon addition of Cu^{II} triflate to an aqueous solution of (*S,S*)-**5.5**, the **5.5** absorption peak in the UV undergoes a rapid increase in intensity, and a corresponding increase in the Cu^{II} *d-d* absorbance at 670 nm is observable as well (Figure 5.70). For both peaks, the change in absorption as a function of Cu^{II} concentration inflects at a [Cu^{II}] equal to the concentration of (*S,S*)-**5.5** (0.25 mM). The absorbance at both peaks continues to increase after one equivalent of

metal is added, presumably due to the ligand to metal charge transfer of the incoming salt but the inflection point is quite apparent nevertheless. A series of metal salts was surveyed in this manner (Table 5.12). The addition of Zn^{II} and Cd^{II} to the (*S,S*)-**5.5** solution also modulated the ligand absorbance and exhibited inflection points similar to those observed in the case of Cu^{II}; however, the spectroscopic change was substantially smaller. No *d-d* transitions were observed for Zn^{II} and Cd^{II}. Having identified a set of metals that bind **5.5**, the next step was to identify which of the **5.5**-metal complexes showed the most promising indicator binding behavior.

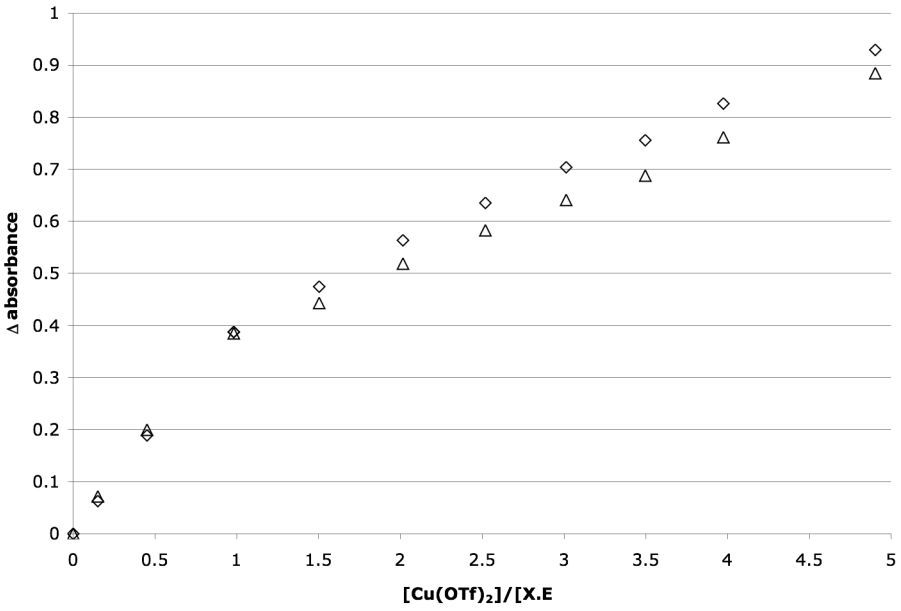

Figure 5.71 ***The change in absorbance of*** **Figure 5.70** ***at 317 nm and 670 nm as a function of*** Cu^{II} ***triflate concentration.*** The change in absorbance of the ligand (◇, 317 nm) exhibits an inflection point around the concentration of (*S,S*)-**5.5** (0.25 mM). The same inflection point is seen in the increase of the incoming peak corresponding to the *d-d* transition of the Cu^{II} ion (△, 670 nm). The change in absorbance of the *d-d* transition has been multiplied by a factor of ten for comparison of the inflection points.

Metal salts	$Cu(OTf)_2$	$CuCl_2$	$Zn(OTf)_2$	$Cd(OAc)_2$	$Co(NO_3)_2$	$CoCl_2$	$Ni(NO_3)_2$
Binding observed?	yes	yes	yes	yes	no	no	no

Table 5.12 ***Metals screened for binding to 5.5.*** Cu^{II}, Zn^{II} and Cd^{II} all modulated the **5.5** absorbance. The triflate salt of copper was used in subsequent Cu^{II}-**5.5** complexes unless otherwise noted.

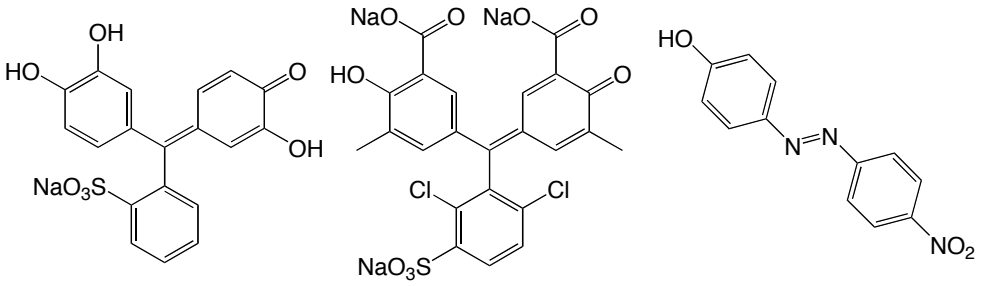

Pyrocatechol Violet **5.6** | Chrome Azurol S **5.7** | 4-(4-nitrophenylazo)phenol **5.8**

Figure 5.72 ***Pyrocatechol Violet, Chrome Azurol S and 4-(4-nitrophenylazo)phenol.*** These indicators were tested for binding to metal-**5.5** complexes.

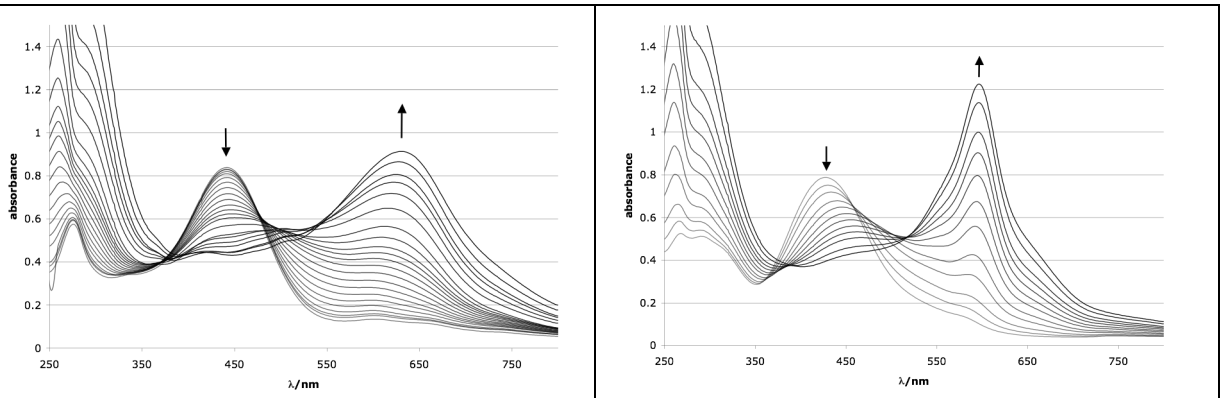

Figure 5.73 ***Spectra of* 5.6 *and* 5.7 *as* Cu^{II}-5.5 *is added.*** *(R,R)*-Cu^{II}-**5.5** was added to **5.6** (52 μM, spectra on left) and **5.7** (52 μM, spectra on right) in a 1:1 water:methanol solution in the presence on 50 mM HEPES buffer at pH 7.0.

5.2.3 Finding an indicator

The Anslyn group is well versed in Cu^{II}-based IDAs, and they have found a number of systems in which pyrocatechol violet **5.6** and chrome azurol S **5.7** have proven to be good indicators, capable of effective binding to Cu^{II} centers, therefore these were the first

indicators that were studied for binding to the currentBAMP-metal system. 4-(4-nitrophenylazo)phenol **5.8** was also tested in hopes that the monodentate indicator would prove especially easy to displace, but **5.8** exhibited no binding to Cu^{II}-**5.5**. The 1:1 Cu^{II}-**5.5** complex was generated *in situ* and titrated into solutions of **5.6** and **5.7** (Figure 5.73). Both (*S,S*)-**5.5** and (*R,R*)-**5.5** were tested for binding to the indicators (52 μM) in aqueous solution (1:1 water:methanol with 50 mM HEPES buffer at pH 7), and the titration data for the enantiomers were nearly identical (Figure 5.74) as is expected when dealing with achiral species like **5.6** and **5.7**. The good agreement between the (*S,S*)-**5.5** and (*R,R*)-**5.5** systems was relieving in light of the difficulties with repeatability and enantiomeric consistency experienced in our earlier endeavor to create an IDA for chiral alcohols using a Ti(IV)-based modified Sharpless catalyst (see Chapter 4).

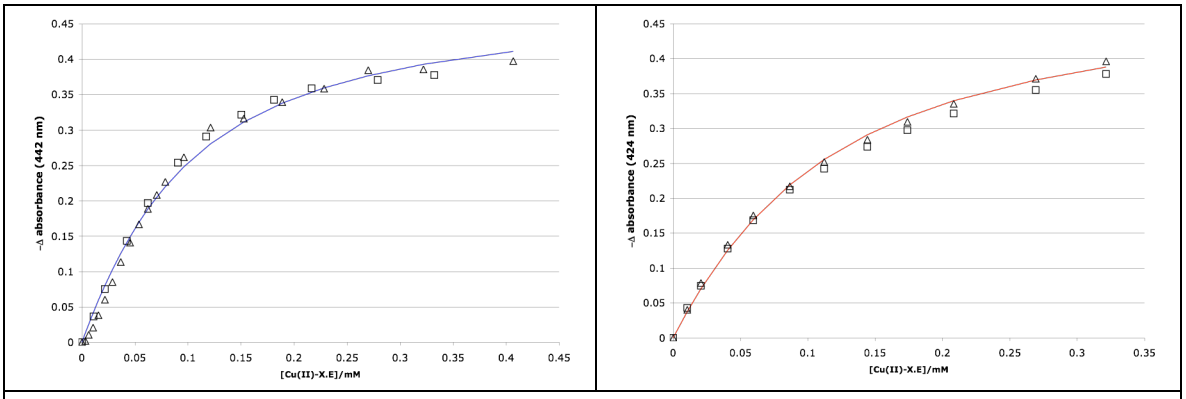

Figure 5.74 ***Isotherms of Cu^{II}-5.5 binding to* 5.6** ***and* 5.7.*** The changes in absorbance of the spectra shown in Figure 5.73 are plotted against the concentration of added Cu^{II}-**5.5**. The decreasing indicator peak was chosen for the isotherm because the incoming Cu^{II} species exhibits a small *d-d* absorbance near the bound indicator absorbance. Therefore, Δ absorbance is plotted as its absolute value (-Δ absorbance). **5.6** (442 nm), on left with blue binding isotherm; **5.7** (424 nm), on right with red binding isotherm; △, (*R,R*)-Cu^{II}-**5.5**; □, (*S,S*)-Cu^{II}-**5.5**.

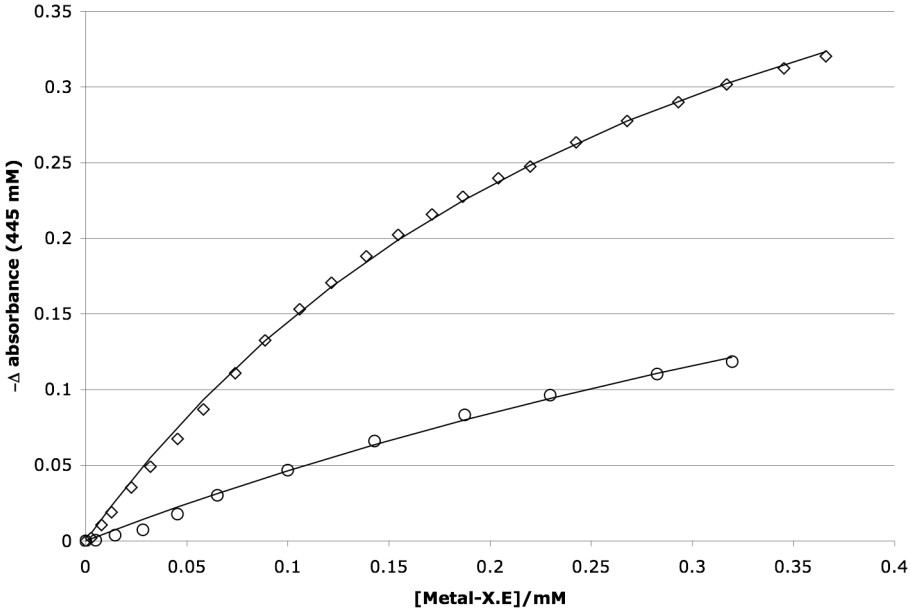

Figure 5.75 ***Zn^{II}-5.5 and Cd^{II}-5.5 into 5.6.*** The change in absorbance of **5.6** (50 μM) is plotted again the concentration of metal-**5.5** complex. The Δ absorbance is plotted as its absolute value (-Δ absorbance). ○, Cd^{II}-**5.5**; ◇, Zn^{II}-**5.5.**

Metal ion	pH	[HEPES] /mM	K_a /M^{-1}
Cu^{2+}	7	50	$1.46 \pm 0.15 \times 10^4$
Cu^{2+}	8	10	$5.59 \pm 1.43 \times 10^4$
Zn^{2+}	7	20	$4.00 \pm 0.20 \times 10^3$
Zn^{2+}	8	10	$1.60 \pm 0.22 \times 10^4$
Cd^{2+}	7	10	$1.20 \pm 0.40 \times 10^3$
Cd^{2+}	8	10	$9.90 \pm 1.00 \times 10^3$

Table 5.13 ***K_a's for metal*-5.5 *binding to* 5.6.** All titrations were carried out in 1:1 water:methanol. The HEPES concentration was higher in early titrations as a precaution but 10 mM was eventually determined to be sufficient. All three metal complexes exhibit stronger binding at higher pH.

The titrations of Cu^{II}-**5.5** into **5.6** and **5.7** were fit to a 1:1 binding isotherm using Origin (Figure 5.74) to give association constants (K_a) of $(1.46 \pm 0.10) \times 10^4$ M^{-1} and $(1.19 \pm 0.89) \times 10^4$ M^{-1} respectively. **5.6** was chosen as the indicator for future studies because precipitate was observed in the Cu^{II}-**5.5**-**5.7** solutions. Therefore, only the binding of **5.6** to Zn^{II}-**5.5** and Cd^{II}-**5.5** was assessed (Figure 5.75). The zinc and cadmium BAMP complexes bind **5.6** at pH 7.0 with affinity constants of an order of magnitude less than that of the Cu^{II}-**5.5** complex (K_a of **5.6** binding to Zn^{II}-**5.5** =

$(4.00 \pm 0.20) \times 10^3\ M^{-1}$; to Cd^{II}-**5.5** = $(1.20 \pm 0.40) \times 10^3\ M^{-1}$). **5.5** complexes with Cu^{II}, Zn^{II} and Cd^{II} were also titrated into **5.6** at pH 8.0. The more basic medium was found to greatly enhance indicator binding (Table 5.13) presumably by assisting the necessary deprotonation of **5.6** to form the catecholate anion that is the actual species binding the metal center. Having established that **5.6** does bind to the metal center of metal-**5.5** complexes, the next step was to study the proposed displacement of the indicator by the BOMP-type α-chiral alcohol derivative **5.3**.

5.2.4 Attempts at indicator displacement

Attempts to displace **5.6** from any of the metal-**5.5** complexes using **5.3** were unsuccessful. (*S,S*)-**5.3** was titrated into multiple metal-**5.5**-**5.6** solutions (Table 5.14) and absolutely no modulation of the **5.6** signal was observed, the only absorbance change being the rising peak of the added BOMP compound (Figure 5.76).

Metal salt	[Metal-**5.5**] /μM	[**5.6**] /μM	[HEPES] /mM	pH
$CuCl_2$	50	50	50	7
$CuCl_2$	100	50	50	7
$Zn(OTf)_2$	100	50	10	8
$Cd(OAc)_2$	100	50	10	8

Table 5.14 ***The displacement of*** **5.6** ***by*** **5.3*****: Conditions tried.*** **5.6** was never observed to displace.

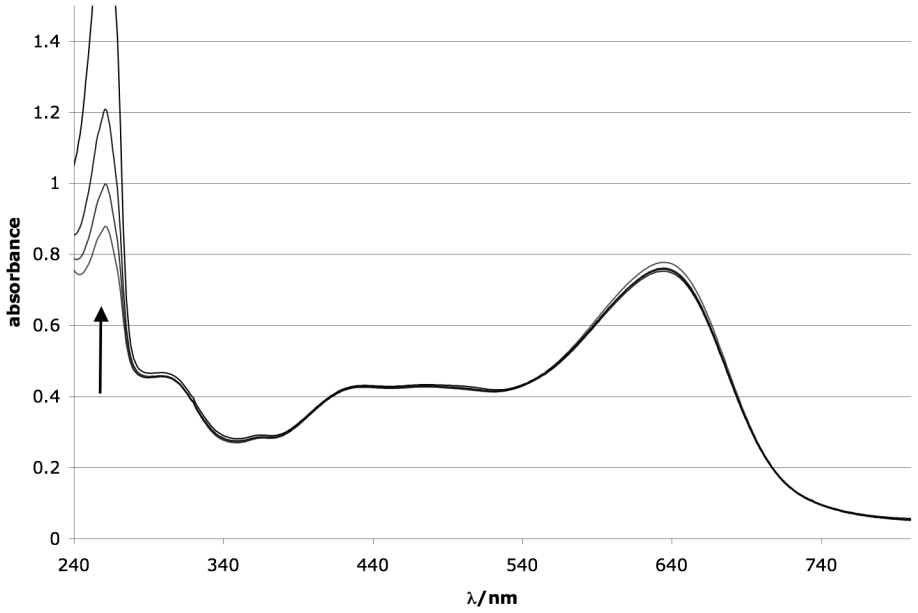

Figure 5.76 ***A sample titration showing no modulation of*** **5.6** ***absorbance as*** **5.3** ***is added.*** The incoming peak at 250 nm is due to **5.3**. The system is (*S,S*)-Zn^{II}-**5.5** (100 μM) with **5.6** (50 μM) in 1:1 water:methanol with 10 mM HEPES buffer at pH 8.0. After the final aliquot was added the total [**5.3**] = 194 μM.

5.3 A Phenanthroline-based Alcohol Derivative

While the anticipated binding affinity of the BOMP-type α-chiral alcohol derivative fell short of expectations, the idea of derivatizing an α-chiral alcohol for use in an IDA was still viable. The key was to find a derivative with sufficient chelating power to displace **5.6** from a BAMP bound metal center, and which can still position its chiral center to interact with the chiral BAMP arms, as calculations indicated in the case of BOMP (Figure 5.69). As before, if a sensing protocol involving a derivatization step is to be viable, then that step must be trivial, with minimal workup and purification. We therefore designed an alcohol derivative having a phenanthroline moiety, as this strongly chelating ligand would at least satisfy our requirement for strong binding affinity.

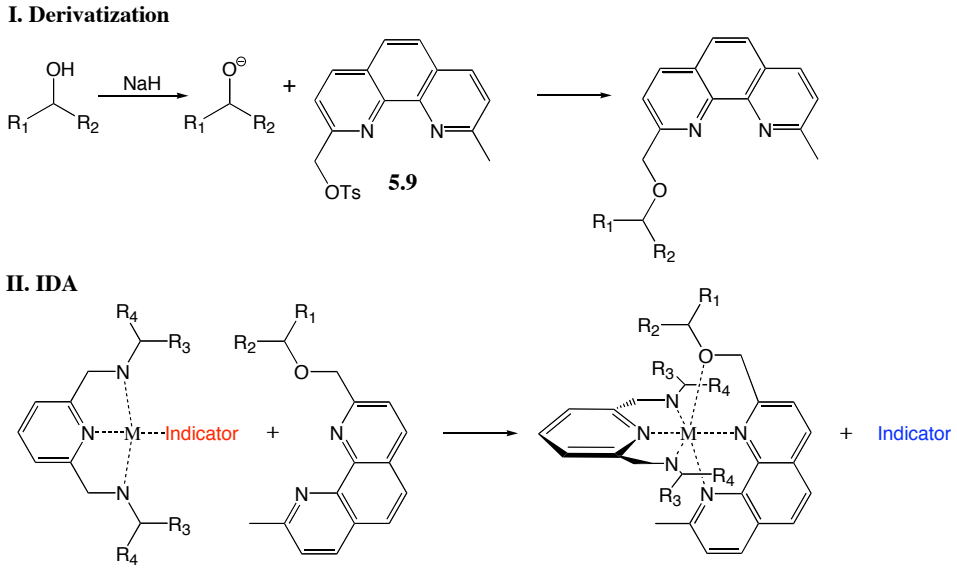

Scheme 5.30 ***Derivatization of a secondary alcohol to form a strongly chelating phenanthroline ether that is capable of displacing an indicator.***

5.3.2 A more strongly chelating secondary alcohol derivative

The poor binding affinity of the BOMP alcohol derivative required the design of a new derivatization process. A phenanthroline bearing an electrophilic center was chosen (Scheme 5.30) because of the well established chelating strength of phenanthroline, and because the chiral ether arm would be positioned near the chiral amino arms of the BAMP ligand upon binding. Besides better metal affinities, a second benefit of this system is the presence of a single tosylate on the derivatizing agent **5.9**. Adding only one ether arm doubles the theoretical yield of the derivative with respect to α-chiral alcohol and negates the possibility of forming *meso* species like those discussed for the BOMP derivative. The downside to having only one ether arm is that the enantiospecific steric interactions between the BAMP ligand and the phenanthroline derivative will decrease, and therefore the difference in energy upon binding the phenanthroline ether enantiomers might be less than that envisioned for the BOMP derivatives.

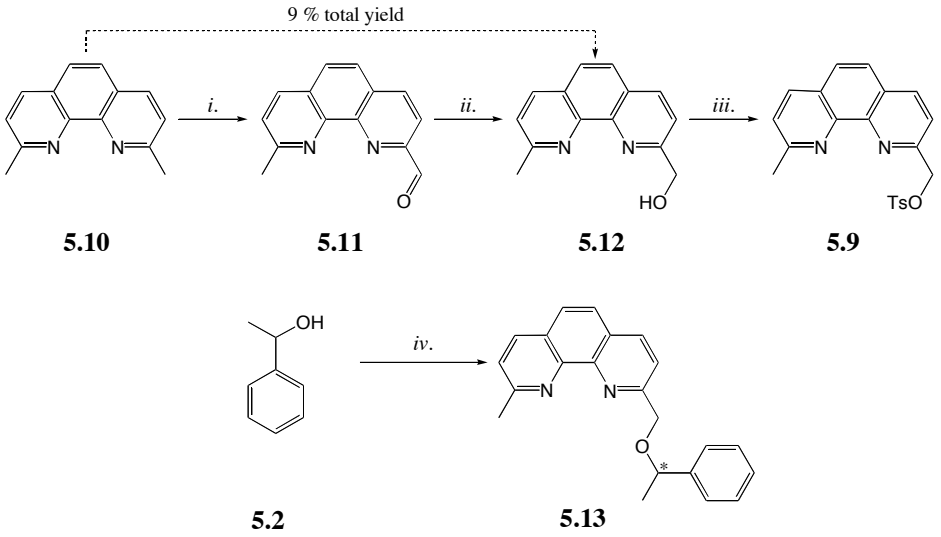

Scheme 5.31 ***Synthesis of phenanthroline-containing derivative 5.13.*** Reagents conditions and yields: (*i.*) SeO_2, 4% H_2O/1,4-dioxane, 80 °C, 3 h (*ii.*) $NaBH_4$, EtOH, 85 °C, 3 h (*iii.*) TsCl, DCM, TEA, 0 °C, 2 h, 42 % (*iv.*) NaH, DMF, 0 °C, 10 min then **5.9**, 23 °C, 2.5 h.

5.3.2 Synthesis of the phenanthroline alcohol derivative

The synthesis of the derivatizing agent **5.9** and subsequent methylbenzyl ether **5.13** begins with neocuproine **5.10**, which is oxidized to the aldehyde **5.11** by selenium dioxide (Scheme 5.31). The crude **5.11** is submitted to reducing conditions without purification to yield **5.12.** Formation of **5.11** also produces the undesired dialdehyde (not shown) double oxidation product. In order to minimize the production of dialdehyde, **5.10** was used in excess and was recovered by silica chromatography after the reduction of **5.11**.

The tosylation of **5.12** to form **5.9** must be kept judiciously at 0 °C and worked up as soon as **5.12** is consumed because the tosyl group of **5.9** is displaced by chloride over time (as observed by mass spectrometry). Keeping the reaction at 0 °C minimizes the solubility of the triethylammonium chloride byproduct to both inhibit the chloride side reaction and to drive the initial tosylation to completion.

Disappointingly, the reaction of 1-phenylethanol **5.2** with **5.9** produced the desired alcohol derivative **5.13** in only 7% yield. Purification was also difficult, requiring a tedious column. *In lieu* of reaction optimization, we decided that the current

derivatization approach was not the most promising for the development of an IDA for the determination of *ee* in α-chiral alcohols.

5.4 Conclusion

This chapter has recounted efforts made in the Anslyn group to develop a system for the quantitative determination of *ee* in α-chiral alcohols *via* the derivatization of the alcohols to effect more potent metal ligands for use in IDAs. Our pursuit of a derivatization approach was an attempt to overcome the basic difficulty of sensing simple alcohols using organometallic-supramolecular systems: the coordination of a single hydroxyl group is too weak to drive most host-guest interactions in the solvent system of choice. By derivatizing the alcohol to create an ether proximal to strong metal-coordinating functional groups, we hoped to form a guest molecule with enough binding affinity to displace an indicator from the metal center of a chiral host. After effecting the transformation of the α-chiral alcohol into a guest capable of displacing an indicator, we intended to explore modular replacement of the chiral ligand used to form the chiral host complex, in order to optimize the system's enantioselectivity. Unfortunately, a suitable derivative was not found.

The incorporation of a derivatization step into a sensing protocol is only valid if the reaction in question is trivial to perform. This means simple reaction setups (stirring at room temperature is ideal), with near quantitative yields and no purification steps beyond filtration of the reaction mixture. The first derivatization we attempted, the formation of BOMP-type diethers, showed promise especially in the ease with which it could be purified by simple filtration through silica gel to afford the desired product in high purity. The BOMP-derivative, however, performed poorly in indicator displacement studies. The second approach attempted, the formation of phenanthroline-based monoethers, failed in the derivatization step because its yield was poor and the product was difficult to purify. Due to the unpalatable nature of requiring a derivatization of any kind in a sensing protocol, we decided to abandon this route and the project has since returned to a

search for a more direct method to sense *ee* in α-chiral alcohols using supramolecular chemistry.

5.5 Experimental Details for Chapter 5

5.5.1 General

Reactions were run under an atmosphere of argon unless otherwise indicated. Glassware was flame dried and let cool under vacuum. The chemicals were obtained from Acros Organics, Aldrich, TCI America, and EM Science and were used without further purification unless otherwise noted. Methylene chloride and triethylamine were distilled from calcium hydride. All water used in analytical experiments was distilled, deionized and filtered. A Varian Gemini 400 MHz NMR was used to obtain ^{1}H and ^{13}C spectra. The chemical shifts were referenced relative to TMS, used as an internal standard unless otherwise noted. A MicroMass AutoSpec-Ultima spectrometer was used to obtain high-resolution mass spectra. The UV-visible absorption measurements were recorded on a Beckman DU640 spectrometer. All products were dried for at least 6 hours prior to spectral analysis.

5.5.2 Synthesis

Pyridine-2,6-diylbis(methylene)bis(toluenesulphonate) (5.1): *p*-toluenesulfonyl chloride (82.486 g, 432.7 mmol) was dissolved in dichloromethane (125 mL) and stirred at 0 °C for 0.5 h with a mechanical stirrer. A slurry of 2,6-pyridine dimethanol (20.068 g, 144.2 mmol) in triethylamine (60 mL) was dripped into the reaction from an addition funnel. The slurry required manipulation with a spatula to completely transfer from the funnel. After 2 h the reaction mixture was diluted with water (200 mL) and the organic phase was removed. The aqueous phase was extracted with dichloromethane (2 x 100 mL). The organic fractions were combined, washed with brine (100 mL) and then dried over anhydrous sodium sulfate. The solution was concentrated *in vacuo* to yield a light brown powder. The crude mixture was purified by sequential recrystallization from dichloroethane:hexanes to yield the desired product in 29% yield (18.746g, 41.89 mmol).

^{1}H NMR ($CDCl_3$): 7.80 (d of t, 4H), 7.69 (t, 1H), 7.33 (d, 6H), 5.05 (s, 4H), 2.44 (s, 6H). ^{13}C NMR ($CDCl_3$): 153.6, 145.1. 137.9, 132.8, 129.9, 128.07, 121.4, 71.3, 21.7. HRMS (CI+) C_{21} H_{22} N O_6 S_2 *m/z*: 448.0882; calcd: 448.0889.

***(S)*- and *(R)*-2,6-Bis-(1-phenyl-ethoxymethyl)-pyridine (5.3):** To dry dimethylformamide (5 mL) was added 1-phenylethanol (264 μL, 2.2 mmol) and the solution was put in a 0 °C ice/water bath. A 60% dispersion of NaH in mineral oil (98 mg, 3.83 mmol) was added and the suspension was let stir for 0.25 h after which **5.1** (448 mg, 1 mmol) was added and the solution warmed to rt. After stirring overnight the solution was diluted with dichloromethane (100 mL). The organic phase was washed with water (3 x 100 mL), brine (1 x 100 mL) and dried over anhydrous sodium sulfate. The solution was concentrated *in vacuo*. The crude mixture was purified by silica gel column chromatography (solvent ramping from hexanes to ethyl acetate) to yield the desired product in 54% yield (151.7 mg, 0.44 mmol). R_f = 0.83 in 1:1 hexanes:ethyl acetate. ^{1}H NMR ($CDCl_3$): 7.72 (t, 1H), 7.41 (d, 2H), 7.37 (m, 8H), 7.29 (t, 2H), 4.58 (q, 2H), 4.50 (q, 4H), 1.55 (d, 6H). ^{13}C NMR ($CDCl_3$): 158.5, 143.6, 137.4, 128.7, 127.8, 126.5, 119.9, 78.4, 71.6, 24.2. HRMS (CI+) C_{23} H_{26} N O_2 *m/z*: 348.1963; calcd: 348.1964.

(*S*)- and (*R*)-N,N'-(pyridine-2,6-diylbis(methylene))bis(1-phenylethanamine) (5.5): To acetonitrile (5 mL) that had been stored over 4Å molecular sieves was added diisopropylethylamine (900 μL, 5.2 mmol) and methylbenzylamine (380 μL, 3 mmol). The solution was heated to 50 °C. Ditosylate **5.1** (450 mg, 1 mmol) was dissolved in dichloromethane (1.5 mL) and added dropwise *via* syringe to the stirring acetonitrile solution over 0.5 h. The reaction was let stir at 50 °C for 1 h after which it was cooled to rt. The reaction mixture was then poured into 1M NaOH (50 mL) and extracted with dichloromethane (4 x 20 mL). The organic phase was washed with brine (1 x 100 mL) and dried over anhydrous sodium sulfate. The solution was concentrated *in vacuo* to a thin brown oil which was stored under nitrogen. The reaction was not left under high vacuum for more than an hour for fear of product evaporation. The crude mixture was

purified by silica gel column chromatography (solvent ramping from dichloromethane to 10% ammonia saturated methanol in dichloromethane) to yield the desired product as an oil in 45% yield (155.6 mg, 0.45 mmol). ^{1}H NMR ($CDCl_3$): 7.52 (t, 1H), 7.38 (d of t, 4H), 7.33 (t of d, 4H), 7.25 (t of t, 2H), 7.05 (d, 2H), 3.88 (q, 2H), 3.76 (s, 4H), 1.45 (d, 6H). ^{13}C NMR ($CDCl_3$): 158.5, 144.7, 136.8, 128.5, 127.1, 126.9, 120.5, 58.0, 52.6, 24.1. HRMS (CI+) C_{23} H_{28} N_3 *m/z*: 346.2286; calcd: 346.2283.

9-Methyl-[1,10]phenanthroline-2-carbaldehyde (5.11): Neocuproine (1g, 4.8 mmol) was suspended in a water (1 mL) and dioxane (25 mL) mixture at 80 °C and treated with SeO_2 (0.266 g, 2.4 mmol). The reaction quickly turned dark brown. The reaction mixture was let stir for 2 h at 80 °C before it was filtered through Celite while still hot. The celite was rinsed with a minimum amount of dichloromethane. The reaction filtrate and rinse fraction were combined and concentrated *in vacuo* to yield a flaky red solid that was used in the next step of the reaction sequence without further purification.

(9-Methyl-[1,10]phenanthrolin-2-yl)-methanol (5.12): Unpurified **5.11** (544.8 mg, 2.45 mmol based on pure compound) was dissolved in ethanol (30 mL) and treated with sodium borohydride (115.9 mg, 3.06 mmol). The solution was heated to 85 °C for 3 h and then let cool to rt. The reaction was quenched with water (50 mL) and then extracted with dichloromethane (2 x 50 mL, 1 x 25 mL). The organic fractions were separated, washed with water (4 x 50 mL), brine (1 x 50 mL) and dried over anhydrous sodium sulfate. The solution was concentrated *in vacuo* to a red oil which became a fluffy solid after some time under high vacuum. The crude mixture was purified by silica gel column chromatography (solvent ramping from dichloromethane to 10% methanol in dichloromethane) to yield the desired product in 15% yield with respect to SeO_2 used in the oxidation of neocuproine (78.9 mg, 0.36 mmol). ~26% of the neocuproine starting material was also recovered at this point (262.2 mg, 1.26 mmol). **5.12** analytical data: ^{1}H NMR ($CDCl_3$): 8.13 (d, 1H), 8.07 (d, 1H), 7.66 (s, 2H), 7.43 (d, 1H), 5.13 (s, 2H), 2.86 (s, 3H). ^{13}C NMR ($CDCl_3$): 160.9, 159.6, 145.3, 144.7, 136.9, 136.6, 128.0, 127.1,

126.1, 125.7, 123.9, 120.6, 65.8, 25.9. HRMS (CI+) C_{14} H_{13} N_2 O *m/z*: 225.1030; calcd: 225.1028.

(9-methyl-1,10-phenanthrolin-2-yl)methyl 4-methylbenzenesulfonate (5.9): The alcohol **5.12** (78.9 mg, 0.35 mmol) was dissolved in dichloromethane (2 mL), treated with triethylamine (0.2 mL, 1.4 mmol) and stirred at 0 °C for 0.25 h. Tosyl chloride (134 mg, 0.704 mmol) was added and the reaction mixture was removed from the ice bath and let stir for 1.75 h. The reaction mixture was passed through a silica plug, which was rinsed with 5% methanol in dichloromethane. The solution was then washed with water (2 x 100 mL) and brine (1 x 100 mL), and then dried over anhydrous sodium sulfate. The solution was concentrated *in vacuo*. The crude mixture was purified by silica gel column chromatography (solvent ramping from dichloromethane to 10% methanol in dichloromethane) to yield the desired product in 42% yield (56.2 mg, 0.149 mmol). ^{1}H NMR ($CDCl_3$): 8.25 (d, 1H), 8.11 (d, 1H), 7.86 (d, 2H), 7.81 (d, 1H), 7.72 (d, 2H), 7.48 (d, 1H), 7.32 (d, 2H), 5.52 (s, 2H), 2.88 (s, 3H), 2.41 (s, 3H). ^{13}C NMR ($CDCl_3$): 159.7, 154.4, 145.14, 145.09, 144.9, 137.2, 136.4, 132.4, 129.9, 128.3, 128.2, 127.0, 126.8, 125.3, 123.9, 120.6, 72.6, 25.9, 21.6. HRMS (CI+) C_{21} H_{19} N_2 O_3 S *m/z*: 379.1121; calcd: 379.1116.

(*S*)- and (*R*)-(9-methyl-1,10-phenanthrolin-2-yl)methyl-methylbenzylether (5.13): To a flask at 0 °C was added 1-phenylethanol (0.1 mL, 0.83 mmol), dry dimethyl formamide (2 mL) and then a 60% dispersion of NaH in mineral oil (33 mg, 0.83 mmol) and the suspension stirred for 10 min. **5.9** (137.4 mg, 0.364 mmol) was dissolved in dichloromethane (0.7 mL) and added to the dimethylformamide solution *via* syringe. The reaction was removed from the ice bath and let stir at rt for 2 h. The reaction mixture was quenched with water (50 mL) and extracted with dichloromethane (3 x 25 mL). The organic layers were combined and washed with water (2 x 50 mL) and brine (1 x 50 mL), and then dried over anhydrous sodium sulfate. The solution was concentrated *in vacuo*. The crude mixture was purified by silica gel column chromatography (very slow solvent ramping from dichloromethane to 10% methanol in dichloromethane) to yield the desired

product in 7% yield (8.8 mg, 0.149 mmol). ^{1}H NMR ($CDCl_3$): 8.25 (d, 1H), 8.12 (d, 1H), 7.93 (d, 1H), 7.73 (d, 2H), 7.49 (d, 1H), 7.43 (d, 2H), 7.36 (t, 2H), 7.29 (t of t, H), 4.97 (s, 2H), 4.68 (q, 1H), 2.91 (s, 3H), 1.60 (d, 3H). ^{13}C NMR ($CDCl_3$): 160.1, 159.4, 145.4, 145.0, 143.5, 136.7, 136.3, 128.5, 127.9, 127.6, 126.9, 126.4, 125.9, 125.6, 123.6, 120.6, 78.4, 72.3, 25.9, 23.9. HRMS (CI+) C_{22} H_{21} N_2 O *m/z*: 329.1654; calcd: 329.1654.

5.5.3 UV-Vis titrations

A sample UV-Vis titration was conducted as follows. The UV-Vis was blanked with air. A cuvette was filled with 0.95 mL of a solution containing Pyrocatechol Violet (**5.6**) (0.052 mM) in a 1:1 water:methanol solvent buffered with HEPES (50 mM; pH 7.0), and the spectrum of this solution was recorded. A second solution of $Cu^{II}(OTf)_2$ (1 mM), **5.5** (1 mM) and Pyrocatechol Violet (**5.6**) (0.052 mM) in a 1:1 water:methanol solvent buffered with HEPES (50 mM; pH 7.0) was added in aliquots to the cuvette and spectra were recorded between each aliquot.

The only exception to the above protocol was the titration of metal salt into **5.5**. The metal salts in this case were dissolved at relatively high concentration (~ 10 mM) in water and added directly to **5.5** (0.25 mM) in a 1:1 water:methanol solvent buffered with HEPES (50 mM; pH 7.0). The high concentration of the metal solution insured minimal dilution of the **5.5** solution over the course of the titration.

5.5.4 Computation

The optimization of the structure shown in Figure 5.69 was performed using the Gaussian 03 program at the unrestricted DFT (B3LYP functional) level of theory.[3]

Route Section: # opt ub3lyp geom=connectivity gen pseudo=read iop(6/7=3) gfinput
Charge = 2 Multiplicity = 2

5.5.5 References for Chapter 5

[1]. Cotton, F. A.; Wilkinson, G. *Basic Inorganic Chemistry*. (John Wiley & Sons, Inc., 1976) ch. 23.

[2]. "A Cationic Host Displaying Positive Cooperativity in Water" Hughes, A. D.; Anslyn, E. V. *Proc. Natl. Acad. Sci. USA*, **2007**, *104*, 6538-6543.

[3]. Gaussian 03, Revision B.05, M. J. Frisch, G. W. Trucks, H. B. Schlegel, G. E. Scuseria, M. A. Robb, J. R. Cheeseman, J. A. Montgomery, Jr., T. Vreven, K. N. Kudin, J. C. Burant, J. M. Millam, S. S. Iyengar, J. Tomasi, V. Barone, B. Mennucci, M. Cossi, G. Scalmani, N. Rega, G. A. Petersson, H. Nakatsuji, M. Hada, M. Ehara, K. Toyota, R. Fukuda, J. Hasegawa, M. Ishida, T. Nakajima, Y. Honda, O. Kitao, H. Nakai, M. Klene, X. Li, J. E. Knox, H. P. Hratchian, J. B. Cross, C. Adamo, J. Jaramillo, R. Gomperts, R. E. Stratmann, O. Yazyev, A. J. Austin, R. Cammi, C. Pomelli, J. W. Ochterski, P. Y. Ayala, K. Morokuma, G. A. Voth, P. Salvador, J. J. Dannenberg, V. G. Zakrzewski, S. Dapprich, A. D. Daniels, M. C. Strain, O. Farkas, D. K. Malick, A. D. Rabuck, K. Raghavachari, J. B. Foresman, J. V. Ortiz, Q. Cui, A. G. Baboul, S. Clifford, J. Cioslowski, B. B. Stefanov, G. Liu, A. Liashenko, P. Piskorz, I. Komaromi, R. L. Martin, D. J. Fox, T. Keith, M. A. Al-Laham, C. Y. Peng, A. Nanayakkara, M. Challacombe, P. M. W. Gill, B. Johnson, W. Chen, M. W. Wong, C. Gonzalez, and J. A. Pople, Gaussian, Inc., Pittsburgh PA, 2003.

Vita

Andrew Dike Hughes was born in Spartanburg, South Carolina on June 30, 1980, the son of William Dike Hughes and Marilyn Justice Hughes. He graduated from Dorman High School in 1998, and entered the University of South Carolina Honors College in Columbia, South Carolina that Fall. During the 2000-2001 school year, Andrew attended Leeds University in Leeds, England as a study abroad experience. He received a Bachelor of Science from the University of South Carolina in December 2002. In September 2003 he entered the Graduate School of the University of Texas at Austin. He married Julie Kathleen Milligan in February 2007.

Permanent Address: 116 Ridgeway Rd., Spartanburg, South Carolina, 29301

This dissertation was typed by the author.